AD-A072 282 TEXAS A AND M UNIV COLLEGE STATION DEPT OF OCEANOGRAPHY F/G 8/3
LONG WAVE COUPLING OF THE MID AND SOUTH ATLANTIC BIGHTS FORCED --ETC(U)
MAY 79 D A BROOKS N00014-77-C-0354
UNCLASSIFIED TAMU-REF-79-3-T NL

1 OF 2
AD A072282

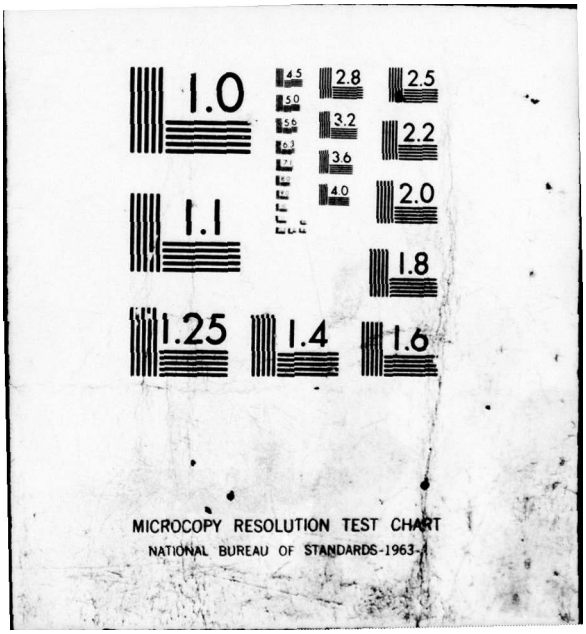
1.0
1.1
1.25
1.4
1.6
1.8
2.0
2.2
2.5
2.8
3.2
3.6
4.0
4.5
5.0
5.6
MICROCOPY RESOLUTION TEST CHART
NATIONAL BUREAU OF STANDARDS-1963-A

LONG WAVE COUPLING OF THE MID AND SOUTH ATLANTIC BIGHTS FORCED BY THE ATMOSPHERE

by

David A. Brooks

REFERENCE 79-3-T

May 1979

Prepared for the National Science Foundation under Grant Number 77-20971

TEXAS A&M UNIVERSITY

COLLEGE OF GEOSCIENCES

SECURITY CLASSIFICATION OF THIS PAGE (When Data Entered)

REPORT DOCUMENTATION PAGE

READ INSTRUCTIONS BEFORE COMPLETING FORM

(14) TAMU-REF-79-3-T

1. REPORT NUMBER
2. GOVT ACCESSION NO.
3. RECIPIENT'S CATALOG NUMBER

4. TITLE (and Subtitle)

(6) Long Wave Coupling of the Mid and South Atlantic Bights forced by the atmosphere

5. TYPE OF REPORT & PERIOD COVERED

6. PERFORMING ORG. REPORT NUMBER

7. AUTHOR(s)

(10) David A. Brooks

8. CONTRACT OR GRANT NUMBER(s)

(15) ONR N-00014-77-C-0354
NSF-OCE 77-20971

9. PERFORMING ORGANIZATION NAME AND ADDRESS

Texas A&M University
College Station, TX 77843

10. PROGRAM ELEMENT, PROJECT, TASK AREA & WORK UNIT NUMBERS

11. CONTROLLING OFFICE NAME AND ADDRESS

National Science Foundation
1800 G Street, NW
Washington, DC 20550
**see block 18

(11)

12. REPORT DATE

May 1979

13. NUMBER OF PAGES

121

14. MONITORING AGENCY NAME & ADDRESS(if different from Controlling Office)

(12) 131p.

15. SECURITY CLASS. (of this report)

Unclassified

15a. DECLASSIFICATION/DOWNGRADING SCHEDULE

16. DISTRIBUTION STATEMENT (of this Report)

Approved for Public Release Distribution Unlimited

17. DISTRIBUTION STATEMENT (of the abstract entered in Block 20, if different from Report)

18. SUPPLEMENTARY NOTES

This work was sponsored in part by the Office of Naval Research

(Florida Keys to Hatteras)

19. KEY WORDS (Continue on reverse side if necessary and identify by block number)

sea level fluctuations, shelf waves, mid and south Atlantic Bights

(Hatteras to Gulf of Maine),

20. ABSTRACT (Continue on reverse side if necessary and identify by block number)

The eastern United States continental margin profile is relatively uniform throughout the Middle Atlantic Bight, but in the South Atlantic Bight it bifurcates into an inner and outer slope region. Coastal tide gage records indicate that sea level oscillations with periods longer than one week can propagate southward as continental shelf waves in both Bights, thereby providing a coupling mechanism between the Bights. However, several-day period motions appear to be confined to the South Atlantic Bight and may result from backscattering of long wave energy by the variable topography and the Gulf

DD FORM 1 JAN 73 1473 EDITION OF 1 NOV 65 IS OBSOLETE
S/N 0102-LF-014-6601

402 203

SECURITY CLASSIFICATION OF THIS PAGE (When Data Entered)

(cont)

20. Stream. The coastal sea level phase data for the several-day period motions is not easily attributable to a monochromatic propagating wave; rather, it appears that wave group properties may lead to a more consistent explanation of the phases. Cross-shelf and longshelf wind stress components were both strongly coupled to sea level fluctuations for long periods; short period motions were more closely associated with dynamic responses to atmospheric pressure fluctuations.

Texas A & M University
Department of Oceanography
College Station, Texas
77843

LONG WAVE COUPLING OF THE MID AND SOUTH ATLANTIC BIGHTS FORCED BY THE ATMOSPHERE

by

David A. Brooks

REFERENCE 79-3-T

May 1979

Prepared for the National Science Foundation under Grant Number 77-20971

TABLE OF CONTENTS

LIST OF FIGURES

ACKNOWLEDGMENTS

This study was funded principally by Grant Number 77-20971 from the National Science Foundation. Some of the calculations in Section 4 were carried out with support under Contract Number N-0014-77-C-0354 from the Office of Naval Research. Most of the raw tide gage data was originally purchased under DOE Contract E(38-1)-902 as part of another project. This project was begun and most of the analysis carried out at North Carolina State University (Raleigh). The final analysis and synthesis were done at Texas A&M University. Most of the multiple regression plots in Appendix B were meticulously done by Ms. Cindy Knapp. I also acknowledge many helpful and ongoing discussions with Dr. John Bane concerning long waves in the Gulf Stream.

Abstract

The eastern United States continental margin profile is relatively uniform throughout the Middle Atlantic Bight, but in the South Atlantic Bight it bifurcates into an inner and outer slope region. Coastal tide gage records indicate that sea level oscillations with periods longer than one week can propagate southward as continental shelf waves in both Bights, thereby providing a coupling mechanism between the Bights. However, several-day period motions appear to be confined to the South Atlantic Bight and may result from backscattering of long wave energy by the variable topography and the Gulf Stream. The coastal sea level phase data for the several-day period motions is not easily attributable to a monochromatic propagating wave; rather, it appears that wave group properties may lead to a more consistent explanation of the phases. Cross-shelf and longshelf wind stress components were both strongly coupled to sea level fluctuations for long periods; short period motions were more closely associated with dynamic responses to atmospheric pressure fluctuations.

1. Introduction

The eastern United States coastal and continental shelf zone may be conveniently divided into two major embayments or bights (Fig. 1). The South Atlantic Bight (SAB) extends from the Florida Keys to Cape Hatteras, and the Middle Atlantic Bight (MAB) extends from Cape Hatteras to at least as far north as the Gulf of Maine. Cape Hatteras provides a salient coastal demarcation between the Bights.

The "boundary" between the SAB and MAB is much less distinct when one considers the shelf and slope topography. The 200 m and 2000 m isobaths in Fig. 1, which approximately bound the most steeply sloping shelf zone in the MAB, have considerably less curvature than the Cape Hatteras coastline in the Bight transition region. Since the continental shelf and slope topography can be expected to play an important role in determining low frequency water movements through angular momentum (vorticity) constraints, the Bights may in fact be quite strongly coupled.

The Bights differ in several dynamically significant ways. As suggested by the isobaths in Fig. 1, the continental slope is a single coherent feature throughout the MAB (and possibly farther north to the Grand Banks), but in the SAB it bifurcates into an upper slope that follows the coast and a lower slope that turns offshore and becomes the Blake Escarpment. The bottom profiles along lines roughly perpendicular to the 200 m isobath are shown in Fig. 2 for the four Carolina Capes and for the Chesapeake and Delaware Bay areas. The bottom slope changes by a factor of 2 or 3 between Capes Hatteras and Romain, but relatively little over the entire extent of the MAB. The inshore Gulf Stream front generally follows the upper SAB slope, and the n turns seaward at Cape Hatteras. The velocity

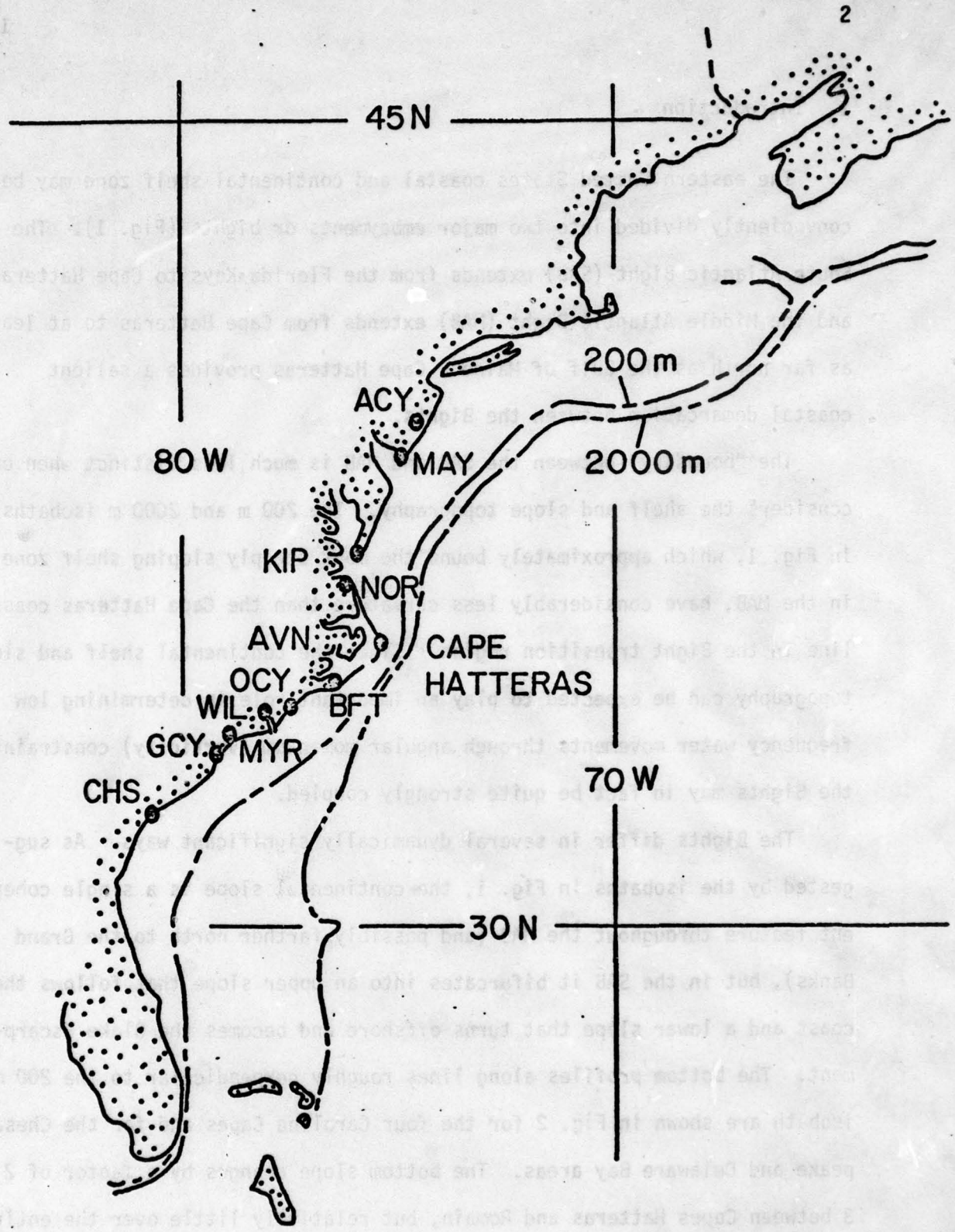

Fig. 1 Map of the eastern United States continental margin, showing the Middle and South Atlantic Bight sea level and meteorological observation station locations. The steepest continental slope zones are shown by the 200 m and 2000 m isobaths.

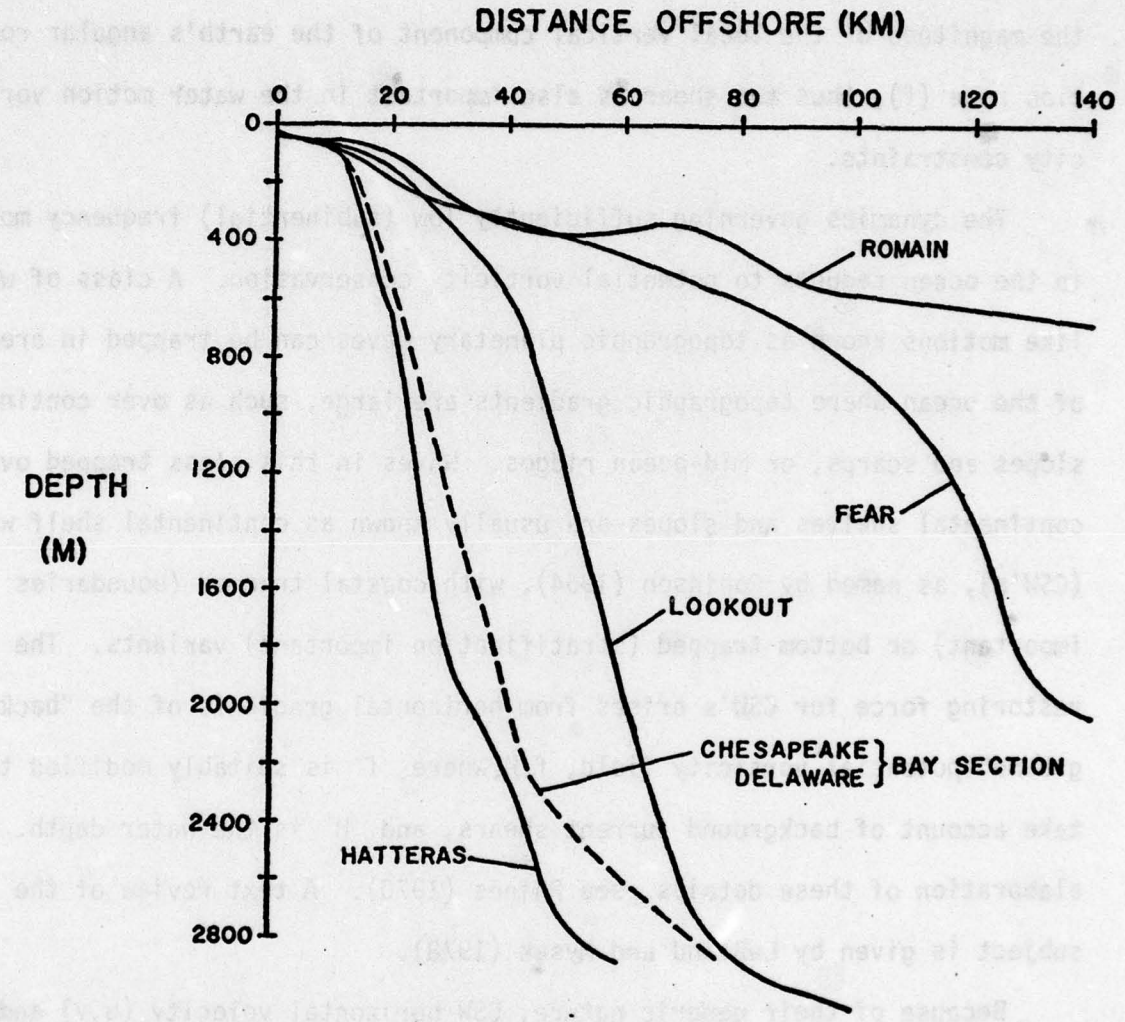

Fig. 2 Topographic profiles of the continental shelf. Profiles are shown for the four Carolina Capes in the SAB and for the Chesapeake-Delaware Bay region, which is typical of the entire MAB.

structure of the Stream perpendicular to a section off Cape Fear averaged over two summer months is shown in Fig. 3 (from Richardson, Schmitz and Niiler, 1969). The maximum horizontal shear of the mean Stream approaches the magnitude of the local vertical component of the earth's angular rotation rate (f); thus the shear is also important in the water motion vorticity constraints.

The dynamics governing sufficiently low (subinertial) frequency motions in the ocean reduces to potential vorticity conservation. A class of wave-like motions known as topographic planetary waves can be trapped in areas of the ocean where topographic gradients are large, such as over continental slopes and scarps, or mid-ocean ridges. Waves in this class trapped over continental shelves and slopes are usually known as continental shelf waves (CSW's), as named by Robinson (1964), with coastal trapped (boundaries important) or bottom trapped (stratification important) variants. The restoring force for CSW's arises from horizontal gradients of the "background" potential vorticity field, f/H, where f is suitably modified to take account of background current shears, and H is the water depth. For elaboration of these details, see Rhines (1970). A text review of the subject is given by LeBlond and Mysak (1978).

Because of their generic nature, CSW horizontal velocity (u,v) and sea level displacement (η) fields are trapped over steep bottom slopes, generally with oscillatory cross-slope structure in those regions and exponentially decaying structure in regions of gentle slope. Because CSW's do not depend on gravity for their existence, associated sea level displacements are small [O(10 cm)] and may become undetectable away from the steeply sloping zone, because the wave motion is evanescent there. Typical CSW velocities are O(30 cm s^{-1}), with wavelengths of O(100 - 1000 km) and

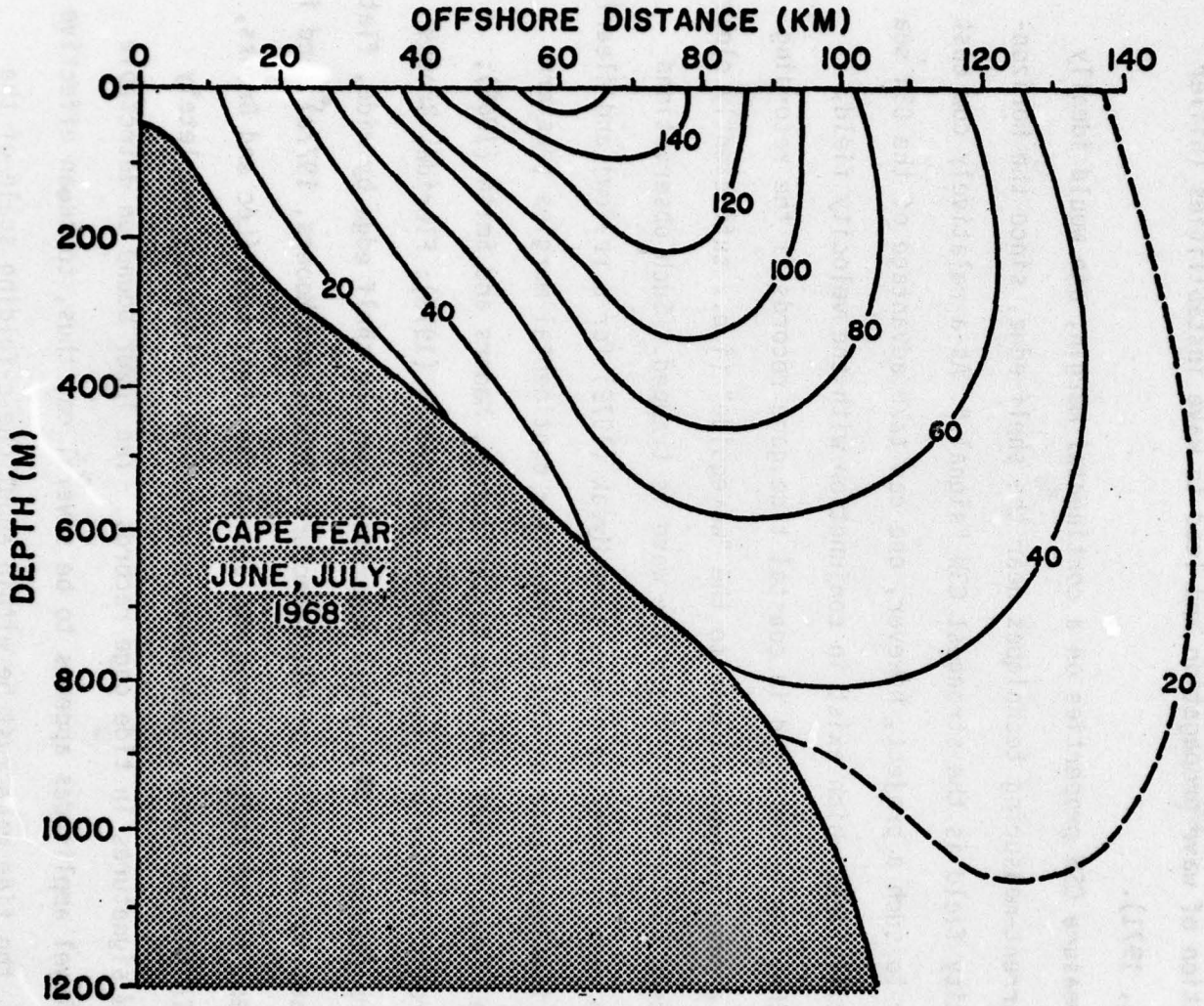

Fig. 3 Two-month summer mean longshore Gulf Stream isotachs off Cape Fear, after Richardson *et al.* (1969). The mean surface axis approximately overlies the 550 m isobath.

"normal" phase propagation *cum sole* (i.e., in the Kelvin wave sense) at speeds of O(100 km day^{-1}). An opposing background current, such as the Gulf Stream in the SAB upper slope case, can strongly modify these characteristics (Brooks and Mooers, 1977a), and, under certain conditions, reverse the direction of wave propagation and lead to wave instabilities (Niiler and Mysak, 1971).

To measure CSW properties on a continental margin, one would ideally employ current-measuring techniques near the shelf edge, since the horizontal velocity field is the strongest CSW "signal." As a relatively cow cost precursor to such a project, however, one can take advantage of the CSW sea level oscillations which exist in conjunction with the velocity field, because they can be detected in coastal tide gage records if the recording stations are sufficiently close to the "waveguide" (i.e., sufficiently close to the steep bottom slope, where the wave is trapped. Such observations have been made in numerous places (see Mysak (1979) for a review) and clearly indicate the importance of CSW motions over continental margins [eastern Australia, Hamon (1962); western United States, Mooers and Smith (1968); North Carolina, Mysak and Hamon (1969), and Brooks (1978); Florida, Brooks and Mooers (1977a)]. Tide gages separated from the shelf edge by wide, flat shelves are not as useful as CSW detectors (Brooks and Mooers, 1977a), and in some cases, may be isolated from motions at the shelf edge (Lee and Brooks, 1979). In shallow water, near shore wind-driven motions may completely swamp CSW signatures in tide gage records. The lower bound on detectable CSW sea level amplitudes appears to be several cm; thus, to be an effective detector, the tide gage must be within about one e-folding scale of the shelf edge. For CSW?s this scale is $\lambda/2\pi$ where λ is the wavelength.

From the regional tide gage studies in the SAB just mentioned,

indications of southward traveling CSW's have been found between Cape Hatteras and Southport, North Carolina, and along the southern half of the east Florida shelf. However, the signal "fades out" of tide gage records along the relatively wide and shallow Georgia shelf which joins the two regions (Lee and Brooks, 1979). In the MAB, the evidence seems quite convincing that CSW's are forced by longshore winds in the New York Bight area, and then propagate southward as free waves at least as far as Kiptopeake Beach (Wang, 1979).

The principal objective of the present study is to use tide gage records to see if CSW's can propagate "around the corner" at Cape Hatteras, thereby linking the Bights. Such a link would provide a potentially important mechanism by means of which storm or otherwise generated vorticity anomalies in the MAB could be introduced into the SAB. An additional objective is to examine the relationship between the tide gage sea level records and the coastal meteorological forcing fields of wind stress and atmospheric pressure. The remainder of the body of the report discusses: (a) the data set and the methods of analysis used, b) summary results of the data analysis, and c) implications concerning the importance of CSW's in the SAB and MAB in light of some simple model calculations. The supporting data set from which the summary figures were extracted are contained in appendices.

2. Data Sources and Processing Techniques

The raw data set used for analysis in this study was extracted from the NOAA archives (hourly coastal tide gage observations, National Ocean Survey, Rockville, Maryland; three-hourly coastal meteorological observations, National Climatic Center, Asheville, North Carolina). The observation stations were chosen to provide reasonable symmetry with respect to Cape Hatteras, the "vertex" station of the array. An additional goal was to obtain data subsets of about four months duration for winter and summer meteorological conditions, to permit a seasonal comparison of meteorological forcing characteristics and effectiveness. The raw subsets finally chosen as the best compromise between the goals and the available data span the periods 18 Apr-21 Aug 74 ("summer") and 1 Nov 74-15 Mar 75 ("winter"), with start times of all data records of 0100 local time. These choices avoided all data gaps, except for the winter Garden City, South Carolina tide gage record, where gaps of 19, 6, 3 and 14 days occurred at random intervals. The gaps were filled with the mean value of the record over suitably-determined intervals before and after the gap. The resulting time series preserves the phase coherence of "good" portions, but suffers spectral blurring in proportion to the amount of data lost, which is 30.7% for Garden City.

The raw meteorological data used in this study consisted of wind speed and direction and atmospheric pressure at observation height. The wind velocity vectors were converted to wind stress vectors $(\vec{\tau})$, using the formula

$$\vec{\tau} = -\rho_a C_D |u| \vec{u}$$

where ρ_a is the air density at sea level, the drag coefficient

$C_D = 1.5 \times 10^{-3}$ is assumed, $\vec{u}$ is the wind velocity vector, and the minus sign results in the positive wind stress vector sense corresponding with the direction toward which the wind blows. The wind stress vectors were then resolved into offshore (τ_x) and longshore (τ_y) components in rotated coordinate systems, with the longshore direction parallel to the alignment of the 200 m isobath immediately offshore of the meteorological station. This rotation scheme, while in general resulting in different rotation angles for each station, emphasizes the expected importance of the continental slope in the relation between the wind and sea level fields.

The raw data were then low-pass filtered[1] to remove diurnal and semi-diurnal tidal and inertial (the Cape Hatteras inertial period is about 21 hours) variance, and the resulting "40HRLP" time series were decimated to a common six-hour interval, with start and stop times of 0100 and 2200 local time, respectively. The low-passed sea level time series were "barometrically adjusted" to remove the static sea level height changes associated with barometric pressure changes; this was accomplished by adding 1.01 cm to the sea level height at each station for each mb of pressure increase relative to the mean pressure at the nearest meteorological station. The filtered, "working" time series span the periods 22 Apr-17 Aug 74 (summer) and 5 Nov 74-11 Mar 75 (winter), with record lengths of 118 (127) days in summer (winter). Station names and abbreviations and coordinate rotation angles are given in Table 1, and station locations are shown in Fig. 1.

---

[1] A 40-hour quarter-power (-6 db) point low-pass Lanczos filter kernel with 33 (97) weights was used to filter the 3-hourly meteorological (hourly sea level) data, resulting in a data loss of 4 days at the beginning and end of all time series. Filter attenuation at diurnal and higher frequencies is $>10^6$. The standard filter programs are called "METFIL" and "SLVFIL," respectively, and are available from the author.

Table 1. Meterological and sea level stations for the summer (S, 22 Apr-17 Aug 74, 118 days) and winter (W, 5 Nov 74-11 Mar 75) 40-hour low pass filtered data sets. The meteorological station coordinate rotation angles are with respect to north, positive clockwise. Station locations are shown in Fig. 1.

A. Meteorological Stations

Station name	Abbreviation	Coordinate rotation (degree)
Norfolk, VA	NOR	10
Cape Hatteras, NC	HAT	56
Wilmington, NC	WIL	56
Charleston, SC	CHS	56

B. Sea Level Stations

Station name	Abbreviation and season (S/W) used	Nearest meteorological station for comparison
Atlantic, City, NJ	ACY (W)	NOR
Cape May, NJ	MAY (S)	NOR
Kiptopeake Beach, VA	KIP (S and W)	NOR
Avon, NC	AVN (S and W)	HAT
Beaufort, NC	BFT (S)	HAT
Ocean City Beach, NC	OCY (W)	WIL
Wilmington, NC	WIL (S and W)	WIL
Myrtle Beach, SC	MYR (S)	WIL
Garden City, SC*	GCY (W)	WIL
Charleston, SC	CHS (S and W)	CHS

* 30.7% gappy

Spectrum estimates were computed from the working data set by Fourier transforming cosine-tapered correlation functions (Blackman and Tukey, 1958). The resulting estimates covered the frequency range from 0 to 0.5 cycles per day (CPD) with an effective bandwidth of 0.033 CPD and 16 (17) degrees of freedom for the summer (winter) case. Coherence squared (γ^2) and phase (θ) functions between two time series were computed from the (complex) cross spectrum squared normalized by the product of the autospectra. For brevity, γ^2 will be referred to as "coherence." The (coherence, phase) vector is a measure of linear dependence between two time series, expressed as a complex function of frequency.

A frequency-dependent multiple regression technique (Groves and Hannan, 1968) was used to investigate meteorological forcing of sea level. The "input" variables were the two wind stress components and atmospheric pressure. Multiple coherence between different combinations of inputs and sea level, and complex partial transfer functions between individual inputs and sea level were computed. This technique has the advantage of accounting for possible input variable correlations, so that, for example, the transfer function between atmospheric pressure and sea level can be corrected for coherence between wind stress and pressure.

3. Summary Analysis Results

The spectrum and regression analysis results in condensed format are presented in this section as contoured fields in the ω-y plane, where ω is frequency and y is the distance from the Avon sea level station measured along the 200 m isobath.

3.1 Sea level interstation analysis

The coherence and phase of adjusted sea level at all stations relative to AVN is shown in Figs. 4-7 for winter and in Figs. 8-11 for summer. The 95% null hypothesis level for coherence is about 0.4, and the 95% confidence interval for phase is about ±(3, 12, 18) degrees for coherences of (0.9, 0.8, 0.7), respectively. The sign convention for the phase is such that positive (negative) values indicate fluctuations leading (lagging) with respect to AVN.

The adjusted sea level coherence in both seasons (Figs. 4 and 8) shows selective interstation coupling over both Bights in period bands of approximately 2.5 to 3.5 and $\geq$ 10 days. The relative coherence maxima in these bands can be traced over most of the extent of the array, in the winter 2.5 to 3.5 day band, for which the coherence decreases rapidly north of KIP. The coherences are generally lower for the unadjusted sea level (Figs. 6 and 10), except for periods greater than about one week. An additional band of high coherence occurs in the MAB unadjusted sea level at a period of about six days, corresponding to the mean cold front interval for the Eastern United States coastal margin (Mooers, *et al.*, 1976). This effect is most noticeable in the winter and in the MAB, as one would expect. The barometric adjustment procedure effectively removed the six-day sea level response, as evidenced by a comparison of Figs. 4 and 6. In the summer,

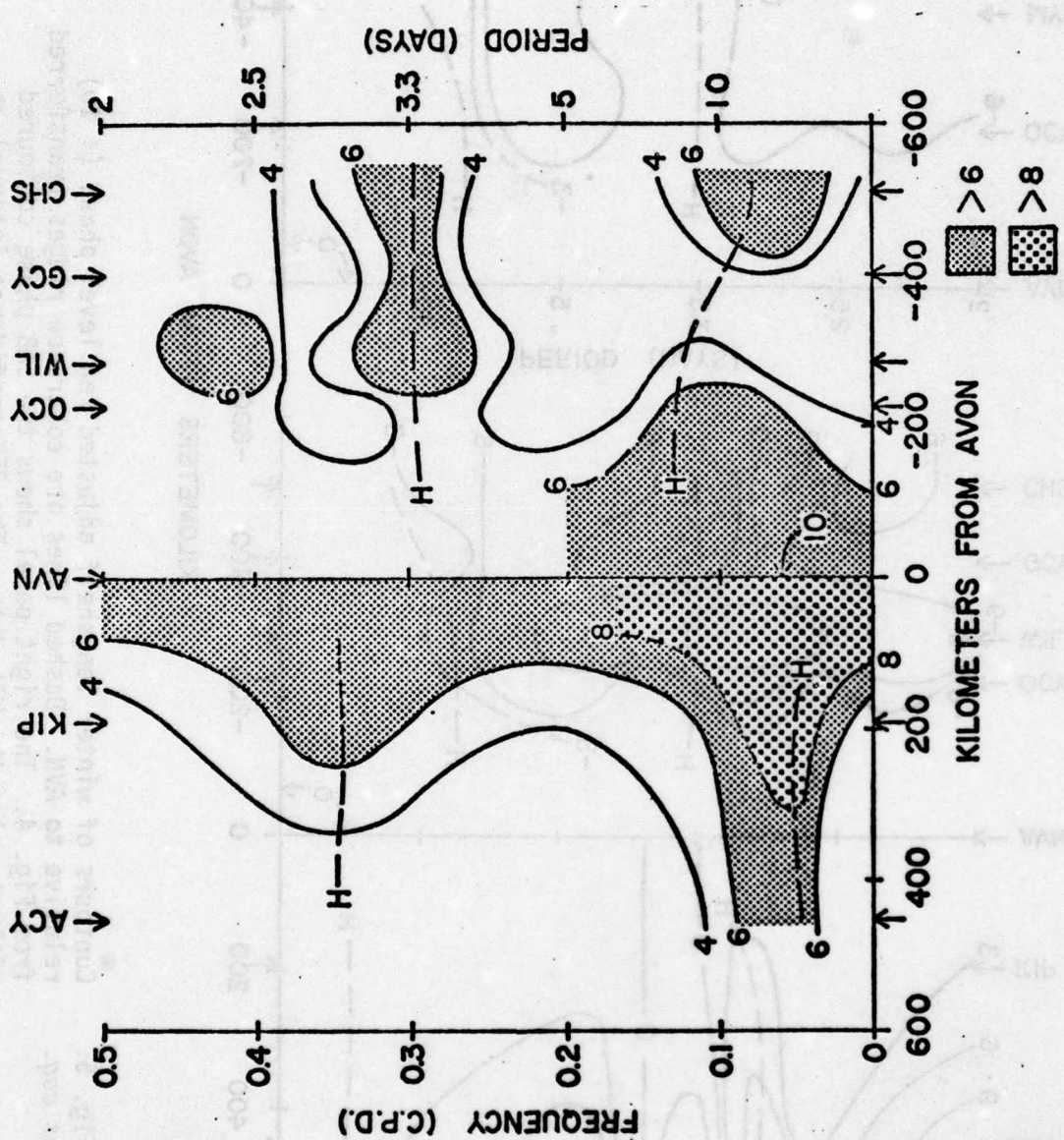

Fig. 4 Contours of winter longshelf adjusted sea level coherence (× 10) *et seq.* relative to AVN. Ridges are identified by the dashed lines, and station locations are shown by vertical arrows. The 95% null hypothesis level for coherence is about 0.4.

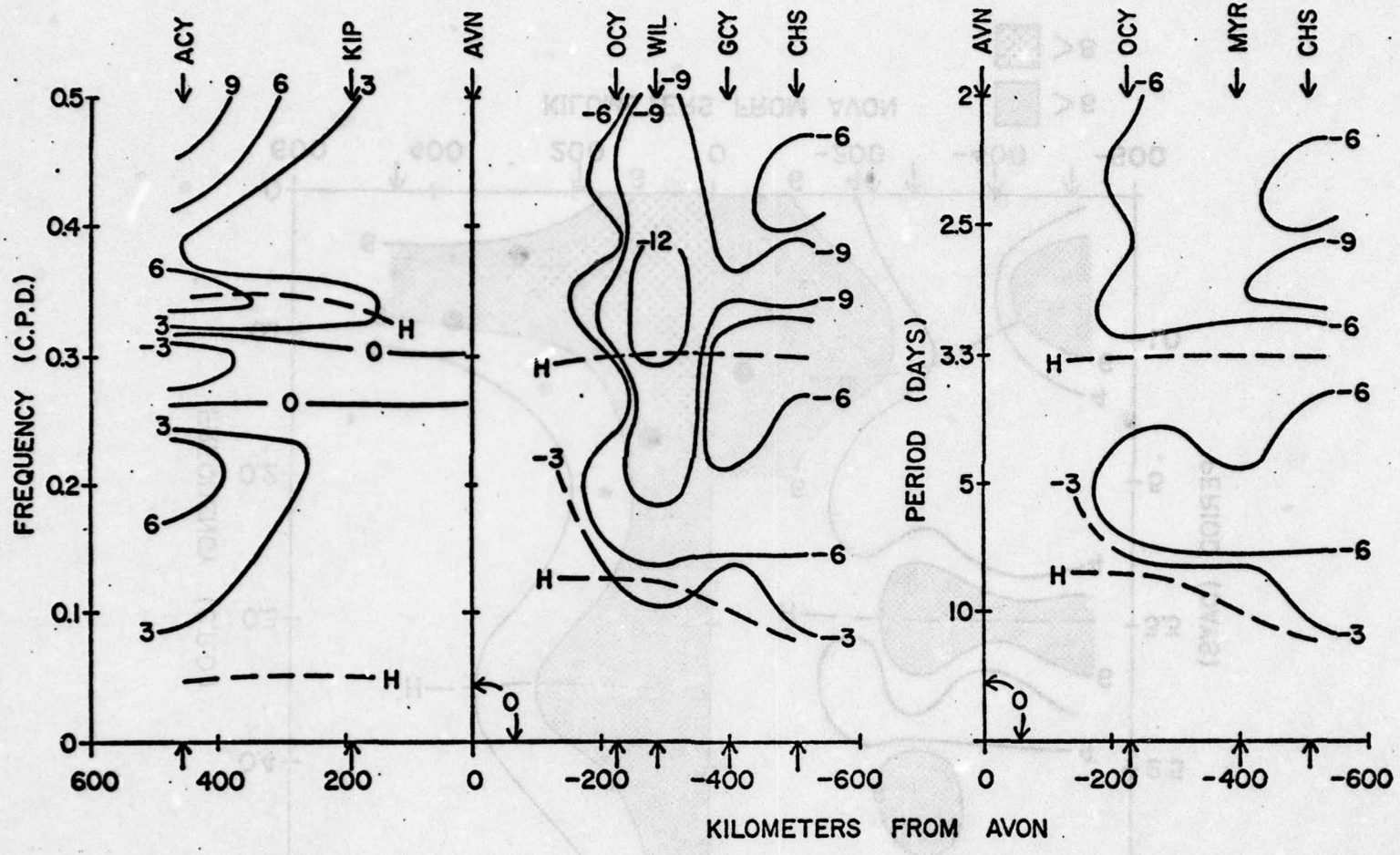

Fig. 5. *et seq.* Contours of winter longshelf adjusted sea level phase (÷ 10) relative to AVN. Dashed lines are coherence ridges transferred from Fig. 4. The right panel shows the SAB phase contoured without using the WIL data. The 95% confidence interval on phase is ±(3,12,18) degrees for a coherence squared of (0.9, 0.8,0.7). Positive phase indicates fluctuations leading those at AVN.

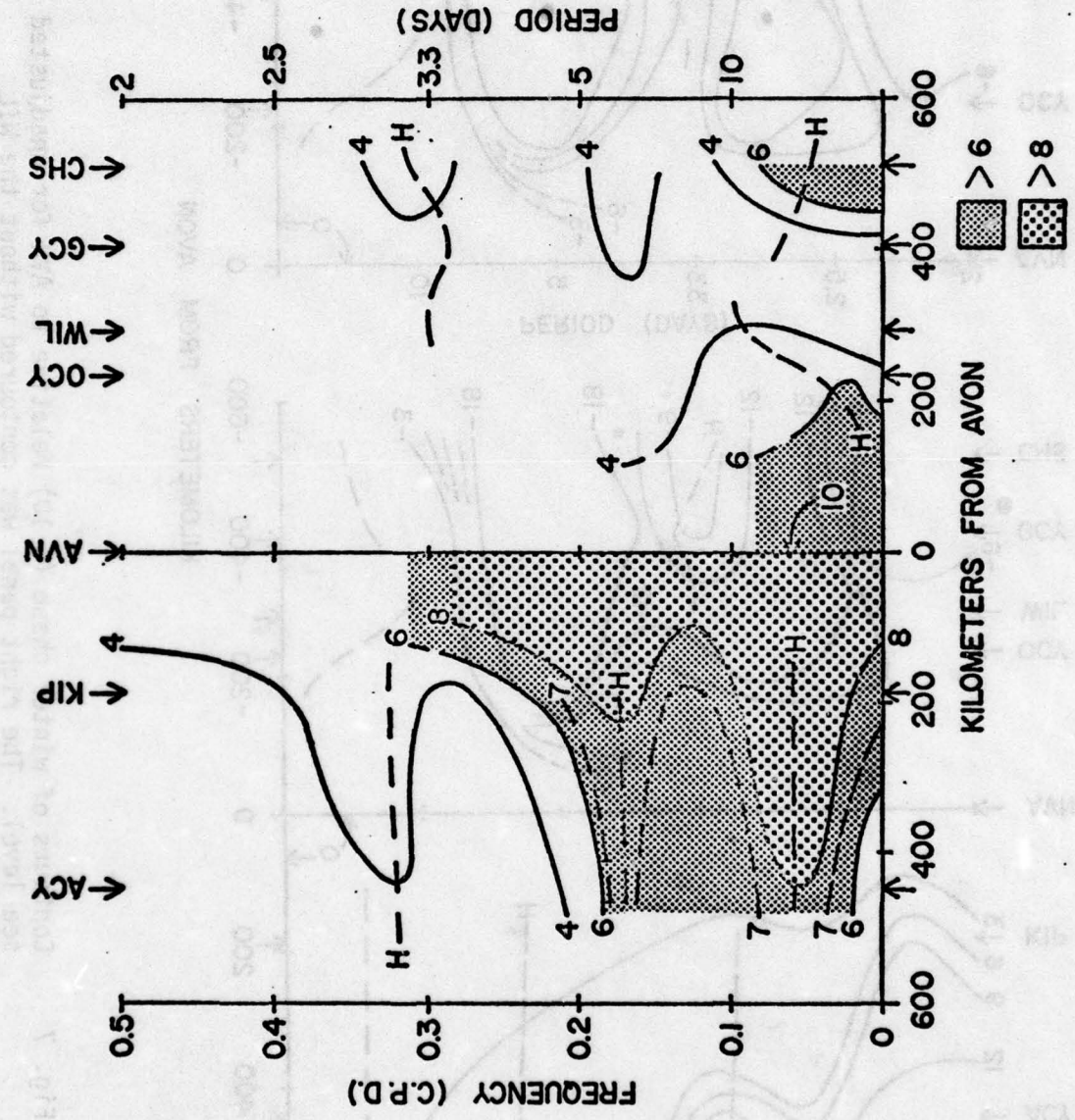

Fig. 6 Contours of winter coherence (× 10) relative to AVN for unadjusted sea level (*cf.* Fig. 4).

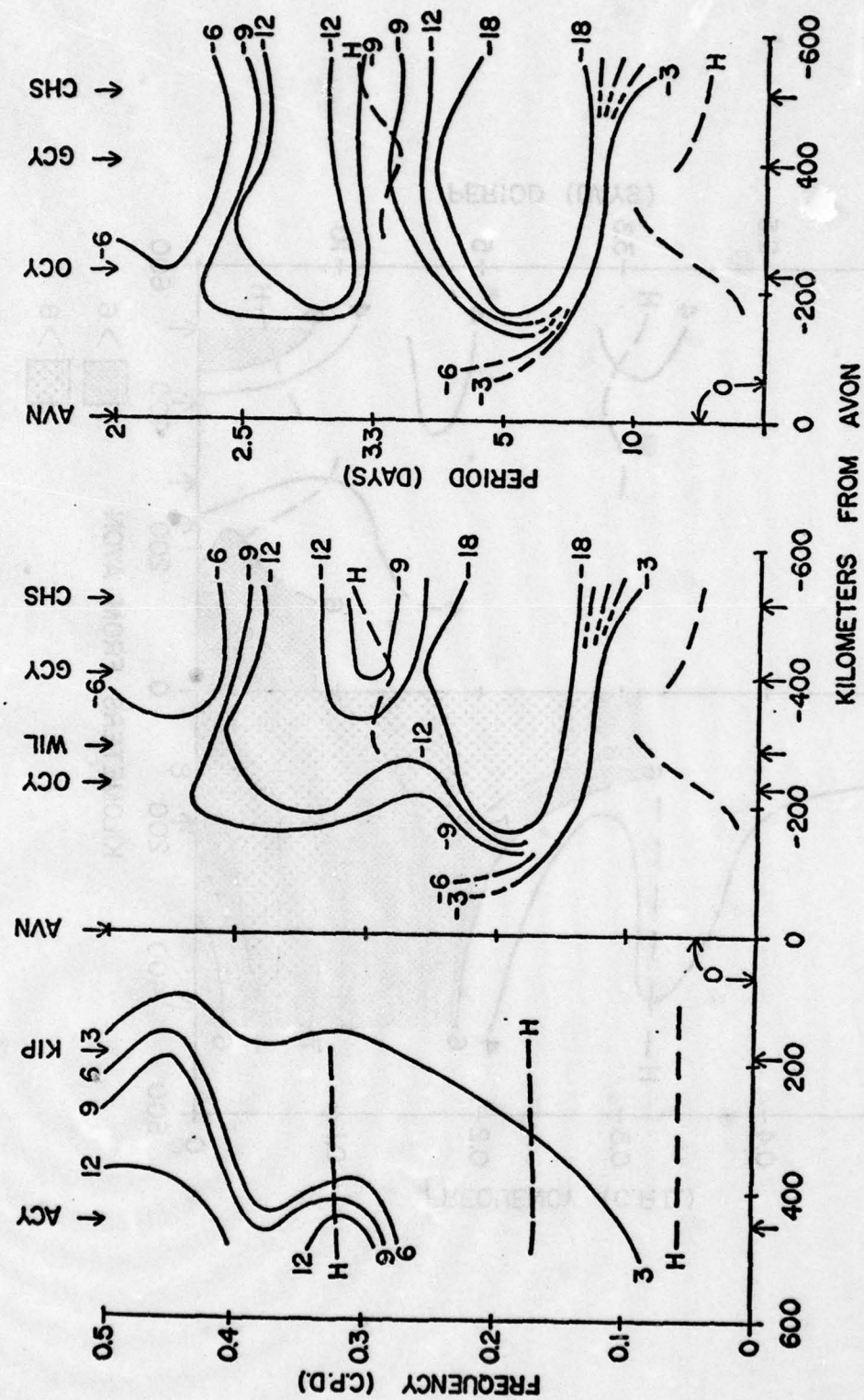

Fig. 7 Contours of winter phase (÷ 10) relative to AVN for unadjusted sea level. The right panel was contoured without the WIL phase (*cf.* Fig. 5).

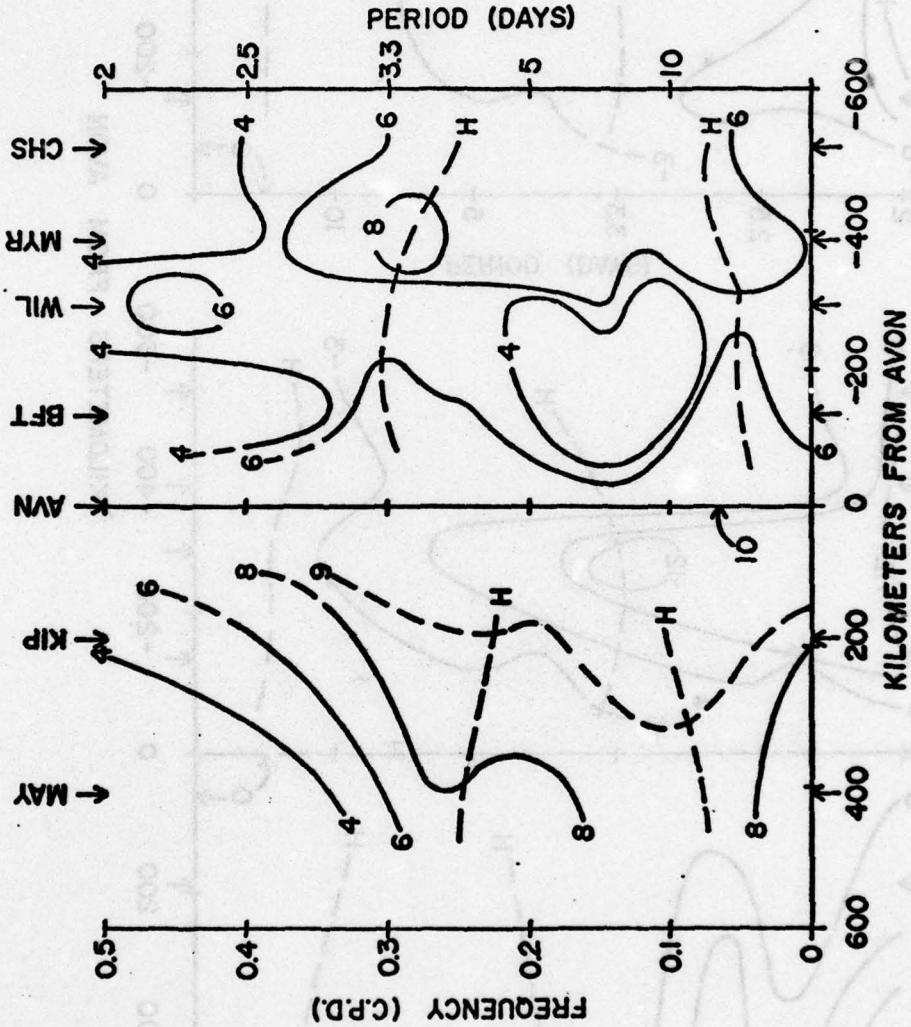

Fig. 8 Contours of summer coherence (× 10) relative to AVN for adjusted sea level (*cf.* Fig. 4).

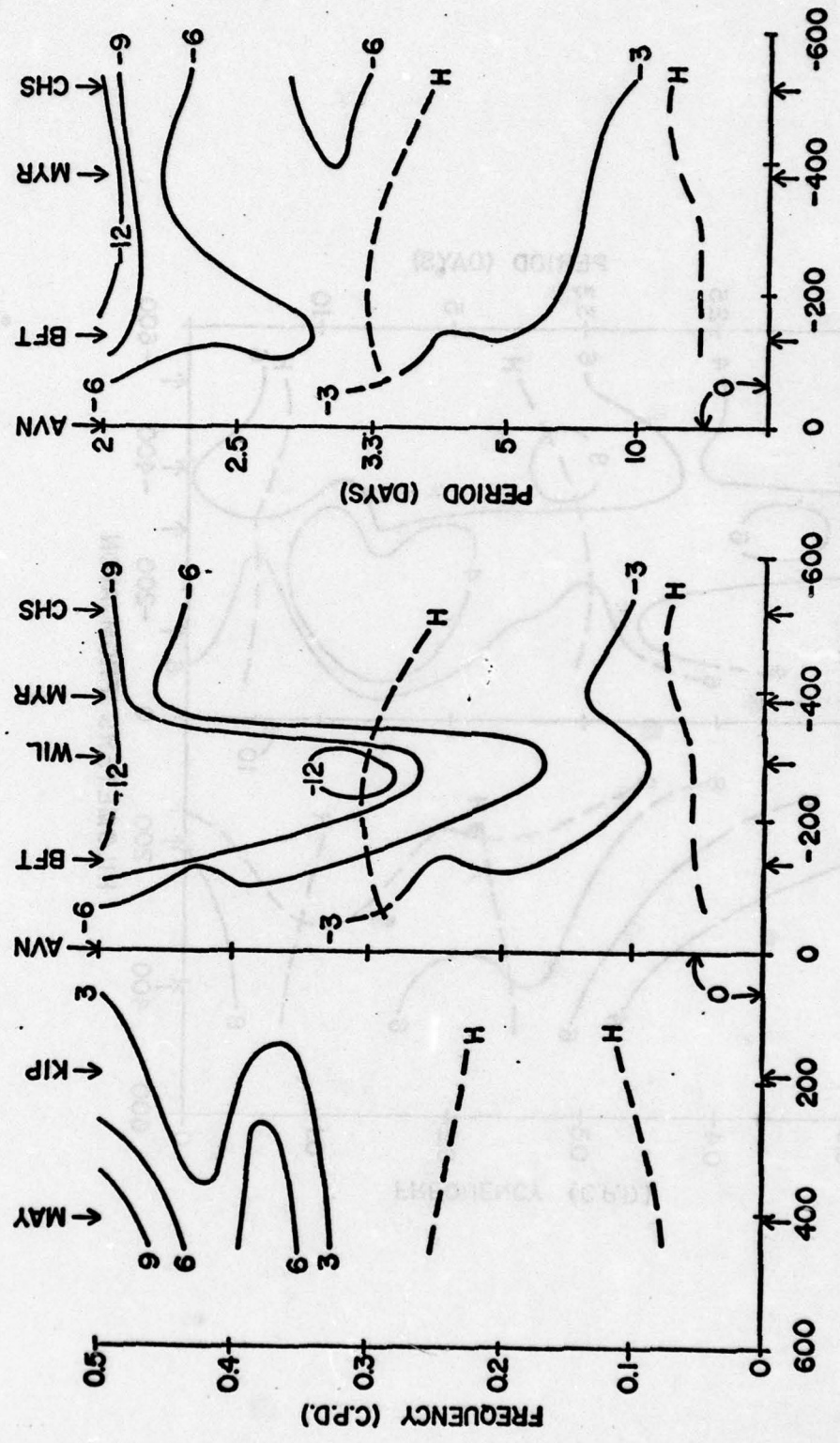

Fig. 9 Contours of summer phase (÷ 10) relative to AVN for adjusted sea level. The right panel was contoured without the WIL phase (*cf.* Fig. 5).

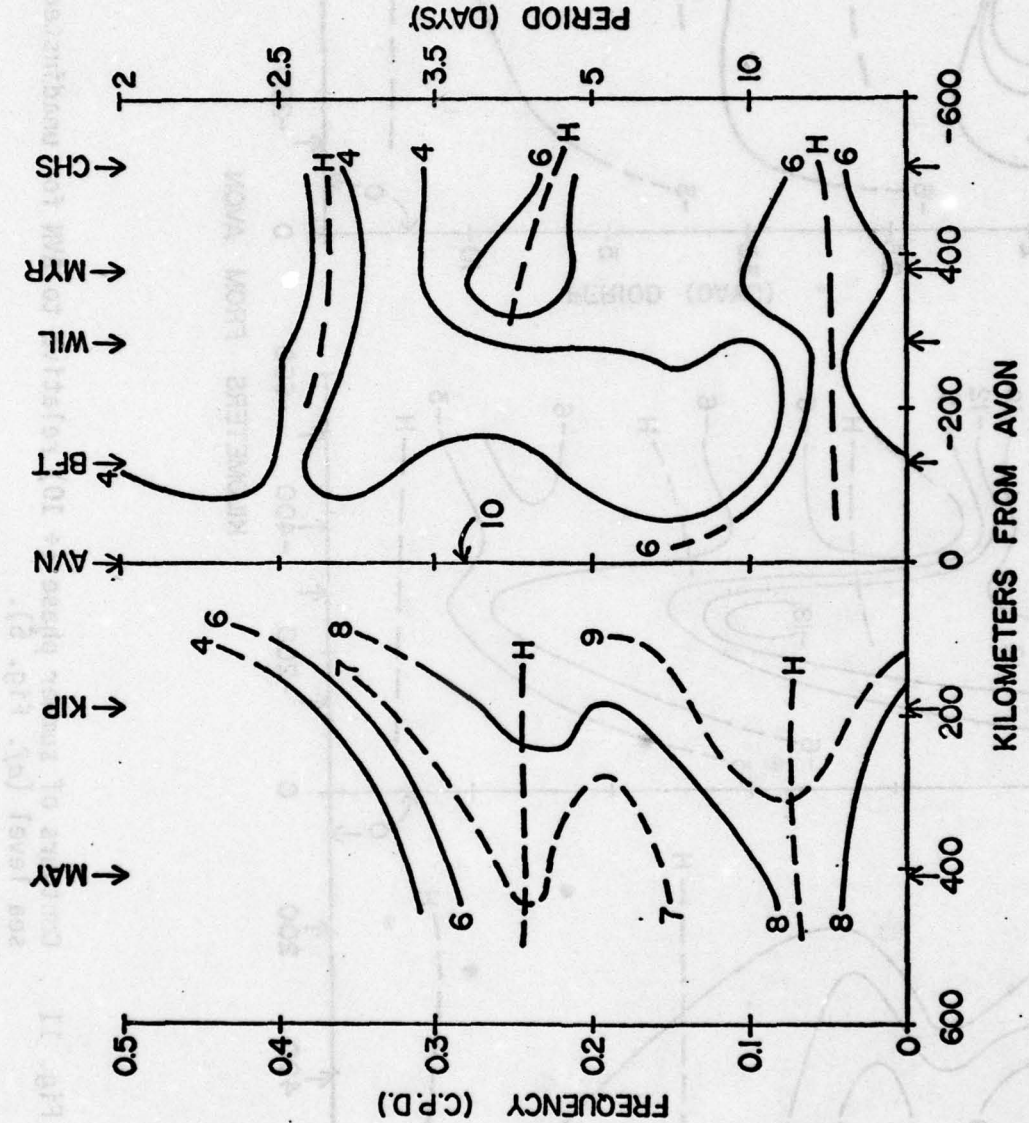

Fig. 10 Contours of summer coherence (× 10) relative to AVN for unadjusted sea level (*cf.* Fig. 4).

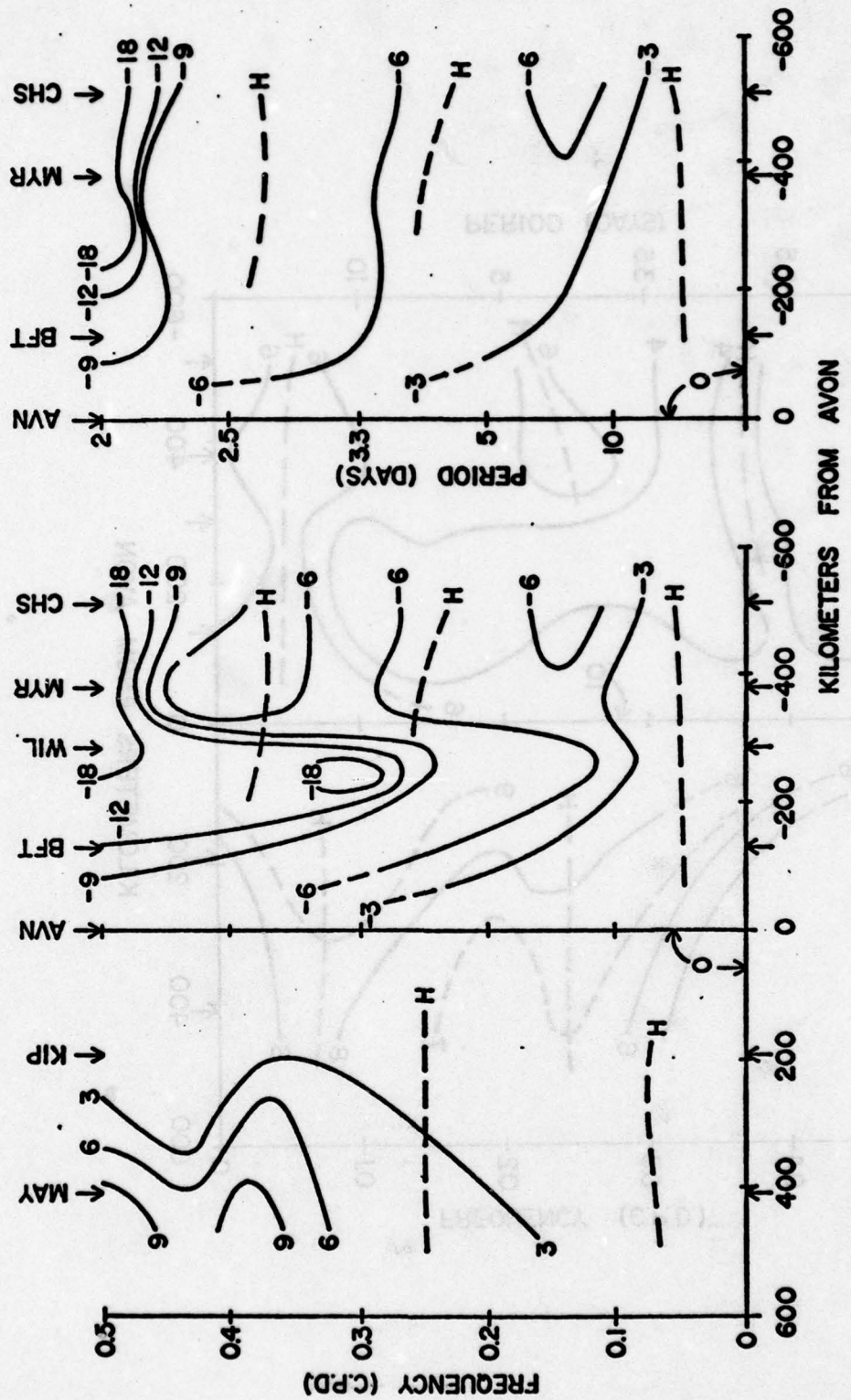

Fig. 11 Contours of summer phase (÷ 10) relative to AVN for unadjusted sea level (*cf.* Fig. 5).

when cold front passages over the array area are infrequent, the adjustment process essentially resulted in a broad-banded coherence increase in both Bights (Figs. 8 and 10).

The winter and summer phase results for both the adjusted (Figs. 5 and 9) and unadjusted (Figs. 7 and 11) sea level are consistent with disturbances traveling southwestward in the high coherence bands over the entire array. The indicated propagation speeds in the 2.5 to 3.5 day band range from a low of several hundred km d^{-1} near AVN to essentially infinite (within the contouring resolution of the figure) in the southern half of the SAB. Indicated speeds in the $\geq$ 10-day band are of the order of several hundred km d^{-1}, but the data resolution is insufficient to justify an interbight or seasonal comparison.

The Wilmington sea level fluctuations have anomalously large phase lags, as evidenced by the tendency toward vertical contours near WIL in the center panels of the phase figures (Figs. 5 and 9). The anomaly is 45-60 degrees, or about 3/8 to 1/2 day in the 2.5 to 3.5 day band, and may be due to a river delay (the gage is located about 30 km upstream from the Cape Fear river mouth). However, lagging phases in the southwestward direction are confirmed without using the WIL data in the contours (right-hand phase panels in Figs. 5, 7, 9, and 11).

The above analysis suggests that the MAB and SAB are selectively coupled in the 2.5 to 3.5 and $\geq$ 10-day period bands. However, the 2.5 to 3.5 day band has a longer coherence scale in the SAB than in the MAB. It is also apparent from the coherence figures (a clear example being Fig. 4) that the coherences relative to AVN are higher and better organized (smoother contours) in the MAB than in the SAB. Part of the relative organization in the MAB may simply be a result of fewer stations to contour there. However, AVN

may not be well suited as a vertex station, because it biases the analysis toward the MAB, since the AVN tide gage is located about 15 km north of Cape Hatteras and is partially sheltered from the SAB by Diamond Shoals. A better location for a vertex station would probably be the Diamond Shoals light tower.

Plotting the adjusted sea level coherences between adjacent stations shows that the sea level fluctuations differ substantially between the Bights, especially in the winter (Fig. 12, winter; Fig. 13, summer). Generally the coherences are highest at long periods in the MAB and lowest at long periods in the SAB. The SAB coherences generally show repeatable structure, with resolved peaks occurring in both winter and summer. The CHS record has the highest coherences in both seasons, possibly because the sea level amplitudes at CHS are relatively large (see Appendix A). The MAB coherences show simpler structure, the principal feature north of KIP being a sudden drop in coherence for periods shorter than about three days.

The adjacent-station coherence analysis suggests that a more appropriate SAB "vertex" station is OCY in the winter and BFT in the summer (*cf.* Fig. 1), thus avoiding the MAB bias of the AVN tide gage. The results of this calculation are shown in Fig. 14 (winter) and Fig 15 (summer), in which the SAB coherences are with respect to the SAB vertex station and the MAB coherences with AVN are reproduced from Figs. 4 and 8. The SAB sea level field, when examined independently of the MAB field, appears to be organized in three bands, the periods of which vary considerably with longshelf position and with season. The longest SAB coherence scales (of order 500 km) occur for periods of about 2.5 and 3.0 days in the winter and summer, respectively. In contrast, the highest MAB coherences occur for very long periods ($\simeq$ several weeks) motions, especially in the winter.

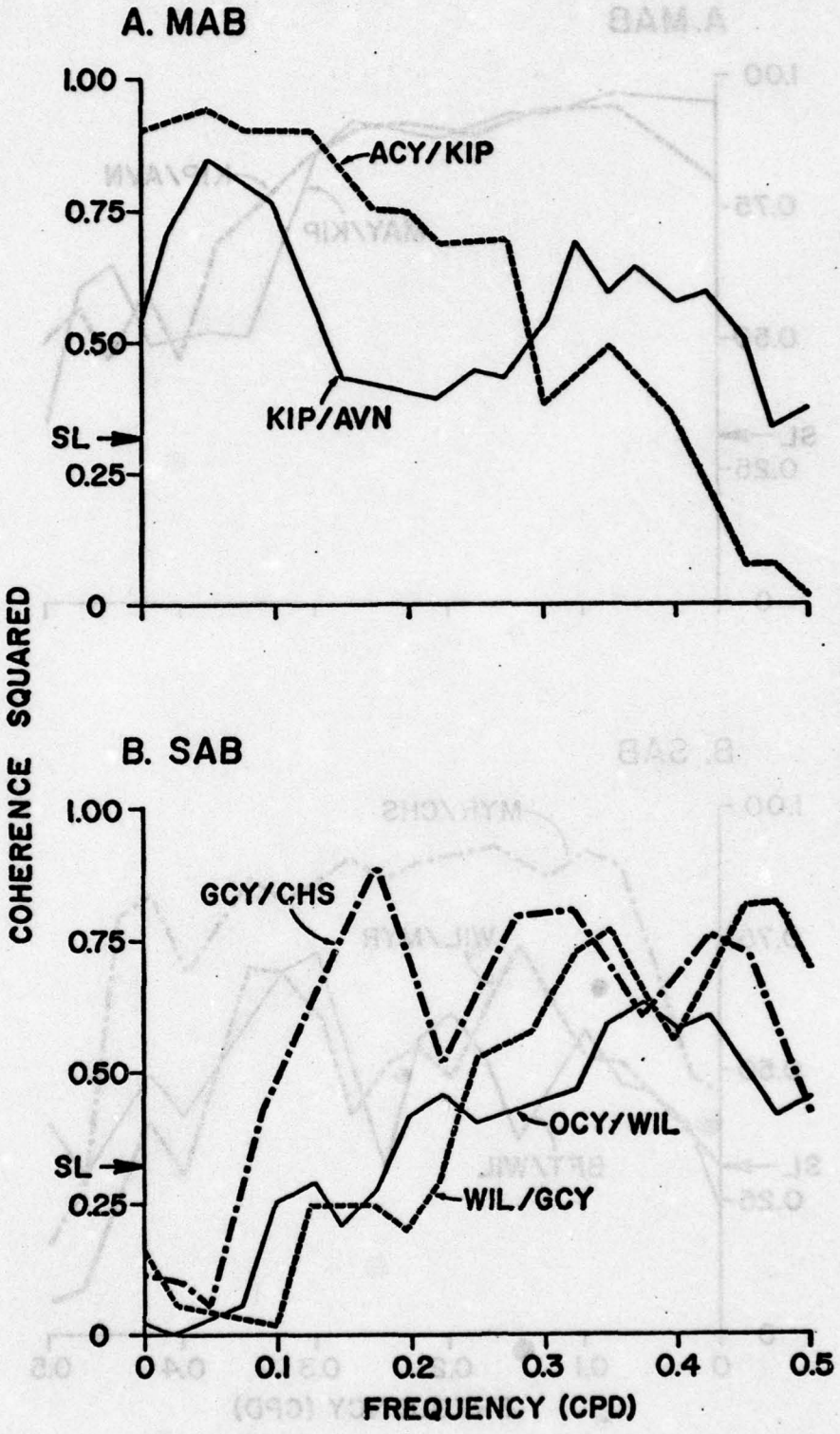

Fig. 12 Interstation winter adjusted sea level coherence by pairs in each Bight. The 95% significance (null hypothesis) level is shown by the horizontal arrow.

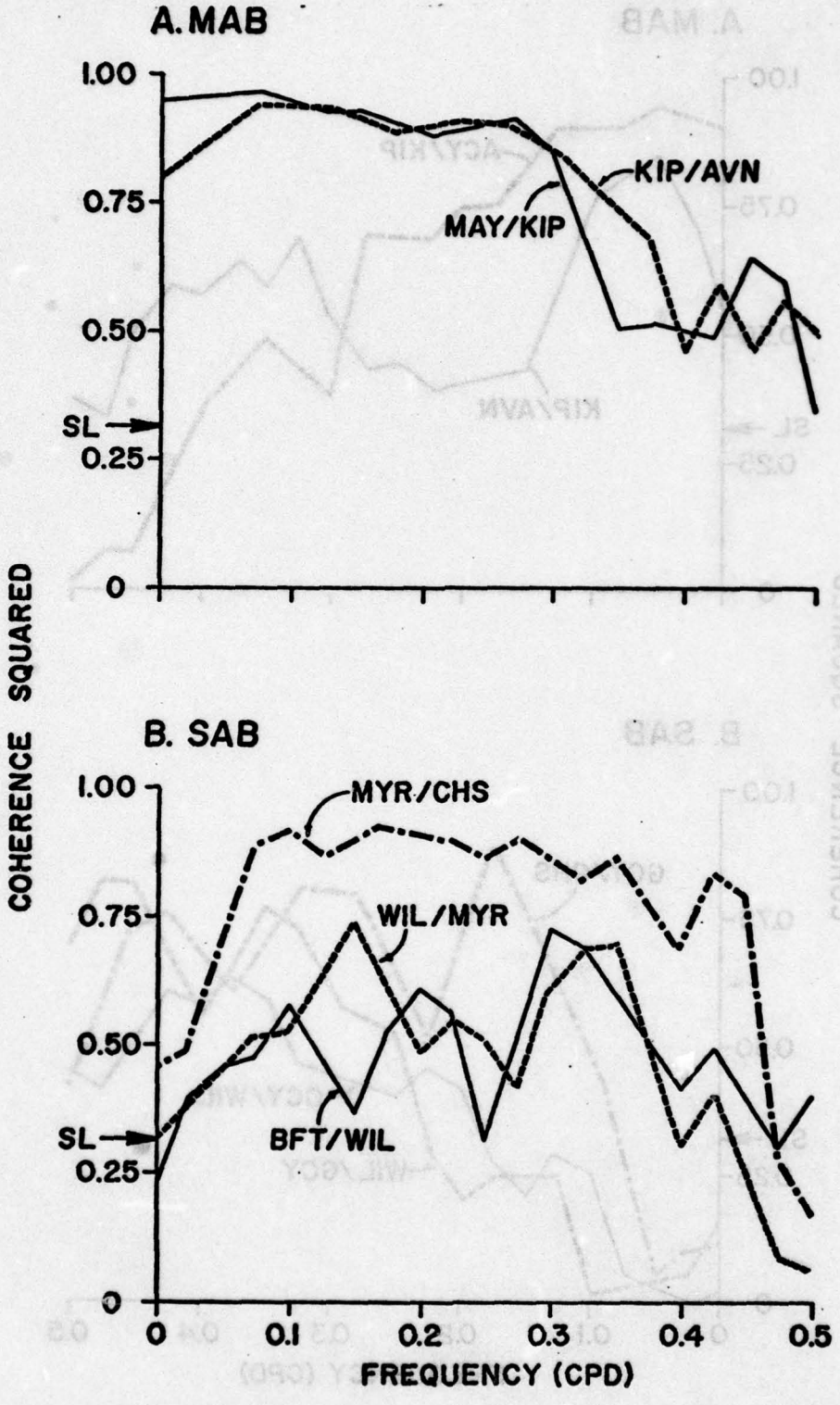

Fig. 13 Interstation summer adjusted sea level coherence by pairs in each Bight. The 95% significance (null hypothesis) level is shown by the horizontal arrow.

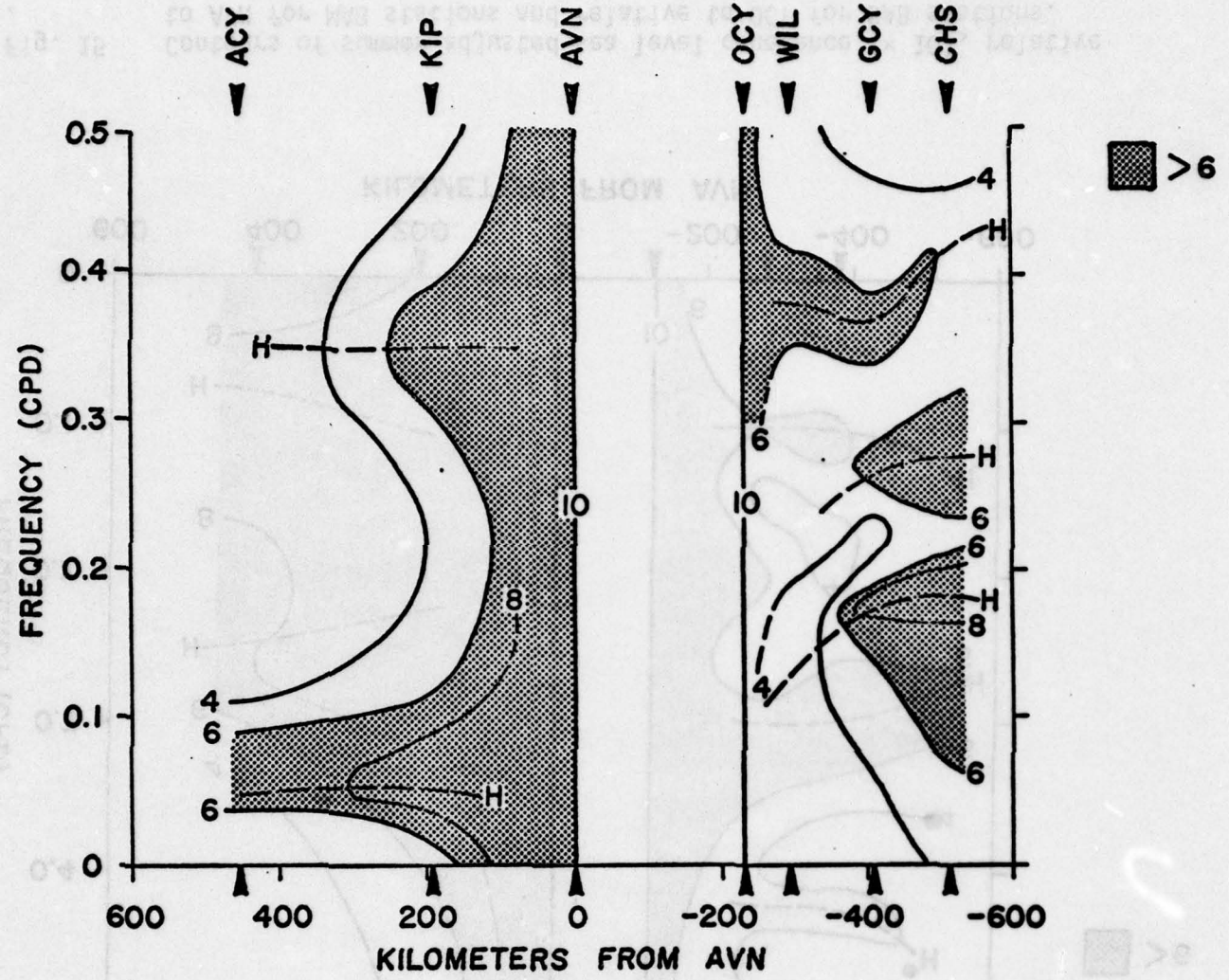

Fig. 14 Contours of winter adjusted sea level coherence (× 10), relative to AVN for MAB stations and relative to OCY for SAB stations. Dashed lines in Figs. 14 and 16 to 20 trace coherence ridges.

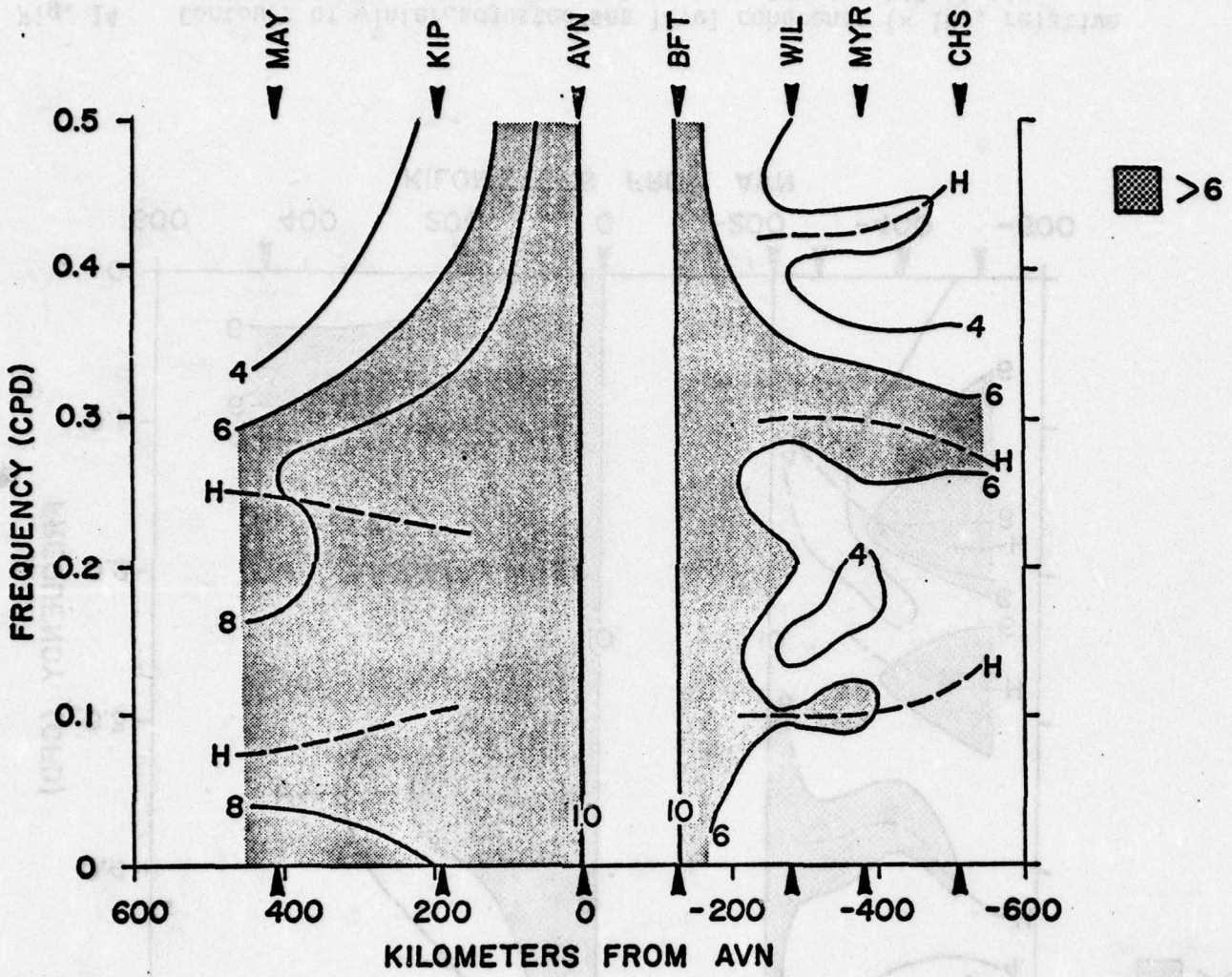

Fig. 15 Contours of summer adjusted sea level coherence (× 10), relative to AVN for MAB stations and relative to OCY for SAB stations. Dashed lines in Figs. 15 and 21 to 25 trace coherence ridges.

The SAB sea level array phase relative to the SAB vertex station (not shown) indicated a WIL river lag of 45-60 degrees in the coherent bands with periods shorter than about one week, as before. The other SAB stations were not significantly out of phase with the SAB vertex station (for a coherence of 0.6, the 95% confidence interval on phase is about ± 20 degrees), although in most cases small (of order 10 degrees) southwestward lags were indicated in both seasons. Reexamining Figs. 5 and 9, one sees that most of the SAB phase lag relative to AVN occurs between AVN and the SAB vertex station, and that the remaining SAB stations (WIL excepted because of the river lag) are nearly in-phase in the coherent bands.

3.1.1 Discussion. The low frequency sea level fluctuations in both Bights are organized in several distinct period bands, with longshelf coherence scales of at least 500 km in the SAB and 400 km in the MAB. However, there are seasonally dependent interbight differences between the periods of the coherent bands. The clearest picture emerges when each bight is considered separately, suggesting important differences in the processes affecting the SAB and MAB coastal sea level and therefore (by inference) affecting the water motions over the continental margin. Three candidate explanations for the differences between the SAB and MAB are: a) differences in meteorological forcing characteristics, b) differences in the continental margin topography, and c) the presence of the Gulf Stream in the SAB. The first possibility is considered in Section 3.2 and the latter two are addressed in Section 4.0.

The coherence structure noted here is consistent with that found in several previous sea level investigations in the MAB-SAB area. In a study of BFT and WIL data, Brooks (1978) found three distinct peaks in the low frequency coherence between the barometrically adjusted sea level records,

which he interpreted as near-zero group speed CSW responses to wind forcing. In an MAB sea level study extending from AVN to Nantucket Shoals (about 400 km northeast of MAY in Fig. 1, Wang (1979) found only very long period coherent motions north of KIP, with evidence of short period motions appearing between AVN and KIP. Thus it seems that subtidal coastal sea level motions with periods shorter than about a week are a feature of the SAB but are evanescent north of AVN.

The most prominent feature of the longshelf sea level phase analysis is the WIL tide gage river lag of 45-60 degrees, equivalent to a time lag of about 3/8 day in the three-day period band. The other station phases generally show small lags in a southwestward direction, but they are only questionably different from zero at the 95% confidence level. Thus the evidence for longshelf propagation of disturbances is murky at best and is not easily explained in terms of a single propagating wave. It is now also apparent that the BFT to WIL phase lag reported by Brooks (1978) may be partly accounted for as Cape Fear river lag, a possibility raised in that paper, and that in fact the sea level fluctuations at BFT and at the river mouth are nearly in-phase. In an earlier study of BFT and Southport, NC (at the Cape Fear river mouth) tide gage data, Mysak and Hamon (1969) found maximum low frequency lags of about 10 degrees, consistent with the southwestward traveling disturbances, but implying propagation speeds considerably larger than expected from a free CSW model. Their 10 degree lag was barely significant at the 95% level, because a full year's data set was used for the analysis. In view of the consistency of the southwestward but small lags over the present array, the statistical significance test based on only one "realization of the process" (i.e., on only one tide gage) may be unduly conservative. If one adopts this view, it can be argued that the

phase results indicate southwestward traveling disturbances over most of the array in the coherent bands. However, the very small lags (tens of degrees) involved lead to implied wavelengths many times longer than the longshelf coherence scales, whence the concept of a traveling monochromatic wavelike disturbance becomes untenable. A more attractive alternate interpretation may be that locally forced disturbances overwhelm remotely forced disturbances, as suggested by Mysak and Hamon (1969). A related possibility is that wave group properties may be more appropriate than phase properties when trying to explain the coastal sea level fluctuation field.

3.2 Meteorological forcing

In this section, a frequency-domain linear regression technique is used to investigate the combined and individual effects of atmospheric pressure and wind stress on sea level height. Since the pressure and wind stress forcing contributions can be expected to be correlated to some degree, it is useful to consider their collective influence using a multiple input statistical model which corrects individual transfer functions for the coherent contributions of other inputs. Thus, for example, the transfer function between pressure and sea level fluctuations can be corrected in each frequency band to remove the effects of coherent wind stress (Bendat and Piersol, 1968; Groves and Hannan, 1968).

Meteorological (MET) time series of pressure (p), cross shelf wind stress (τ_u) and longshelf wind stress (τ_v) at NOR, HAT, and WIL were used as forcing inputs for five winter and four summer sea level stations spanning both Bights (see Table 1.B for correspondence between meteorological and sea level stations). The results are contoured in ω-y space, and supporting calculations are shown in Appendix C. For each season, the

following quantities are discussed: a) the multiple coherence $\gamma^2_{p,\tau_u,\tau_v,\cdot SL}$ which is a measure of the simultaneous linear dependence of the sea level (SL) fluctuations on all three input variables; b) the pressure and wind stress component partial transfer function moduli $(H_{p\cdot SL;\tau_u,\tau_v})$, $(H_{\tau_u\cdot SL;p,\tau_v})$, $(H_{\tau_v\cdot SL;p,\tau_u})$, where the transfer function between the two dotted subscript variables has been corrected for remaining ones; and c) the coherent fraction of longshelf wind stress compared to total wind stress $[\tau_v/(\tau_u+\tau_v)]$, which is a measure of the importance of wind forced coastal Ekman flux divergence. The interstation coherence ridges identified in Figs. 14 and 15 have been transferred to the figures in this section for comparison.

The WIL transfer functions all had anomalously large moduli, indicative of shallow water or closed basin responses atypical in magnitude from coastal responses. For this reason, the WIL moduli were not used in the contours, although frequencies of relative maximum and minimum values often were identifiable with those at coastal stations. The WIL sea level record, while evidently biased by river lag and shallow basin effects, still contains a useful "signature" of coastal processes.

3.2.1 The winter case. The multiple coherence (Fig. 16) indicates significant* coupling between MET and SL fluctuations over a broad area of ω-y space in both Bights. The area includes all the coherent interstation period bands identified earlier (the dashed lines) except the short period MAB band, for which the coherence falls well below the significance level.

---

* The 95% significance level for $\gamma^2_{p,\tau_u,\tau_v\cdot SL}$ is 0.45.

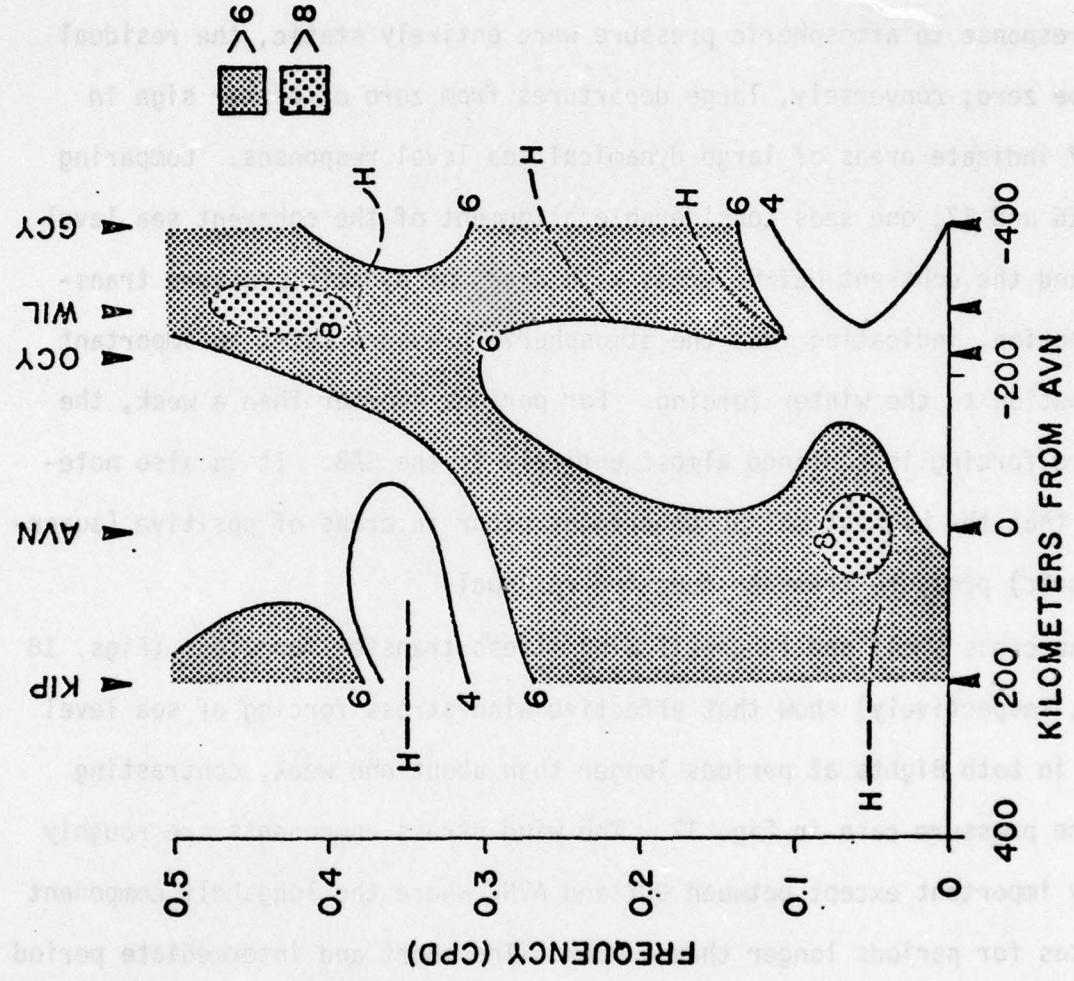

Fig. 16 Contours of winter multiple coherence (× 10) between sea level and the combined effects of atmospheric pressure, cross shelf wind stress, and longshelf wind stress.

This supports the notion raised earlier that short period motions can be forced in the SAB but are evanescent in the MAB.

The non-static residual partial pressure transfer function is shown in Fig. 17. The residual was obtained by subtracting 1.01 cm/mb (the static "barometer factor") from each transfer function estimate. Thus if the sea level response to atmospheric pressure were entirely static, the residual would be zero; conversely, large departures from zero of either sign in Fig. 17 indicate areas of large dynamical sea level responses. Comparing Figs. 16 and 17, one sees considerable alignment of the coherent sea level bands and the coherent MET·SL areas with areas of dynamic pressure transfer function, indicating that the atmospheric pressure makes an important contribution to the winter forcing. For periods shorter than a week, the pressure forcing is confined almost entirely to the SAB. It is also noteworthy that the highest MET·SL coherences occur in areas of positive (superbarometric) pressure transfer function residual.

The cross shelf and longshelf wind stress transfer functions (Figs. 18 and 19, respectively) show that effective wind stress forcing of sea level occurs in both Bights at periods longer than about one week, contrasting with the pressure case in Fig. 17. The wind stress components are roughly equally important except between OCY and AVN, where the longshelf component dominates for periods longer than a week. The short and intermediate period coherent sea level bands (dashed lines) do not seem to be identifiable with features of the wind stress forcing field. For long periods, however, both wind stress components contribute to the MET·SL coherence in Fig. 16; the large τ_v transfer function values are clearly associated with the sea level coherence maximum near AVN. It also can be seen by comparing Fig. 16 and the coherent longshelf wind stress fraction in Fig. 20 that the areas

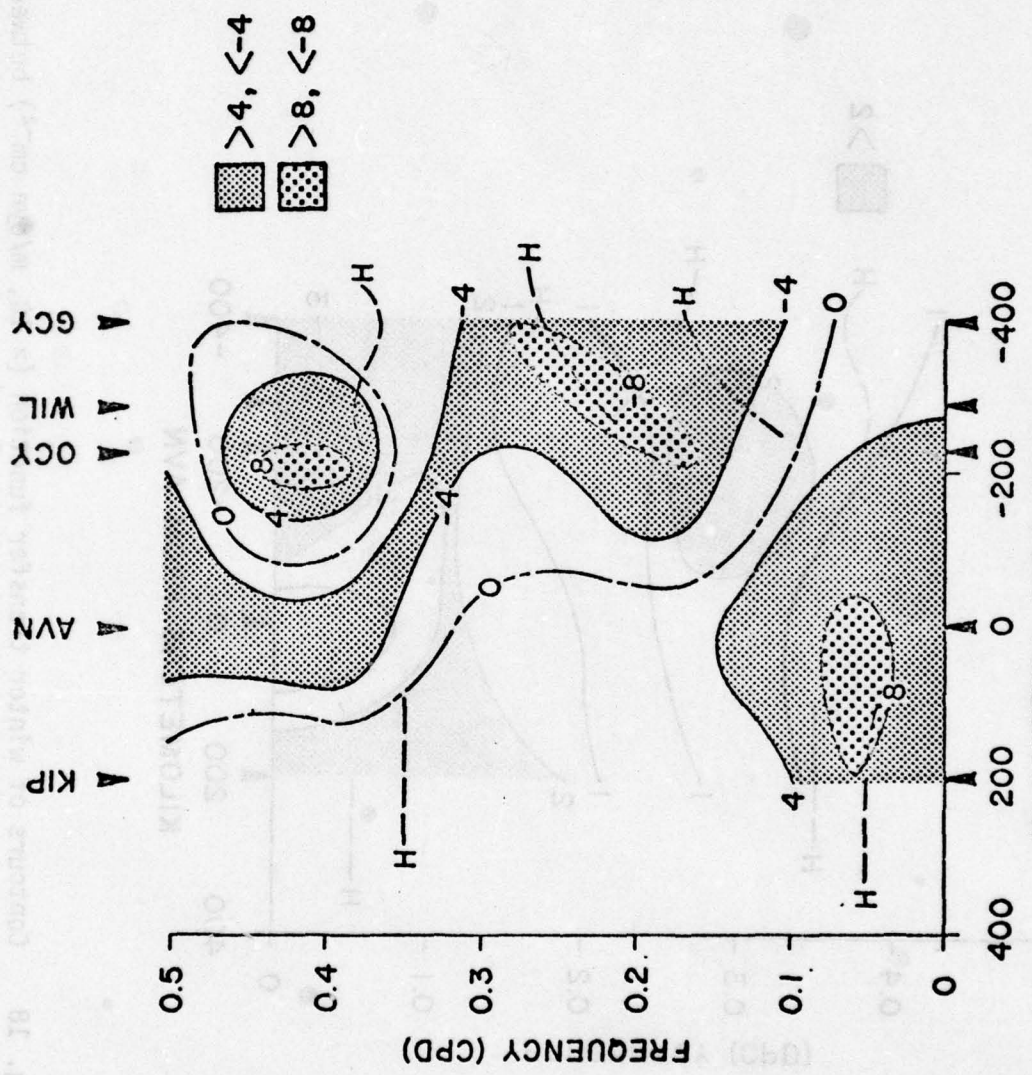

Fig. 17 Contours of winter dynamic transfer function (× 10, cm/mb) between atmospheric pressure and sea level. Departures from zero indicate non-static sea level responses.

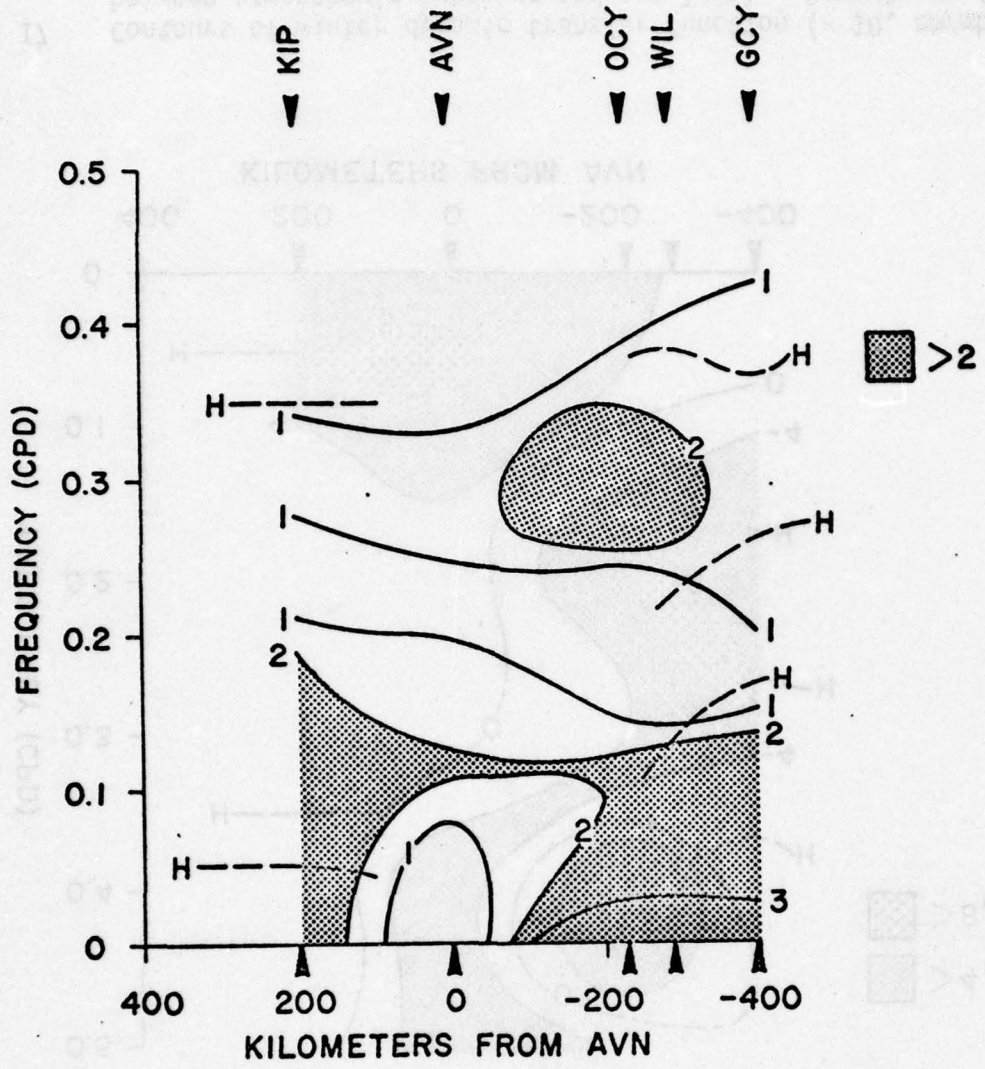

Fig. 18 Contours of winter transfer function (× 10, m/dyn cm^{-2}) between cross shelf wind stress and sea level.

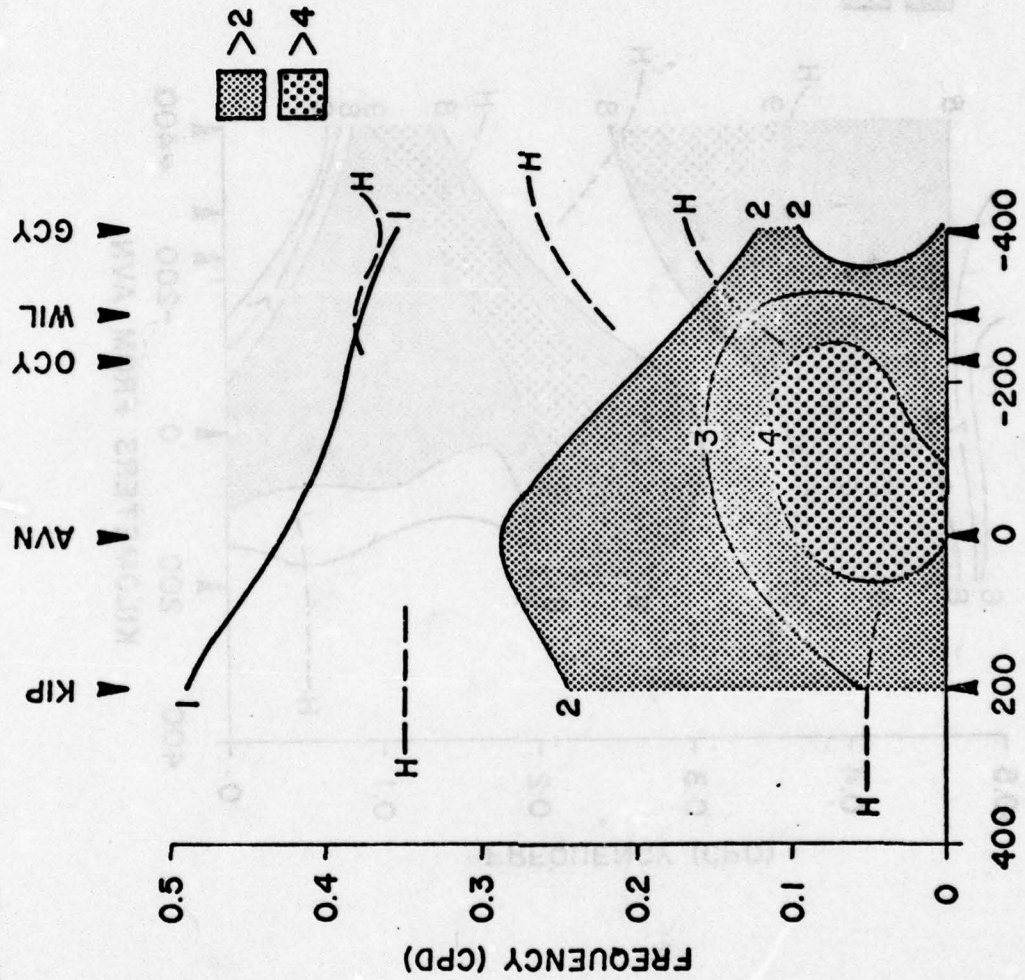

Fig. 19 Contours of winter transfer function (× 10, m/dyn cm^{-2}) between longshelf wind stress and sea level.

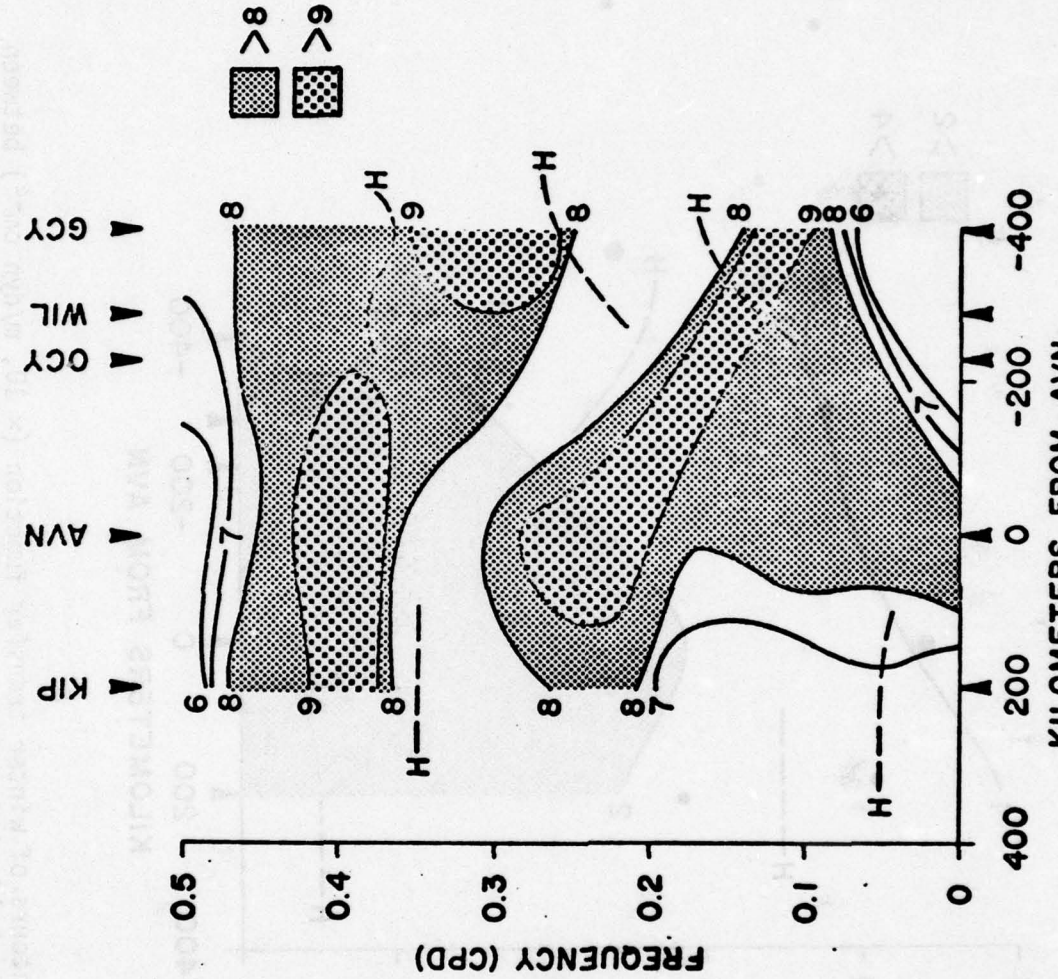

Fig. 20 Contours of winter $\gamma^2_{\tau_v \cdot SL} / \left(\gamma^2_{\tau_u \cdot SL} + \gamma^2_{\tau_v \cdot SL} \right)$ (× 10), the longshelf fraction of the wind stress coherent with sea level.

of highest MET·SL coherence are not aligned with areas of highest values of the fraction; i.e., the cross shelf wind stress plays an important role in the forcing process. A similar effect was noted in the Florida Straits by Brooks and Mooers (1977a). Thus the coastal Ekman divergence shelf wave forcing mechanism described by Gill and Schumann (1974) may not be entirely adequate here, although it is clear from Fig. 20 that, overall, τ_v is more effectively coupled to sea level fluctuations than is τ_u (the area-weighted fraction in Fig. 20 is about 0.8).

3.2.2 The summer case. The summer MET·SL coherence (Fig. 21) has more and larger areas of high coherence (> 0.8) than the winter case. The short and intermediate period sea level bands (dashed lines), while not as clearly associated with high MET·SL coherence as they were in the winter, fall within the 5.5 contour (shown as a special case in Fig. 21), and the long period band in both Bights falls inside or near the 0.8 contour.

Comparing Fig. 21 with the residual pressure transfer function in Fig. 22, one sees correspondence between high MET SL coherence and dynamic pressure forcing in the SAB for periods shorter than a week, but little correspondence elsewhere in the ω-y space. Overall, the summer sea level pressure response was more nearly static than in the winter, but with the largest residuals occurring for short periods in the SAB as in the winter. The MAB coherent sea level fluctuations appear to be unrelated to dynamic pressure fluctuations. Both wind stress components were relatively more effective in the SAB than in than in the MAB for periods longer than about one week (Figs. 23 and 24), but the maximum magnitudes of both components were about 30% less than in the winter. As in the winter, the high MET·SL coherence areas are anti-correlated with areas of high coherent τ_v fraction (Fig. 25), again indicating the importance of the cross shelf wind

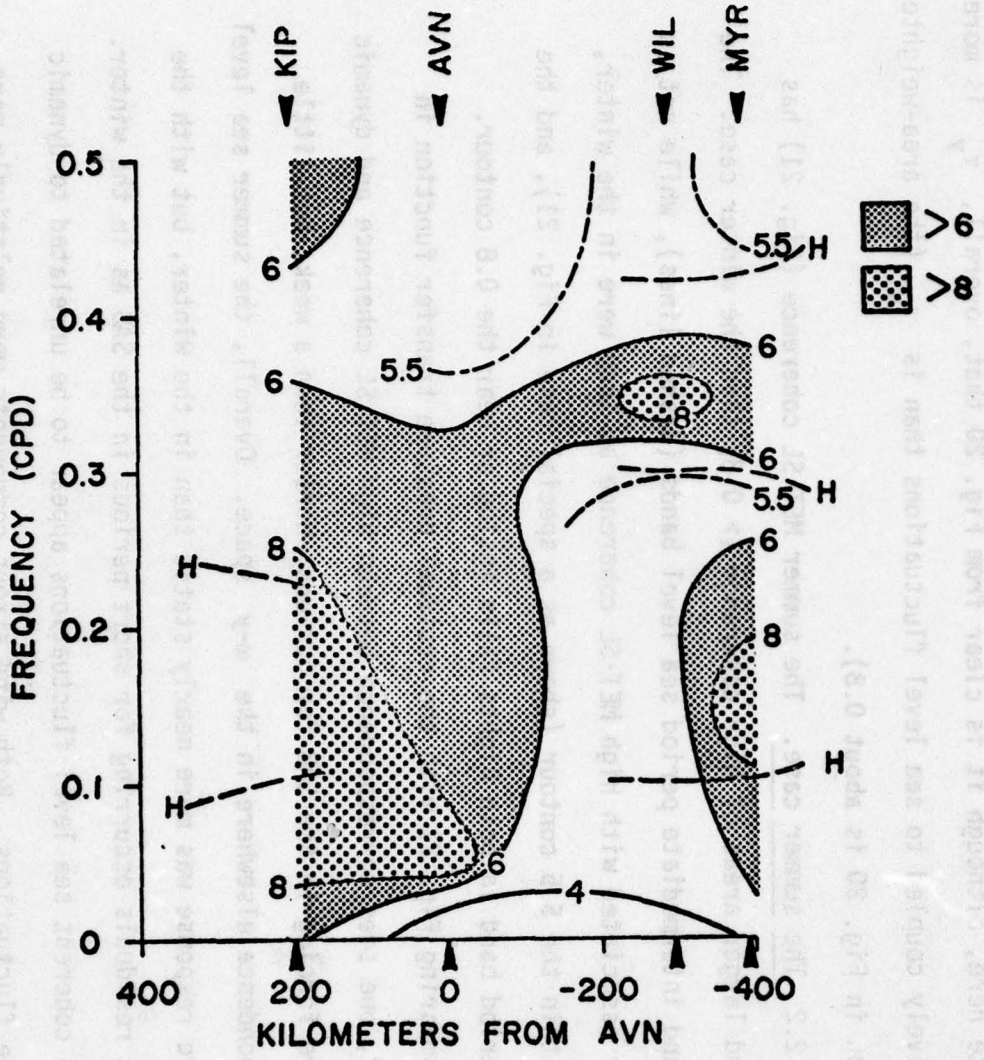

Fig. 21 Contours of summer multiple coherence (× 10) between sea level and the combined effects of atmospheric pressure, cross shelf wind stress, and long shelf wind stress.

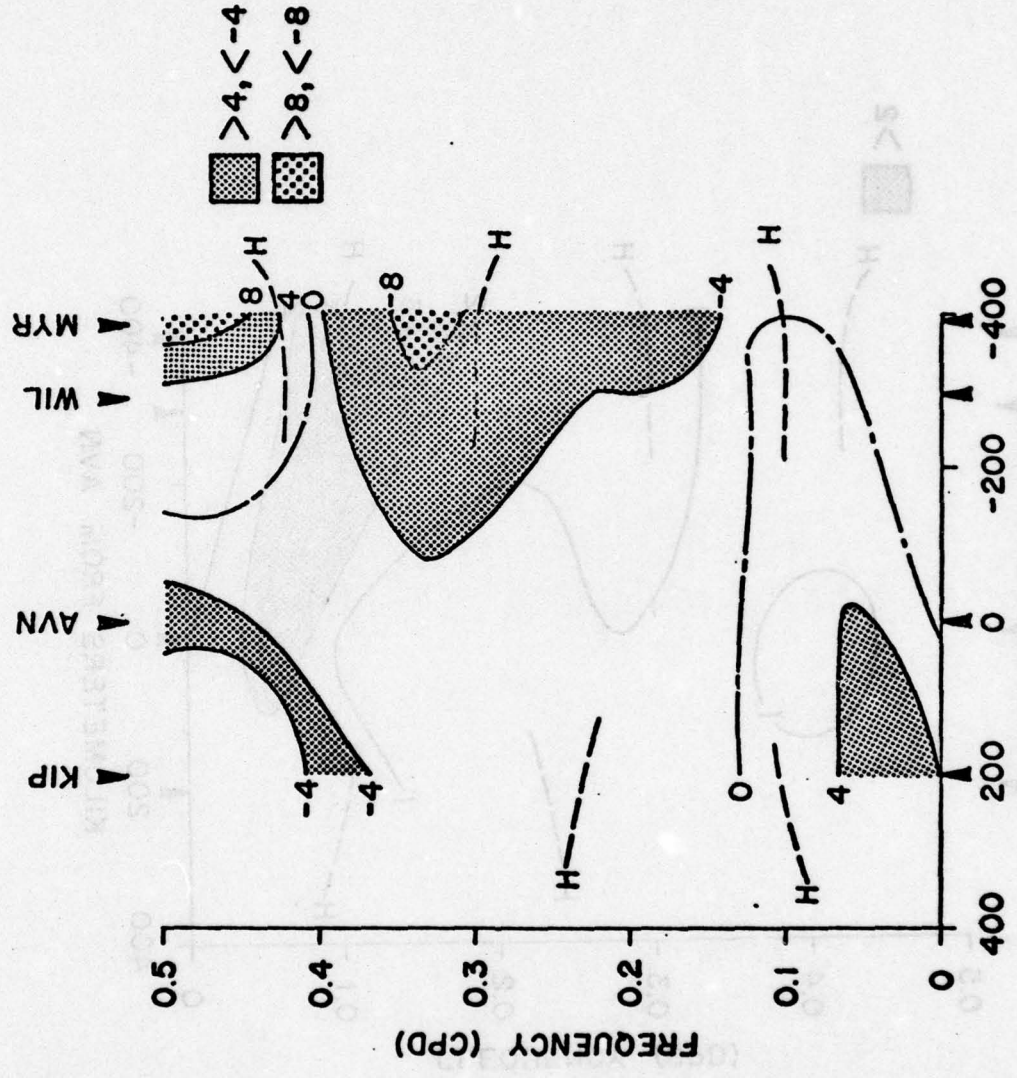

Fig. 22 Contours of summer dynamic transfer function (× 10, cm/mb) Between atmospheric pressure and sea level. Departures from zero indicate non-static sea level responses.

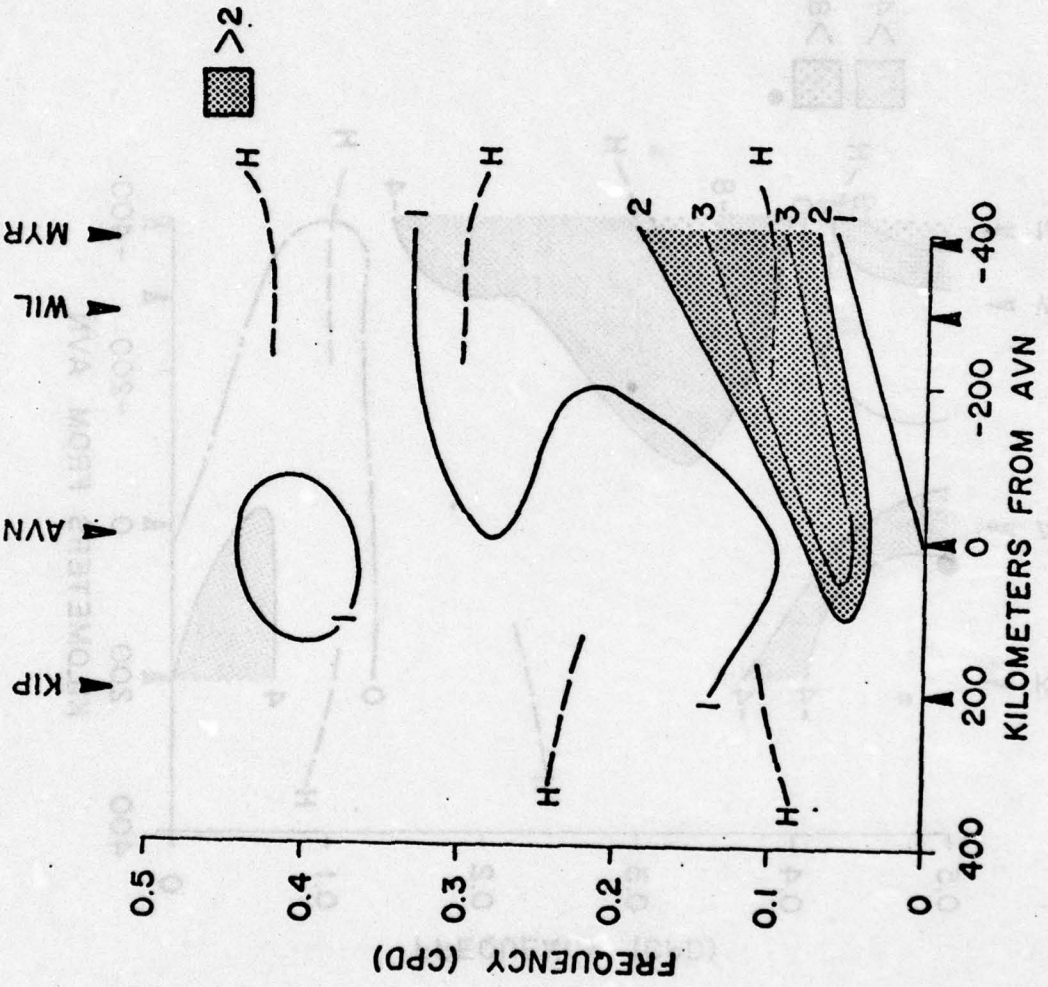

Fig. 23 Contours of summer transfer function (× 10, m/dyn cm^{-2}) between cross shelf wind stress and sea level.

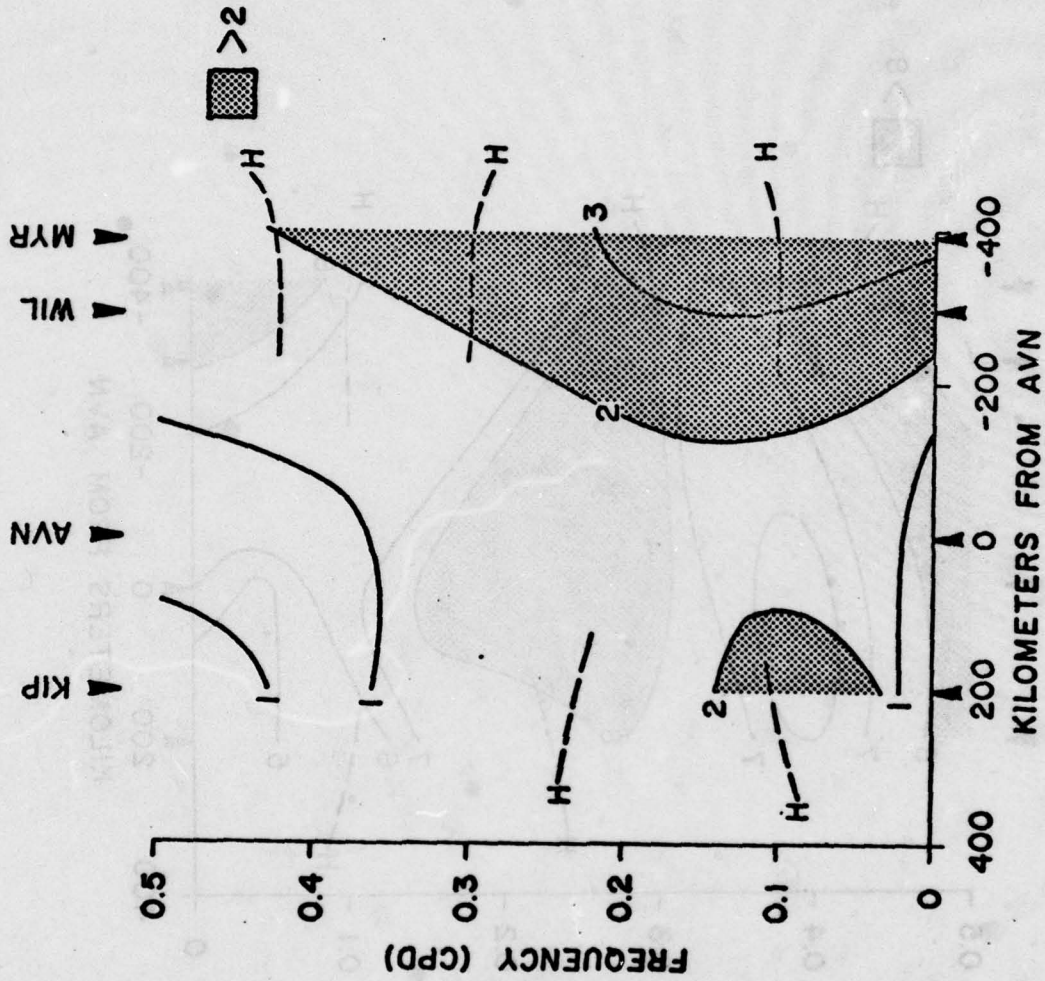

Fig. 24. Contours of summer transfer function (× 10, m/dyn cm^{-2}) between longshelf wind stress and sea level.

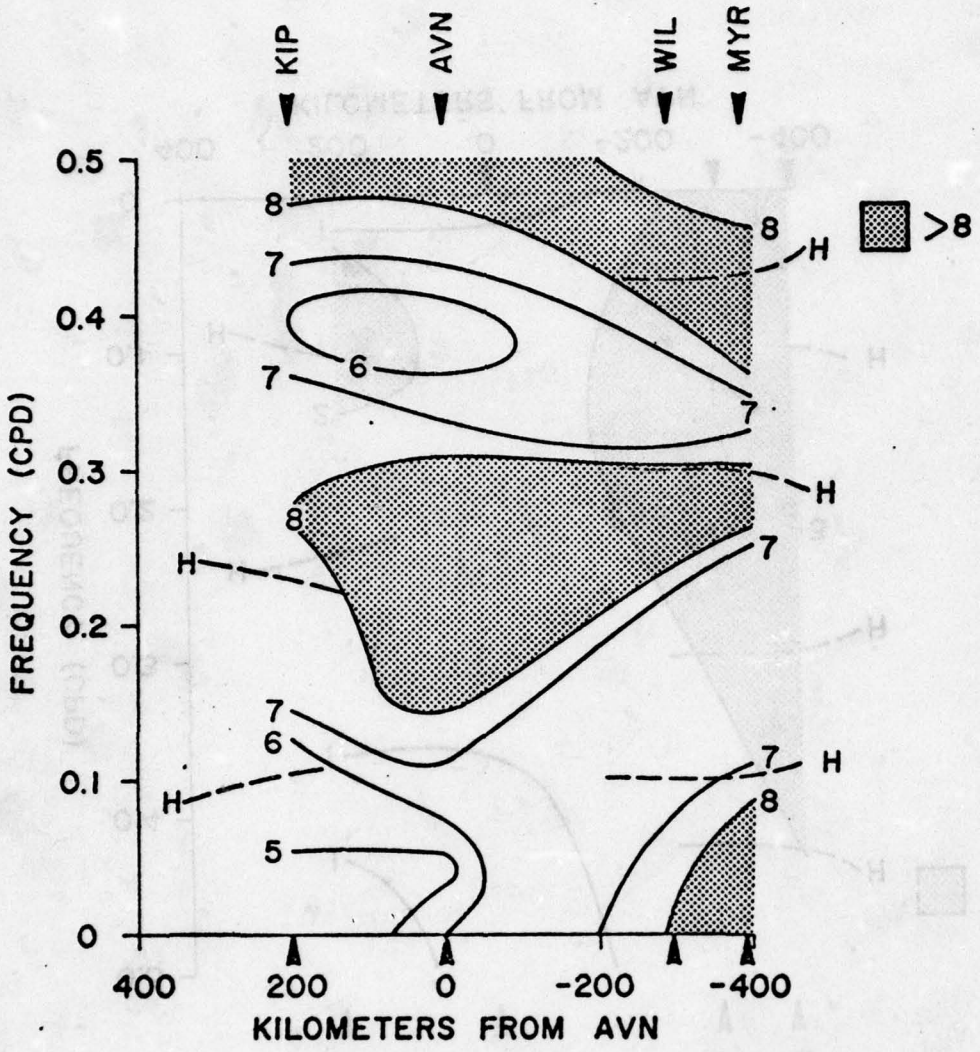

Fig. 25 Contours of summer $\gamma^2 \tau_v \cdot SL \Big/ \left[\gamma^2 \tau_u \cdot SL + \gamma^2 \tau_v \cdot SL\right]$ (× 10), the longshelf fraction of the wind stress coherent with sea level.

stress component.

3.2.3 Discussion. There are several seasonally persistent characteristics of the meteorologically forced sea level field common to both Bights. Strong coupling of the wind stress and sea level fluctuations occurs only for periods longer than about one week, and both the longshelf and the cross shelf wind stress components are important forcing contributors in the coherent sea level bands. The dynamical pressure forcing contribution is important for short period motions, especially noticeable in the SAB, and more prominently so in the winter than in the summer. On the other hand, the effective wind stress forcing in the summer is largely confined to the SAB, whereas in the winter it occurs in both Bights. This result probably reflects seasonal differences in weather patterns, with cold front winds influencing both Bights in the winter and the more gentle and steady southeast trade winds primarily affecting the SAB in the summer.

For several-day periods, the coastal sea level coherence pattern seems to be associated with dynamical sea level responses to atmospheric pressure fluctuations, but only in the SAB. Strong dynamical sea level responses to atmospheric pressure were also found off Australia by Hamon (1966), off North Carolina by Mysak and Hamon (1969) and off Florida by Brooks and Mooers (1977a), suggesting the general importance of pressure forcing. Adams and Buchwald (1968) have argued that the correlation between sea level and pressure observed by Mysak and Hamon is an artifactual consequence of correlation between the pressure and the longshelf wind stress, with the latter providing the "real" vorticity forcing via coastal Ekman flux divergences. The pressure transfer functions presented herein, however, have been corrected for the linear correlation with wind stress, and the non-static responses are still clearly evident. It is furthermore evident that the

pressure and wind stress forcing contributions generally occupy different portions of the frequency domain; i.e., the pressure effect is relatively more important at short periods, and the wind stress effect is more important at long periods.

The argument that pressure fluctuations are ineffective vorticity generators over a shelf is based on the fact that the free surface divergence term in the barotropic long wave equations is scaled by $(L/R_D)^2$, where L is the cross shelf length scale and R_D is the Rossby deformation radius. For typical shelves, this scale factor is $O(5 \times 10^{-2})$; thus, in the absence of resonances, the above argument follows. Adams and Buchwald point out that a resonant response with the pressure disturbance traveling in phase-locked coincidence with the sea level disturbance is not likely to be important, because of the long (1000's of km) coastal distances over which the process must act to be effective. How then are the dynamic sea level responses to pressure fluctuations explained?

The phase-locked resonance mechanism was suggested by Robinson (1964). An alternate type of forcing that may be important for both pressure and wind stress, suggested by Buchwald and Adams (1968), may occur at frequencies for which the group velocity of CSW's is small or zero. Since a CSW packet is stationary or nearly so in the vicinity of zero group velocity frequencies (turning points of the CSW dispersion curves), the energy supplied locally to such a packet of waves must remain in its neighborhood of introduction, allowing the local packet amplitude to grow as long as the forcing energy source is available. Phase locking of the forcing and shelf water disturbances over large coastal distances is not required for this "group resonance" to occur. The group resonance mechanism also provides a potential explanation for the selectivity (i.e., bandedness) of the sea

level coherence structure. Several studies have indicated that peaks in the longshelf coherence between sea level stations can be associated with the zero group velocity frequencies of CSW modes (*cf.* Cutchin and Smith, 1973; Brooks, 1978).

The wind stress and its curl are forcing terms that may be of comparable magnitude for typical event-like cold front wind fields (Brooks, 1978). Historically, the curl term has been neglected compared to the stress term, based on the assumption that the horizontal scale of wind variations is much larger than the shelf width (see LeBlond and Mysak for details of scaling the barotropic vorticity equation). However, it has been pointed out by Brooks (1978) and others that the horizontal scale of wind stress variation near a cold front can be much smaller than the distance between adjacent fronts; a typical curl scale is 100 km, the same as the shelf width scale. Furthermore, the resultant pulse-like time history of a sequence of cold front wind stress curl events at a fixed location produces a forcing spectrum harmonically rich in frequency and wavenumber space. Thus, while the fundamental atmospheric forcing time and space scales may be a week and a megameter, significant forcing energy can also be expected to occur at scales shorter than these,especially for the wind stress curl. A field test of the importance of this idea awaits higher resolution wind stress measurements permitting a reasonable calculation of the local (shelf scale) curl.

The longshelf wind stress can induce cross shelf water motions and coastal sea level set-down or set-up in response to surface Ekman flux divergences (coastal or otherwise generated), which "releases" vorticity by moving fluid columns over variable depth. However, for a straight coastline and parallel isobaths, a uniform cross shelf wind stress can produce only

a uniform longshelf current geostrophically balanced with a coastal sea level set down or set up. This situation would not produce relative vorticity anomalies, assuming the longshelf scales are small enough that variations in f (the "beta-effect") can be neglected, and therefore waves would not be excited. If, however, longshelf coastal and/or isobath variation is significant, or if the cross shelf wind stress is not uniform, then longshelf mass convergences and divergences can occur, resulting in cross shelf (vorticity-generating) water motions to satisfy mass conservation locally. Thus it seems that, while the longshelf wind stress mechanism is more direct, forcing by the cross shelf component is likely to be important in regions of convergent or divergent isobaths, or in regions where isobaths and the coastline are non-parallel, such as in the SAB.

The results of this section indicate that atmospheric pressure and both wind stress components are important contributors to the forcing of low frequency coastal sea level motions. Their relative effectiveness varies according to frequency, season, and longshelf location, but it is apparent that none should be neglected *a priori* as insignificant. It is also clear that the three-input forcing model presented does not consider all possibly relevant contributors, the most notable absence being the wind stress curl. The surprising degree of selectivity of the coupling between the atmosphere and sea level fluctuations suggests the importance of some kind of resonant dynamical mechanism.

4. Dispersion of Barotropic Shelf Waves in the Bights

It was pointed out in the introduction that the continental slope and shelf width change by a factor of 2 or 3 between Capes Romain and Hatteras. A comprehensive theory of coastal trapped waves in the SAB would therefore necessarily be three dimensional and would probably require a complex numerical scheme to obtain solutions. The presence of the mean baroclinic Gulf Stream, which crosses bottom contours in the northern end of the SAB, further complicates matters.

The general problem of CSW's propagating in a stratified ocean with a sheared mean current and longshelf variation of geometry has been approached from several simplified starting points. (For a thorough review of historical and recent progress, see Mysak, 1979). With longshelf variation neglected, and in the absence of stratification, continental shelf waves result (Robinson, 1964). When stratification is included, the more general coastal trapped waves result (Wang and Mooers, 1976). If a vertical coastal wall is present, Kelvin waves appear in both cases which can interact with and modify the dispersion properties of the continental shelf or coastal trapped waves (Wang and Mooers, 1976). For the case of small amplitude longshelf topographic and coastline variations, barotropic shelf waves propagate with the local phase speed and adjust their cross shelf modal structure to agree with the local eigenfunction structure (Allen, 1976). During the adjustment process, scattering of energy into other shelf modes can occur. If a sheared mean current flows parallel to isobaths, the shear and advective effects combined can lead to stable shelf waves propagating in either longshelf direction, or to downstream unstable waves (Niiler and Mysak, 1971; Brooks and Mooers, 1977b). Much work remains to be done for cases which include large longshelf topography variations and baroclinic

mean currents, particularly with regard to critical level wave-mean current interactions (*cf.* McKee, 1979).

As a precursor to a three-dimensional formulation, the SAB problem is addressed in this section with barotropic model in which longshelf variations are assumed to occur over distances much greater than the shelf width. Thus we can expect slow variations in wave propagation speeds and eigenfunctions, as described by Allen (1976). The barotropic model discussed by Buchwald and Adams (1968), modified to include a mean current, will be applied to bottom and mean current profiles representative of each SAB Cape and the MAB, but the y (longshelf) variation is not explicitly included. This method is not entirely satisfactory because scattering effects are ignored and the scale over which the topography changes is too short to justify a WKB approach. Nonetheless, the results suggest how to proceed.

4.1 Formulation

In the presence of a horizontally-sheared basic state current, linear barotropic oscillations of a fluid overlying a sloping bottom are governed by the potential vorticity equation

$$(c_o-\overline{V})\left[\left(\frac{\psi'}{h}\right)' - \frac{\ell^2\psi}{h}\right] + P'\psi = 0 .$$

The mass transport stream function has the wavelike form $\hat{\psi} = \psi(x)e^{i(\ell y-\omega t)}$, and the right-handed coordinate system is oriented with the x-axis perpendicular to isobaths (positive seaward). Longshelf (y) variations in the mean current $\overline{V}(x)$ and the bottom topography $h(x)$ are not explicitly included. The basic state potential vorticity is $P(x) = (f + \overline{V}_x)h^{-1}$, where f is the constant Coriolis parameter. The absolute (i.e., relative to the fixed coordinate frame) wave phase speed is defined as $c_o \equiv \omega/\ell$ where ω is the wave frequency and ℓ is the wave number. For a discussion of the assumptions and details leading to this equation and its

inherent limitations, see LeBlond and Mysak (1979).

With two-point boundary conditions for ψ, the governing equation presents an eigenvalue problem for the phase speed c_o, (upstream propagation for $\omega > 0$ assumed). For downstream waves with $0 \leq c_o \leq \overline{V}_{max}$, the equation has singular (critical) points where $c_o = \overline{V}$, the spectrum is continuous (McKee, 1977), and under certain circumstances the waves may be unstable (Niiler and Mysak, 1971).

For a given $h(x)$, $\overline{V}(x)$, there will be n solutions $(c_o,\psi)_n$ for each wavenumber ℓ_n, with the n^{th} solution determining a point on the dispersion curve for the n^{th} mode. For example, the dispersion diagram is given by Brooks (1978) for the Cape Fear bottom profile (Fig. 2) and a current profile determined by vertically integrating the $V(x,z)$ section in Fig. 3. For general h, $\overline{V}$ profiles, the solutions are most conveniently obtained numerically.

The model calculations were performed for each of the bottom profiles shown in Fig. 2, assuming that the mean current profile was invariant in the SAB, that its axis coincided with the 550 m isobath, and that its transport was fixed at $53 \times 10^6 m^3 s^{-1}$ (reported by Richardson *et al.*, 1969). The MAB case was run with $\overline{V} = 0$ (no Gulf Stream). Dispersion curves for the gravest mode in each case are shown in Fig. 26. The dimensional period scale shown applies only at the Cape Fear latitude but the scale factor (the inertial period) changes by only about 4 percent over the latitude range considered (about 3 degrees). The zero group speed, lowest mode horizontal velocity structure is shown in Fig. 27 for the three southernmost Capes.

4.2 Discussion and relation to observations

For monotonic bottom profiles, the dispersion curve for CSW mode n characteristically exhibits at least one zero group speed (zero slope) point (ω_{no},ℓ_{no}) (Huthnance, 1975). The dispersion curves in Fig. 26

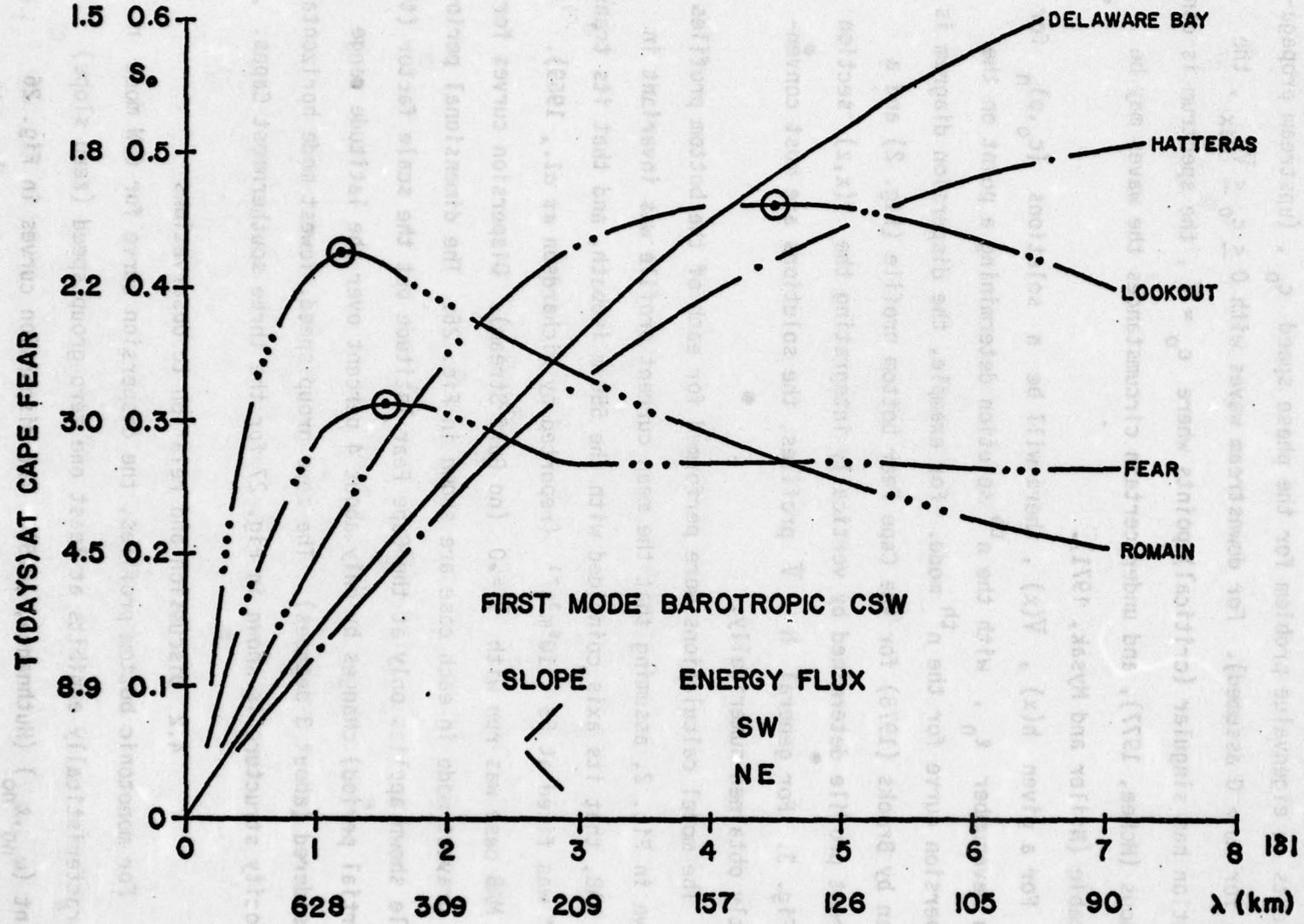

Fig. 26 Gravest shelf wave dispersion curves for bottom and mean current profiles typical of the four Carolina Capes and of the MAB (Delaware Bay). Zero group speed points are circled. The dimensional period scale is strictly correct only at Cape Fear.

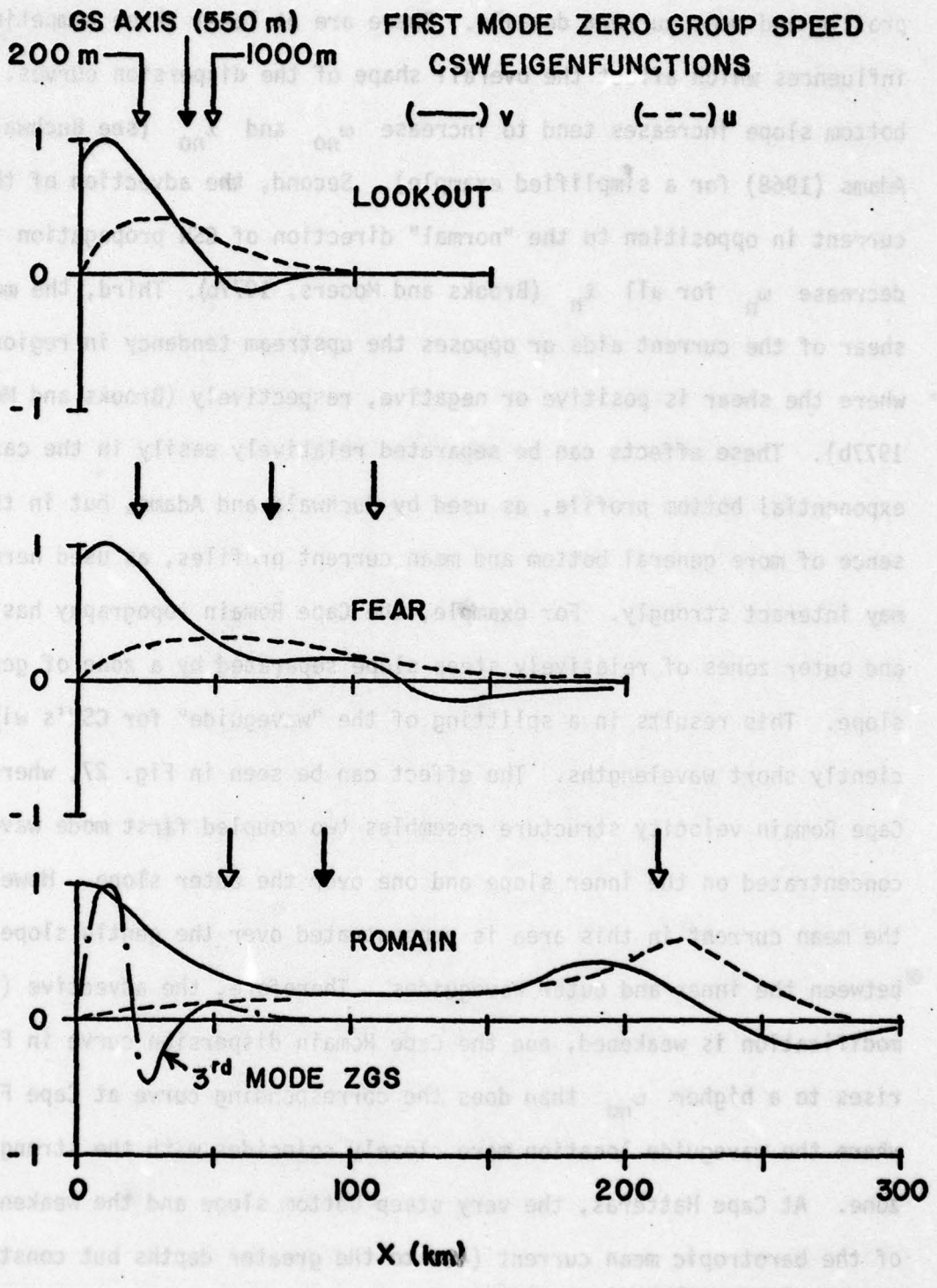

Fig. 27 Gravest mode zero group speed velocity component eigenfunctions for the Carolina Capes. Locations of the 200 m and 1000 m isobaths and the model mean Gulf Stream axis are shown by vertical arrows. Note that the first mode structure over the narrow Cape Lookout shelf divides into two coupled first mode structures over the dual shelf off Cape Romain; in contrast the third Romain mode is trapped entirely over the inner shelf.

illustrate that the location of these points depends strongly on the bottom profile and mean current details. There are at least three competing influences which affect the overall shape of the dispersion curves. First, bottom slope increases tend to increase ω_{no} and ℓ_{no} (see Buchwald and Adams (1968) for a simplified example). Second, the advection of the mean current in opposition to the "normal" direction of CSW propagation tends to decrease ω_n for all ℓ_n (Brooks and Mooers, 1977b). Third, the mean shear of the current aids or opposes the upstream tendency in regions where the shear is positive or negative, respectively (Brooks and Mooers, 1977b). These effects can be separated relatively easily in the case of an exponential bottom profile, as used by Buchwald and Adams, but in the presence of more general bottom and mean current profiles, as used here, they may interact strongly. For example, the Cape Romain topography has inner and outer zones of relatively steep slope separated by a zone of gentle slope. This results in a splitting of the "waveguide" for CSW's with sufficiently short wavelengths. The effect can be seen in Fig. 27, where the Cape Romain velocity structure resembles two coupled first mode waves, one concentrated on the inner slope and one over the outer slope. However, the mean current in this area is concentrated over the gentle slope region between the inner and outer waveguides. Therefore, the advective (kinematic) modification is weakened, and the Cape Romain dispersion curve in Fig. 26 rises to a higher ω_{no} than does the corresponding curve at Cape Fear, where the waveguide location more closely coincides with the strong current zone. At Cape Hatteras, the very steep bottom slope and the weakened effect of the barotropic mean current (due to the greater depths but constant transport) result in ω_{no}, ℓ_{no} being offscale in Fig. 26. Likewise, in the

MAB (represented by the Delaware Bay curve in Fig. 26), the absence of the current allows ω_{no} and ℓ_{no} to increase to relatively large values.

The foregoing results suggest that longshelf energy dispersion by CSW's over the eastern United States continental margin will be complex. For example, consider the case of a forcing event occurring simultaneously in the SAB and the MAB. The event can be characterized as an energy density distribution in ω , ℓ (dispersion) space, which will project into the various free modes of motion available (CSW's in this case) with efficiencies dependent upon the eigenfunction structure and other details involving the othogonality of the modes and critical level effects (*cf.* Wang and Mooers (1975) for a discussion of orthogonality relations of coastal trapped waves and McKee (1979) for forced waves in the presence of critical levels). It is reasonable to expect the gravest mode to be most strongly excited because it has the simplest structure. The energy of the mode propagates with the group speed for that mode, which is equal to the slope of its dispersion curve. For $\ell_n < \ell_{no}$, the energy flux is upstream (southwestward) and for $\ell_n > \ell_{no}$, the energy flux is downstream (Fig. 26). For the frequency and wavenumber ranges in Fig. 26, which correspond approximately with the ranges over which the data studies in Section 3 apply, a downstream energy flux can occur only for periods of about 2-4 days, and only in the SAB. Thus gravest-mode backscattering of CSW energy by topography or mean current variations can be significant only in this period range. This may provide an explanation for the intensity of short period sea level motions in the SAB compared to the MAB, and also for the evanescence of short period motions backscattered into the MAB as long period CSW's encounter the abrupt waveguide change at Cape Hatteras associated with the Gulf Stream.

The response energy at a fixed observation site (e.g., a tide gage) to the simultaneous event forcing would be composed of the sum of the energy introduced locally plus that propagated to the observation site from upstream or downstream forcing sites. The resultant phase distribution along the coast would be determined in a complex way by the relative importance at each observation site of the locally forced, forward propagating, and backscattered energy. The fact that SAB tide gage investigations (*cf.* Section 3) have found longshelf phase lags in the several-day period band too small to conveniently explain by a monochromatic disturbance may be evidence that the locally forced contribution to the total energy at a particular point is dominant. If so, the dominant sea level and attendant circulation variability can be expected to occur at or near zero group speed periods and wavelengths. In the SAB, these periods fall in the 2-3 day period range for the lowest CSW mode, corresponding rather well to the short period coherent sea level bands in Section 3. In the MAB, however, the zero group speed wavelength is very short for the lowest mode -- probably less than the shelf width -- and is not likely to be strongly energized by atmospheric disturbances, even when the relatively small wind stress curl scales (a few hundred km) are considered. Thus the dominant disturbances in the MAB are likely to be those with scales determined externally, i.e., by the atmosphere; this coupling is clearly most effective in the MAB for long periods of a week or more (*cf.* Section 3).

An alternate forcing scheme of interest is that of an isolated North Atlantic storm that impinges on the MAB. One could envision an initially quiescent SAB and then consider the process by which the storm-induced MAB vorticity disturbance would influence the SAB. From the discussion surrounding Fig. 26, all of the significant low mode energy will propagate

southwestward in the MAB. Upon "rounding the corner" at Cape Hatteras, however, an increasingly large fraction of short wave energy will be backscattered as the disturbance proceeds into the SAB. The spectral characteristics and the total energy of the disturbance will change as it travels in the SAB, with long wavelengths (and therefore long periods) becoming relatively more important than short wavelengths, but with the total energy decreasing due to the short wave fraction lost to backscattering. The increasing importance of long period motions as one proceeds upstream in the SAB is suggested in the interstation longshelf sea level coherence (Figs. 14 and 15) and in the MET·SL coherence (Figs. 16 and 21), more notably so in the winter case.

5. Summary and Conclusions

The principal objective of this study was to see if continental shelf waves could propagate "around the corner" at Cape Hatteras, providing a means of communication between the Middle and South Atlantic Bights (MAB and SAB). An additional objective was to investigate the efficiency of atmospheric weather disturbances as forcing functions for these waves. The underlying motivation for the study was the idea that, if the communication between the Bights were effective, it could provide a mechanism for introducing vorticity disturbances caused by North Atlantic storms into the Gulf Stream. The data sets used to test the hypothesis consisted of coastal tide gage and meteorological time series from an array of stations spanning the interbight region.

Analysis of the tide gage data showed that disturbances with periods longer than one week propagated southwestward in both Bights, with no apparent interruption at Cape Hatteras. Similar long period motions have been observed as far north as Nantucket Shoals and as far south as Key West, so it is probably reasonable to consider the entire eastern United States continental margin as a single "waveguide" for long period motions. The wavelengths implied by coastal phase lags are very imprecisely indicated by this study to be of the order of 1000 km, which is approximately the long shelf scale of the observation station array used here.

Several-day period motions were found to be prominent in the SAB but evanescent north of Cape Hatteras in the MAB. Coastal sea level phase lags indicated upstream propagation in the SAB, but the lags were considerably smaller than would be expected for a monochromatic several-day period shelf wave. Also, the phase lags were very non-uniform and of questionable

statistical significance over most of the SAB, leading to the conclusion that a monochromatic wave is an inappropriate descriptor of the several-day period motions in the SAB.

Wind stress and atmospheric pressure fluctuations were coupled with the sea level fluctuations in different proportions, depending on the period of the motion, the season, and the location of the tide gage. Generally, both wind stress components (cross shelf and longshelf) provided important forcing for periods longer than about a week in both Bights, and atmospheric pressure (after correction for coherent wind stress effects) was important for several-day periods in the SAB. Strongest coupling occurred in the SAB in the summer, and in both Bights in the winter, presumably reflecting seasonal differences in prevailing weather patterns.

Consideration of the energy dispersion characteristics of shelf waves in the two Bights suggests that backscattering of long period motions as they enter and propagate through the SAB may explain the presence of several-day period energy there. This result is a consequence of the highly variable bottom slope and shelf width in the SAB, and is also dependent upon the location of the Gulf Stream relative to the shelf profile. If this hypothesis is correct, the absence of short-period motions in the MAB is a result of the relatively uniform shelf profile and the absence of the Gulf Stream there, and not due to MAB-SAB differences in the atmospheric forcing details. It is not entirely clear that scattering is the prime source of short period SAB motions, because strong and very selective dynamical coupling between atmospheric pressure and sea level occurs for short periods in the SAB. The latter is an unexplained result, since the equations indicate that direct forcing by pressure fluctuations should be unimportant. Furthermore, the notion that pressure correlation with sea level is just

an indication of pressure correlation with wind stress is ruled out, at least in a linear relationship, because the pressure transfer functions upon which the above statements are based were corrected for the pressure-to-wind stress linear correlation. A related possibility is that the pressure-to-sea level correlation is an artifactual consequence of the relationship between the pressure and the wind stress curl; this notion is attractive because the curl is more likely to have the requisite short period energy than is the undifferentiated wind stress.

It is clear from this study that provincial treatments of ocean dynamics on the eastern United States continental margin may be inappropriate, particularly for periods of a week or longer. The modeler's field of view must be widened sufficiently to encompass the different but coupled dynamics of the two Bights, if an appropriate understanding of the low frequency motions is to be gained. The dynamical processes that seem most in need of treatment in light of these results are: 1) scattering and energy dispersion of shelf waves by longshelf coastal and topographic irregularities; 2) statistical details of the process by which realistic wind stress and wind stress curl fields can drive oceanic motions over the shelf; and 3) the interaction of shelf waves with the Gulf Stream, particularly with regard to momentum and energy exchange between the two on critical surfaces where the wave speed vanishes relative to the mean current.

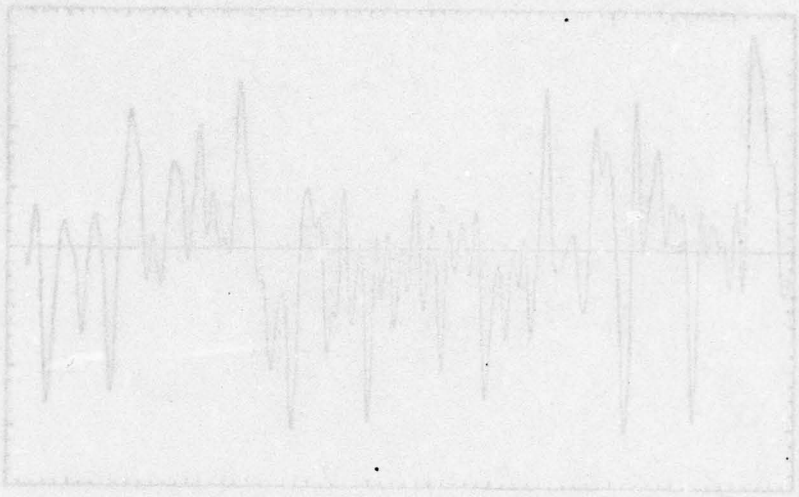

APPENDIX A

Time series of low pass filtered sea level and meteorological data. See Section 2 for details of filter characteristics, calendar start and stop times, and wind vector coordinate rotation angles. The order of sea level subset presentation follows that in the text, proceeding from south to north along the coast.

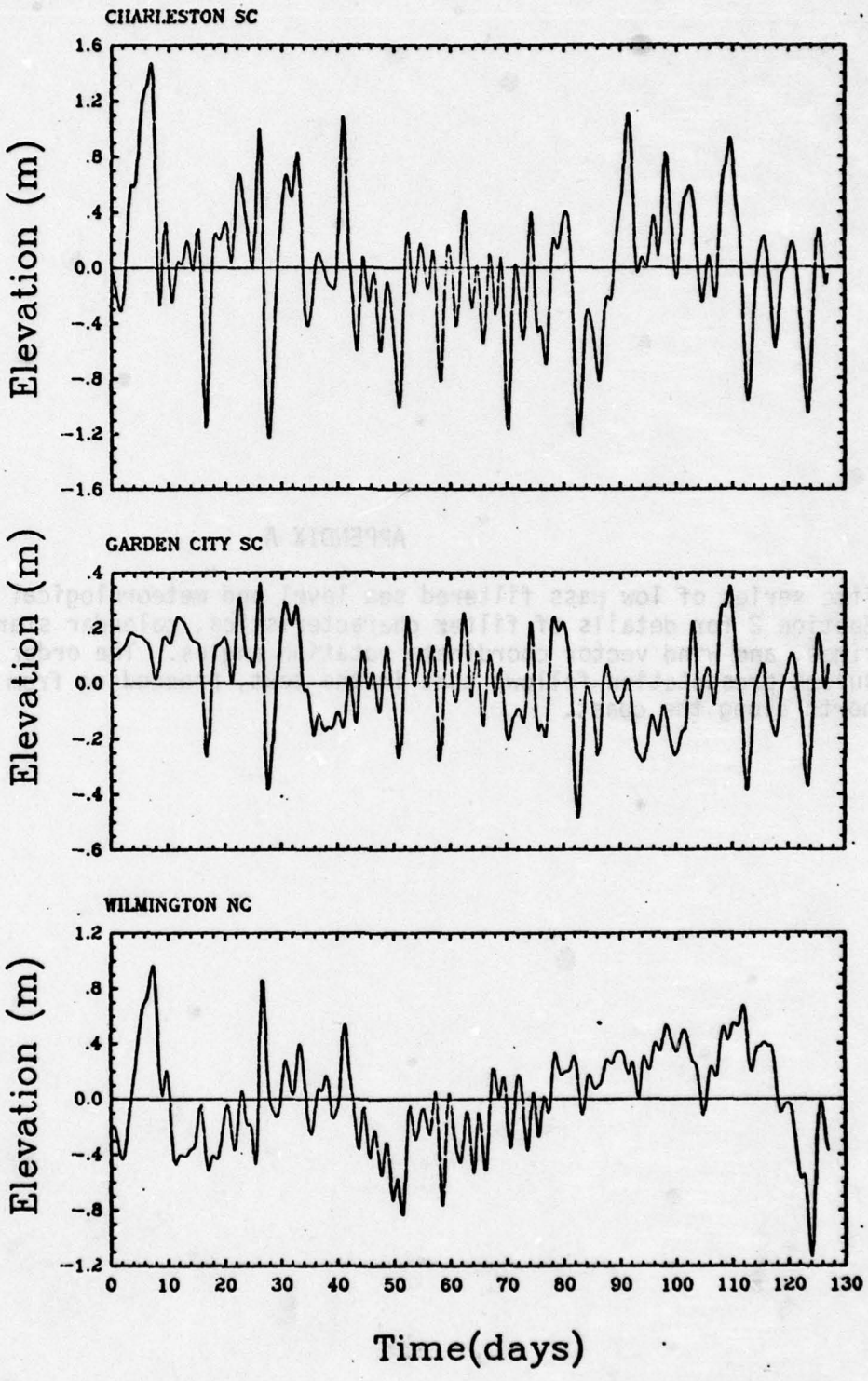

Fig. A.1 Winter adjusted sea level.

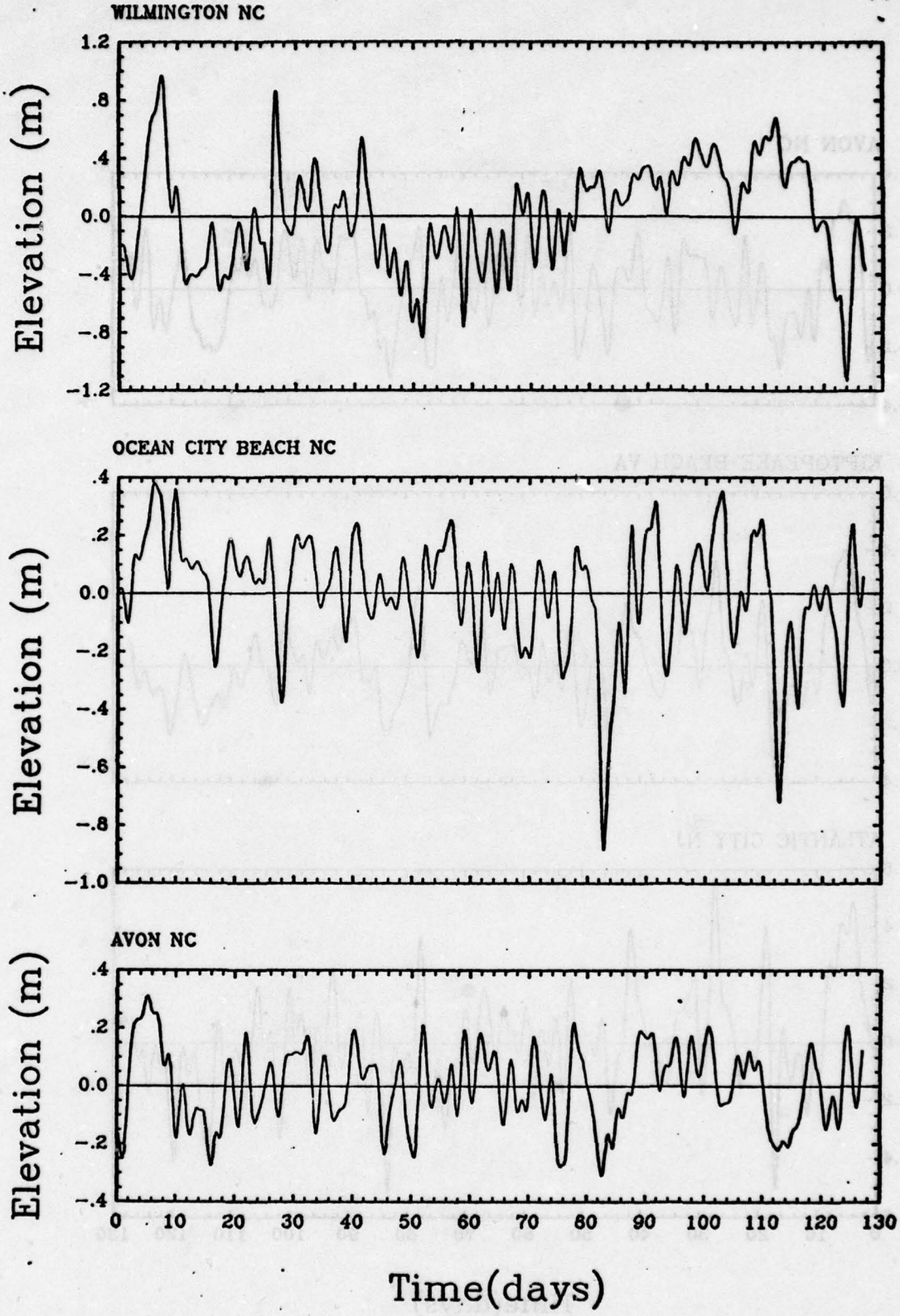

Fig. A.2 Winter adjusted sea level.

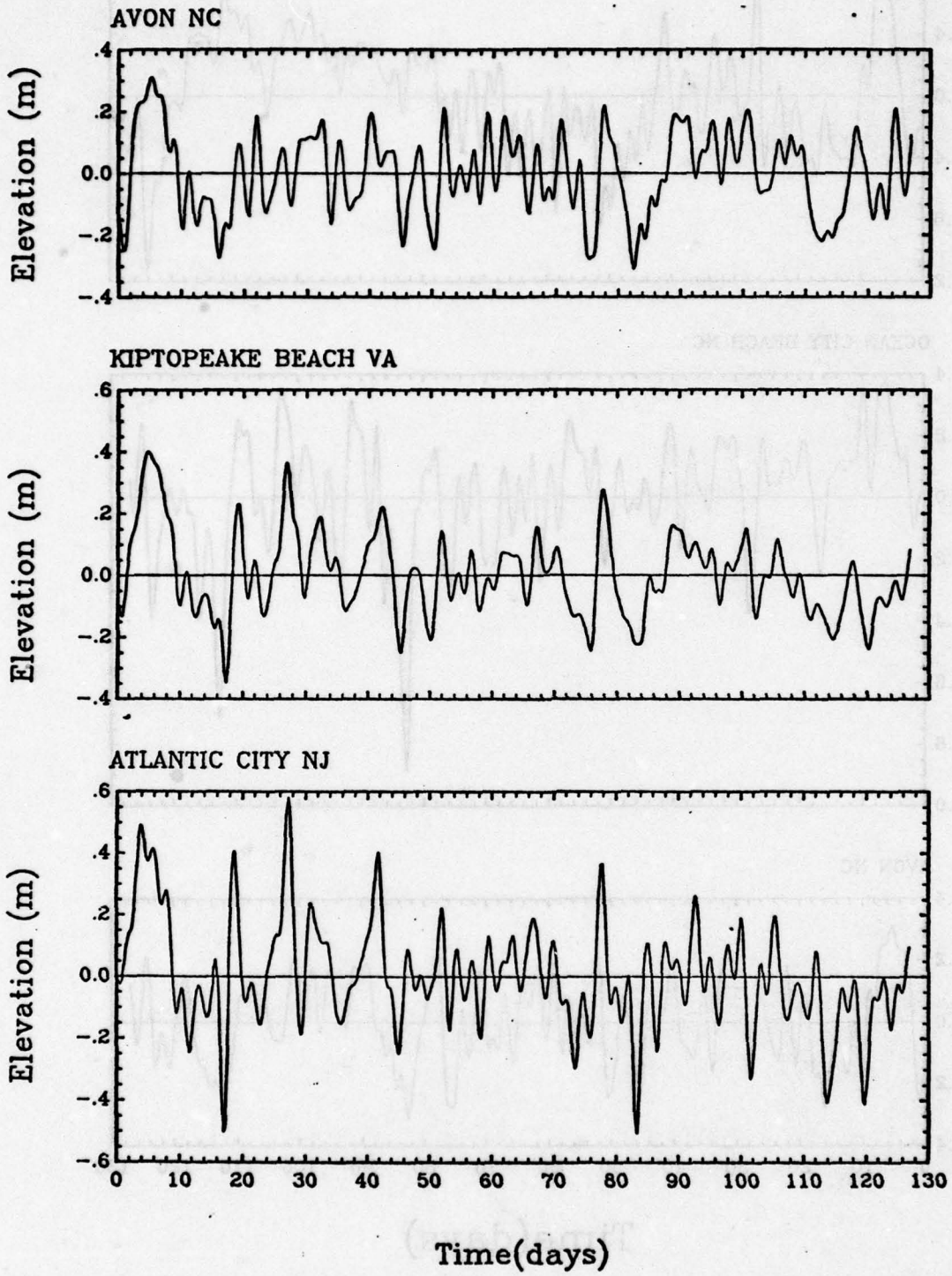

Fig. A.3 Winter adjusted sea level.

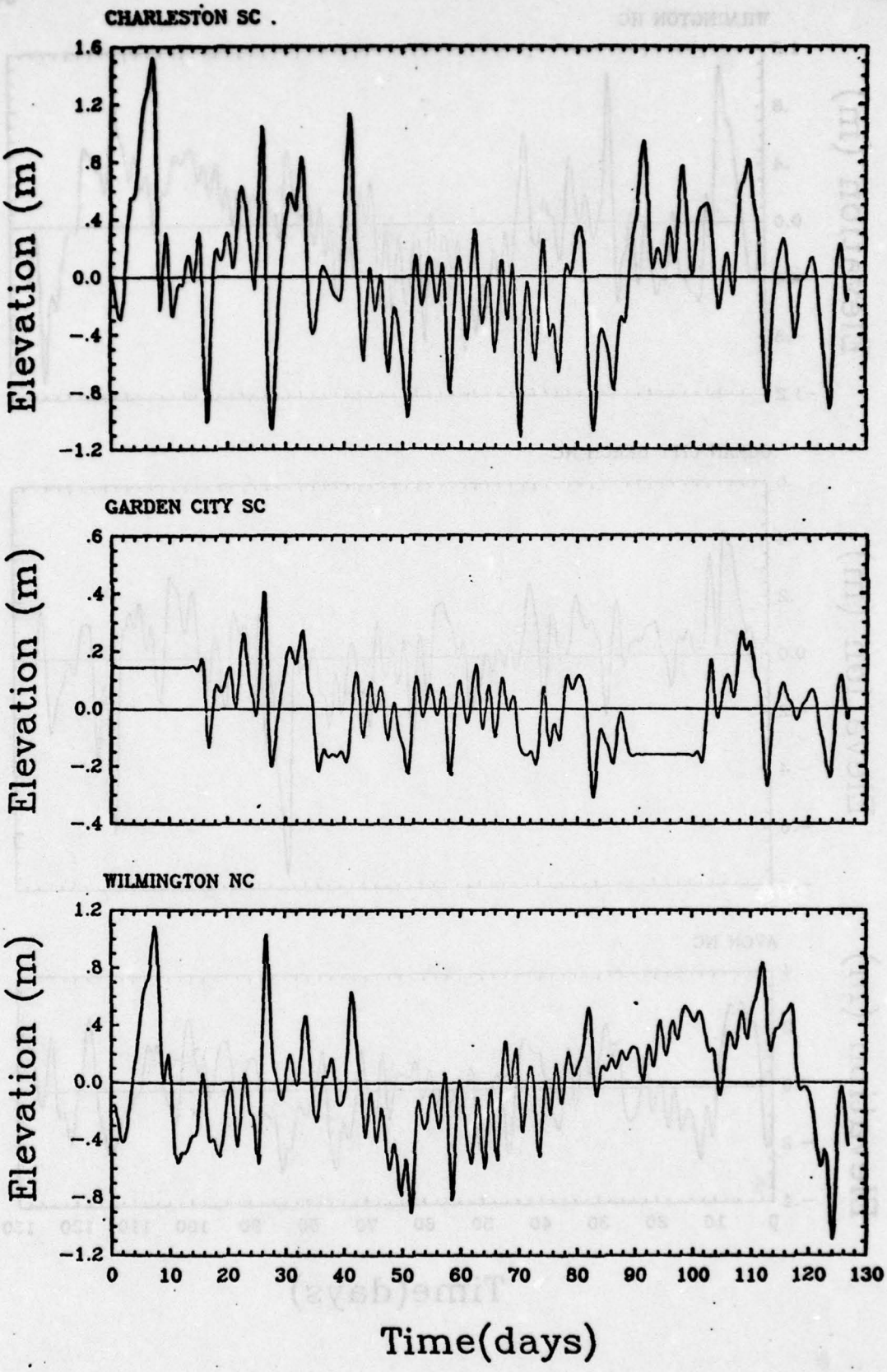

Fig. A.4 Winter unadjusted sea level.

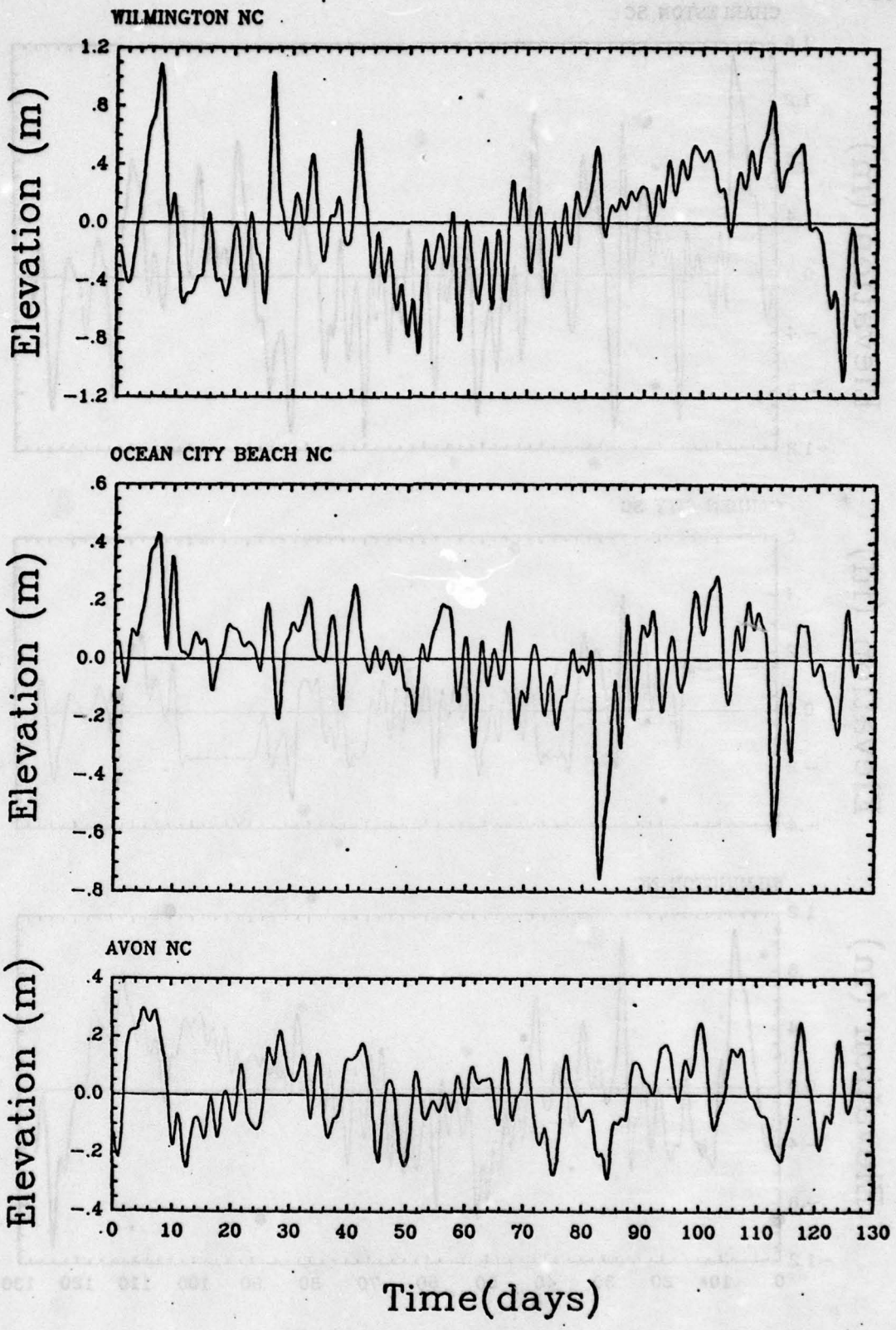

Fig. A.5 Winter unadjusted sea level.

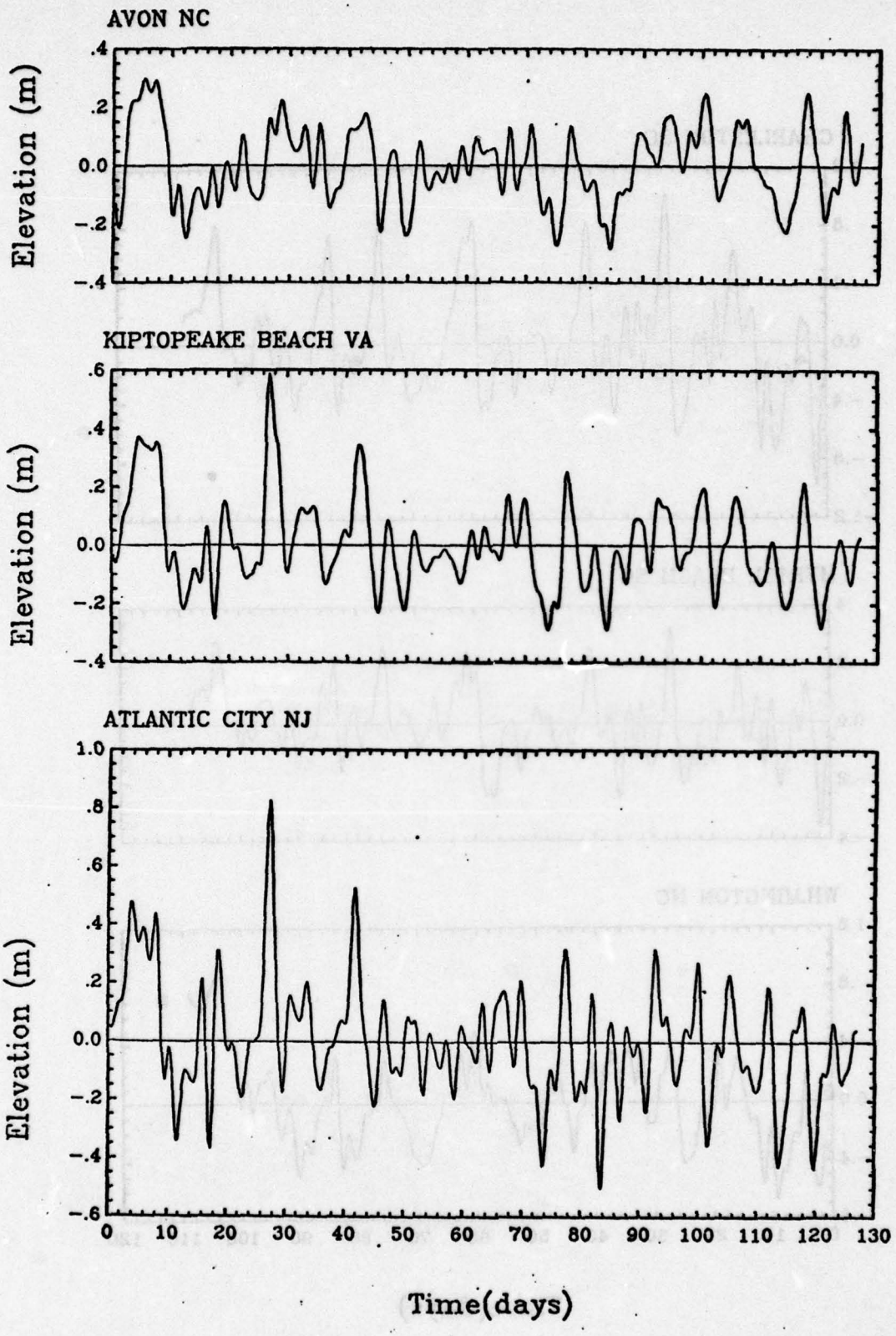

Fig. A.6 Winter unadjusted sea level.

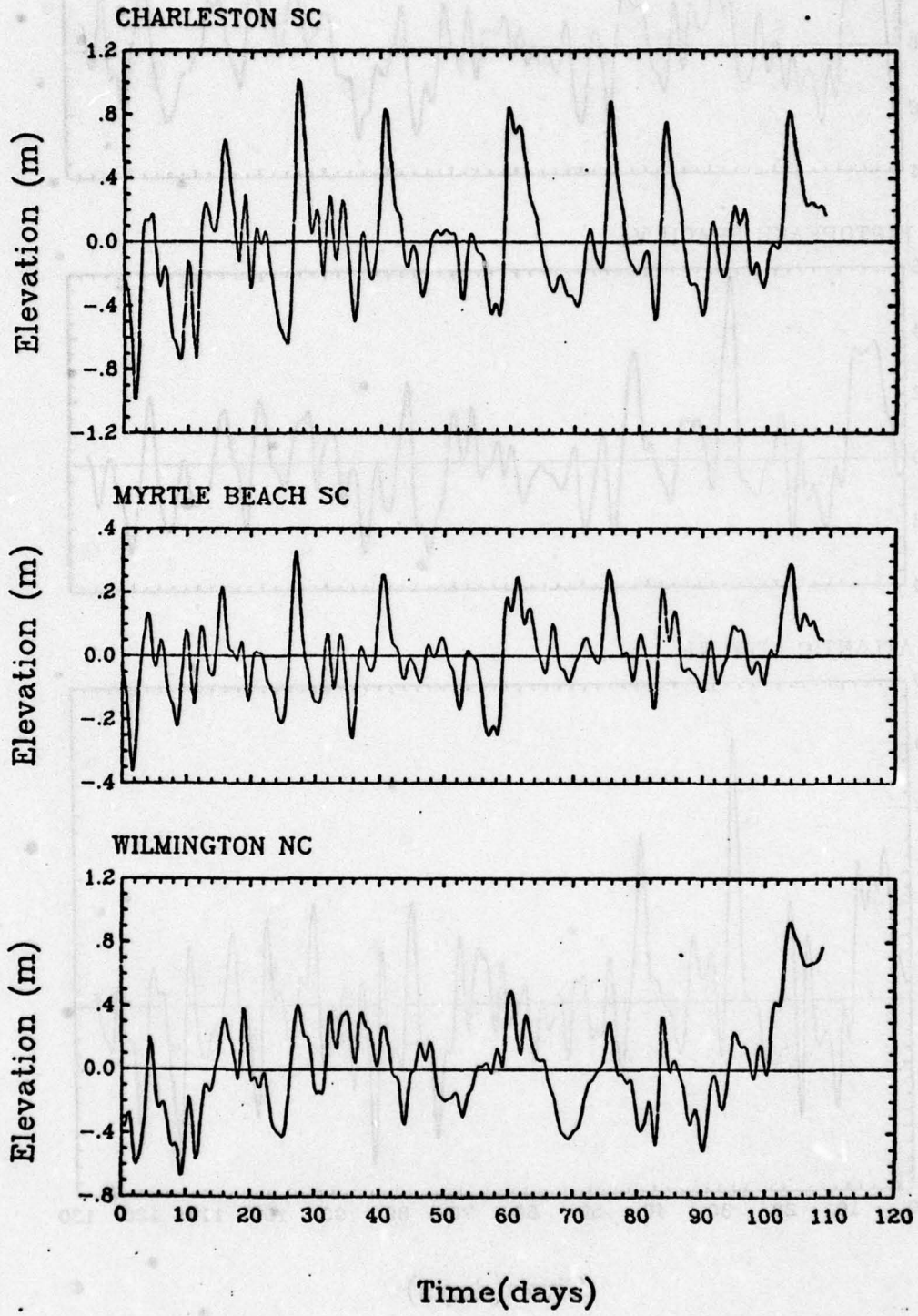

Fig. A.7 Summer adjusted sea level.

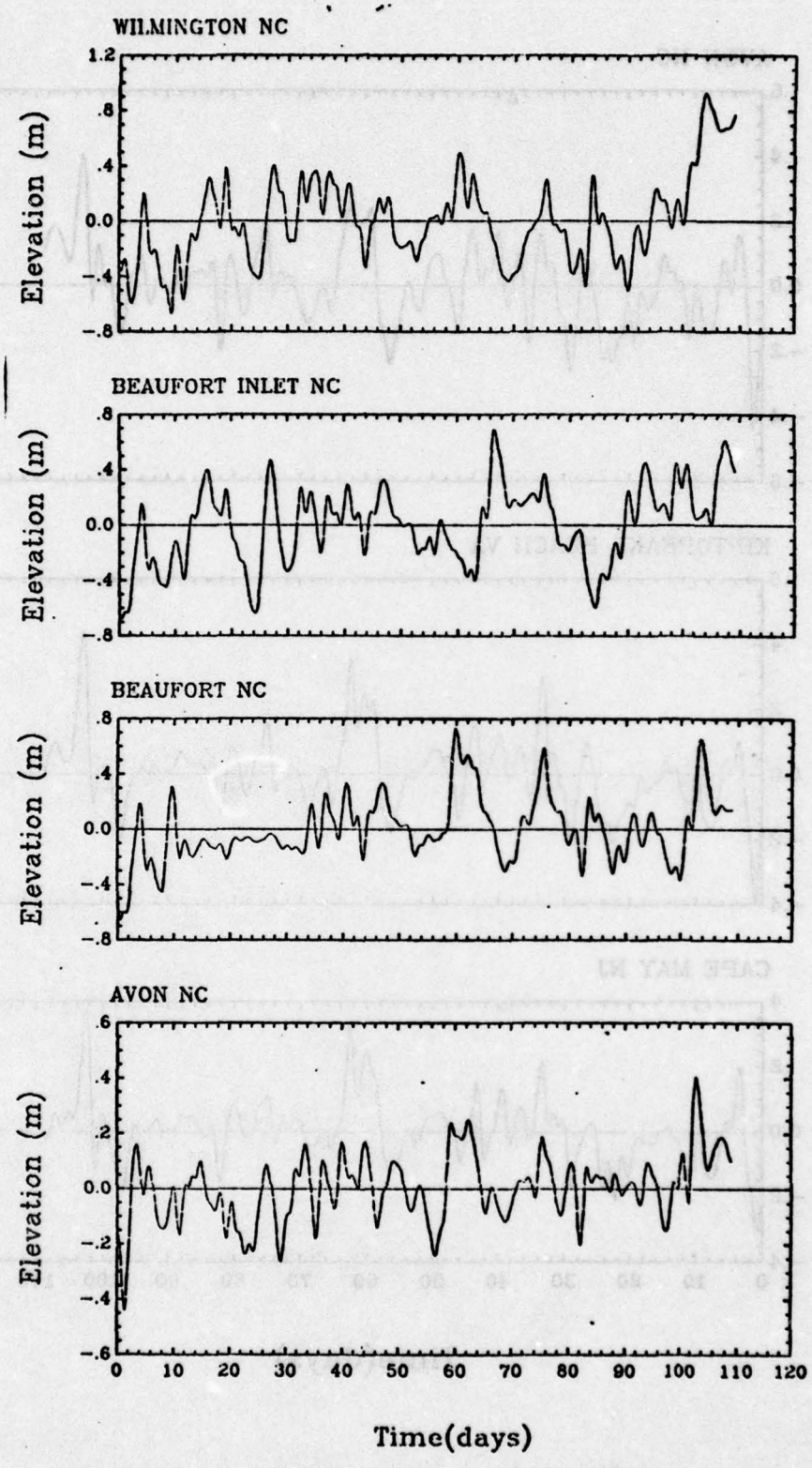

Fig. A.8 Summer adjusted sea level.

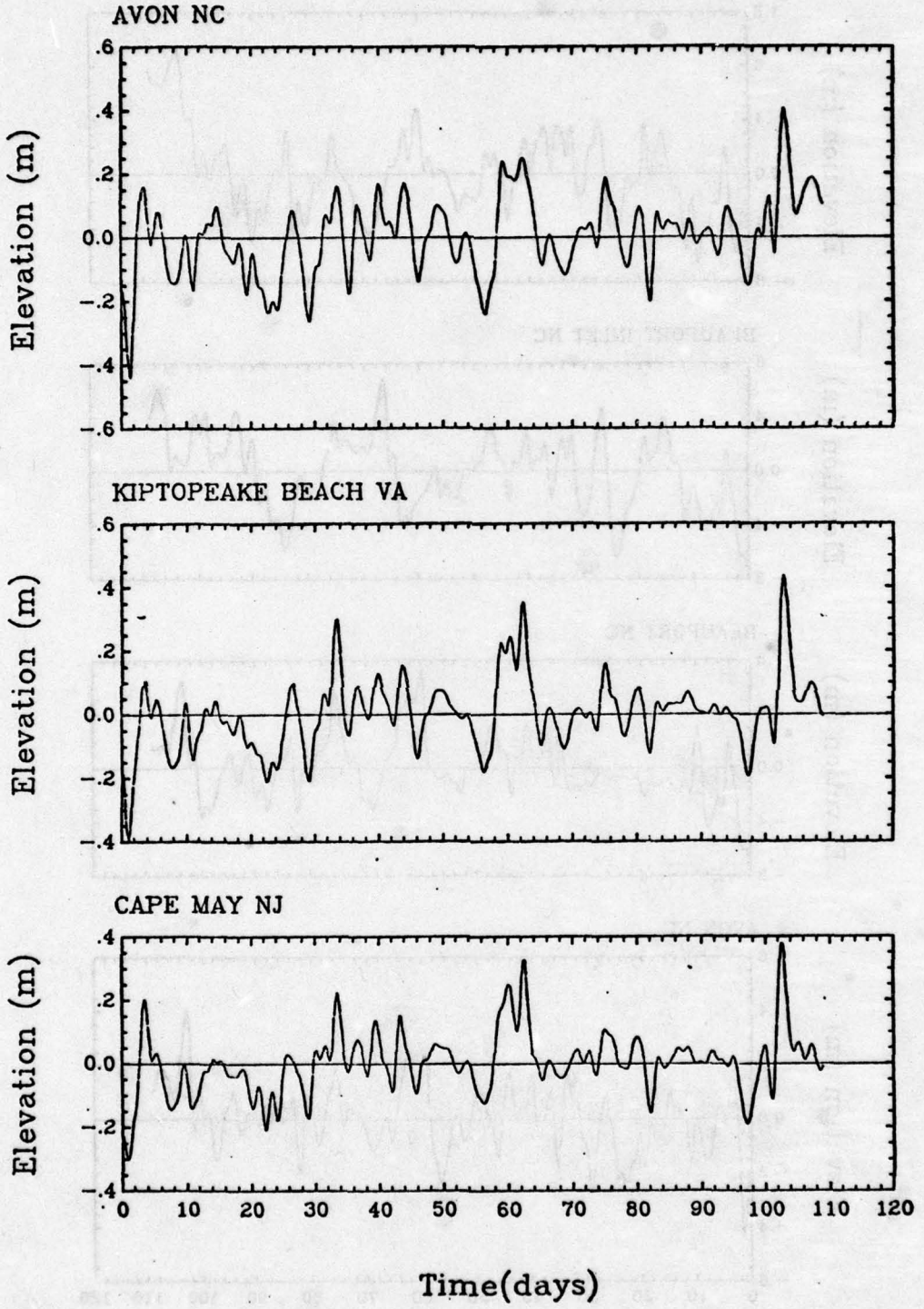

Fig. A.9 Summer adjusted sea level.

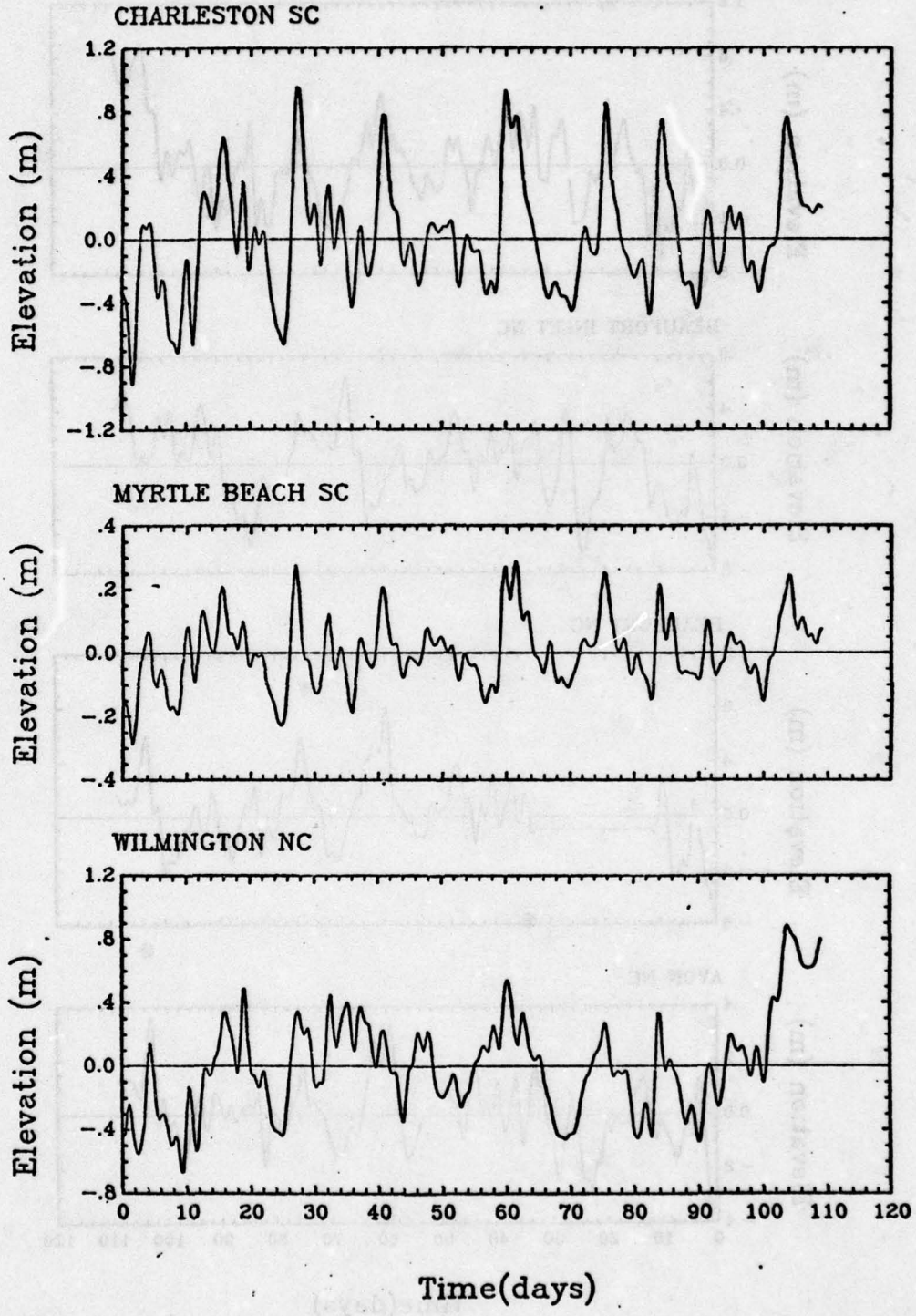

Fig. A.10 Summer unadjusted sea level.

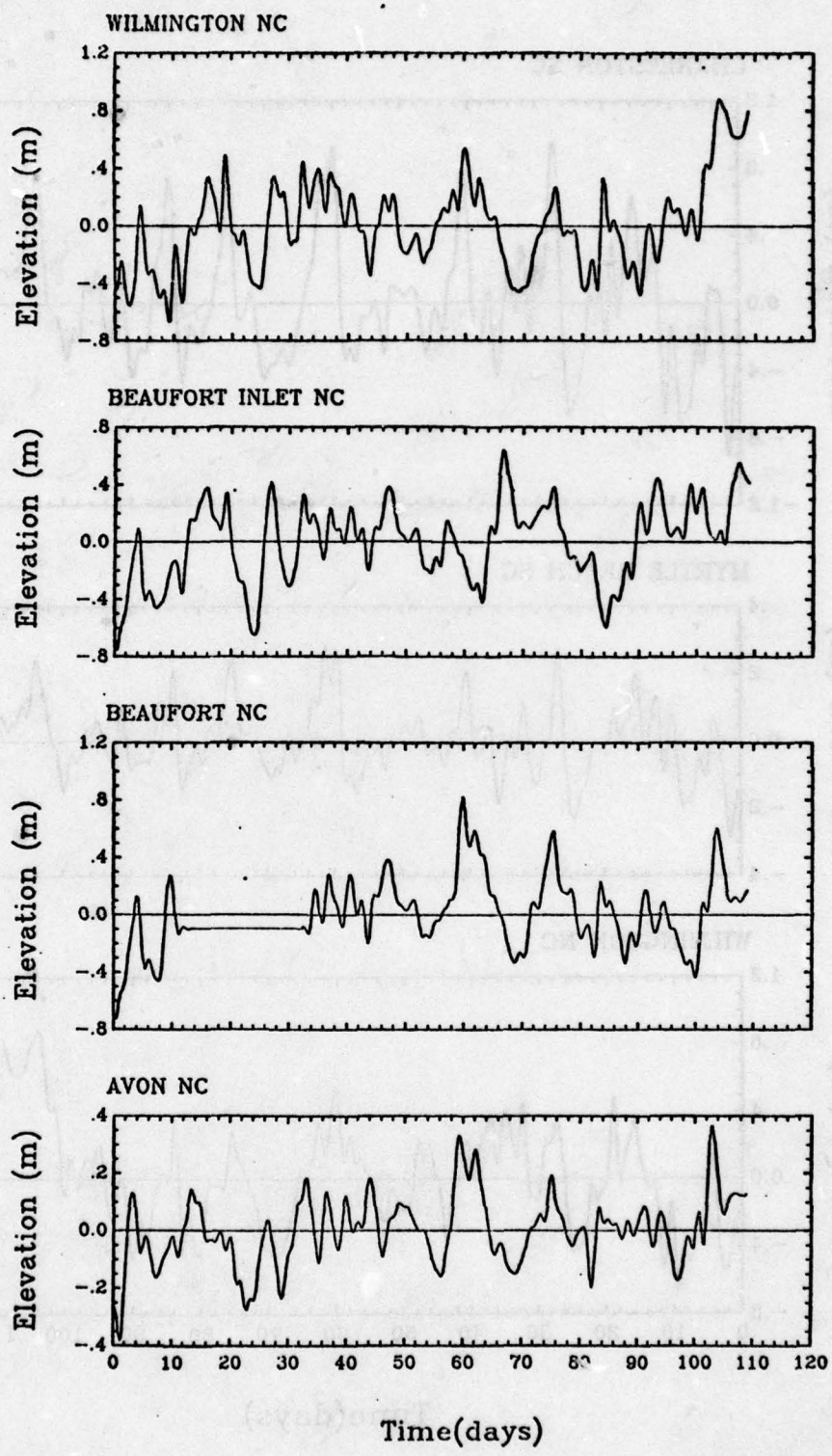

Fig. A.11 Summer unadjusted sea level.

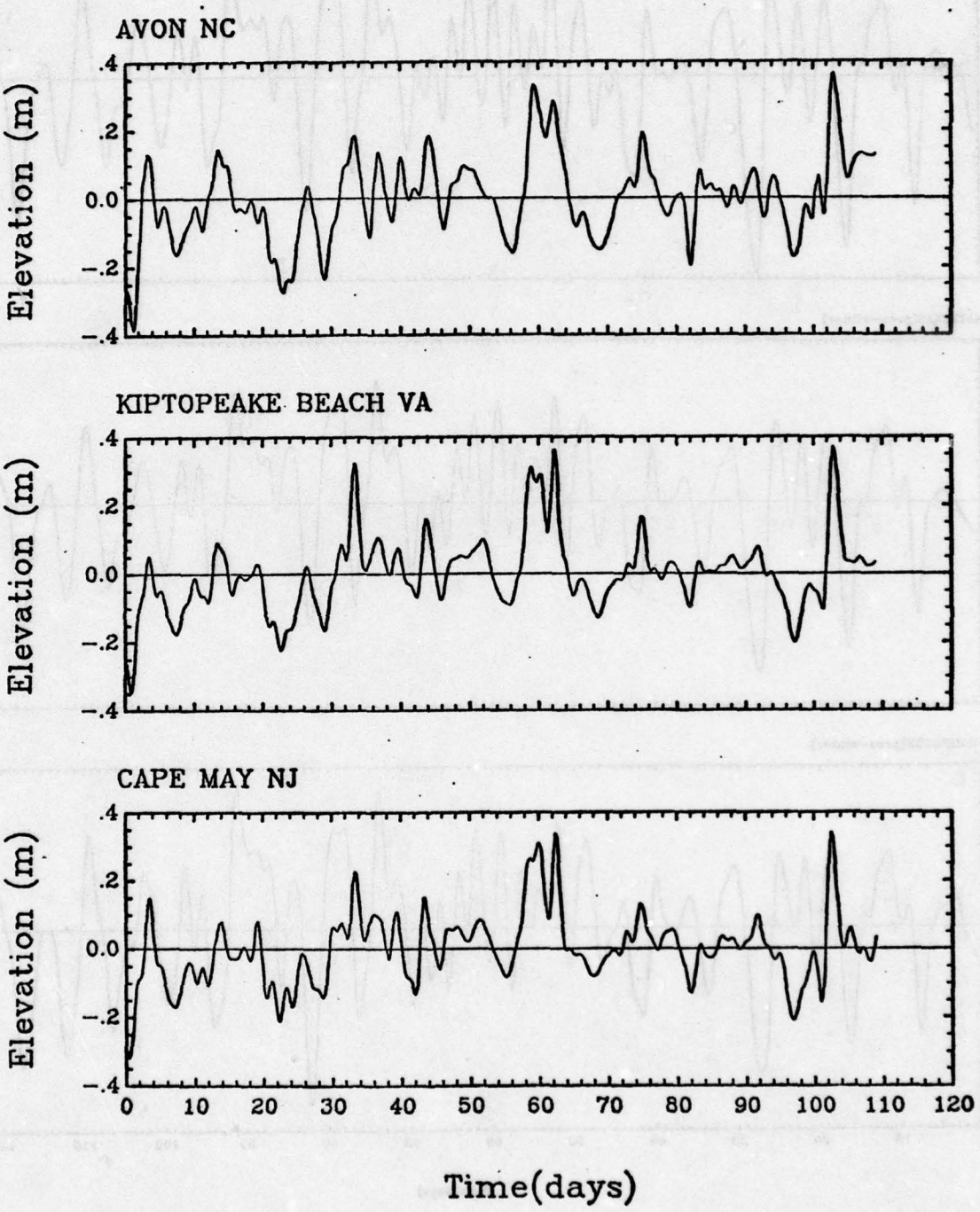

Fig. A.12 Summer unadjusted sea level.

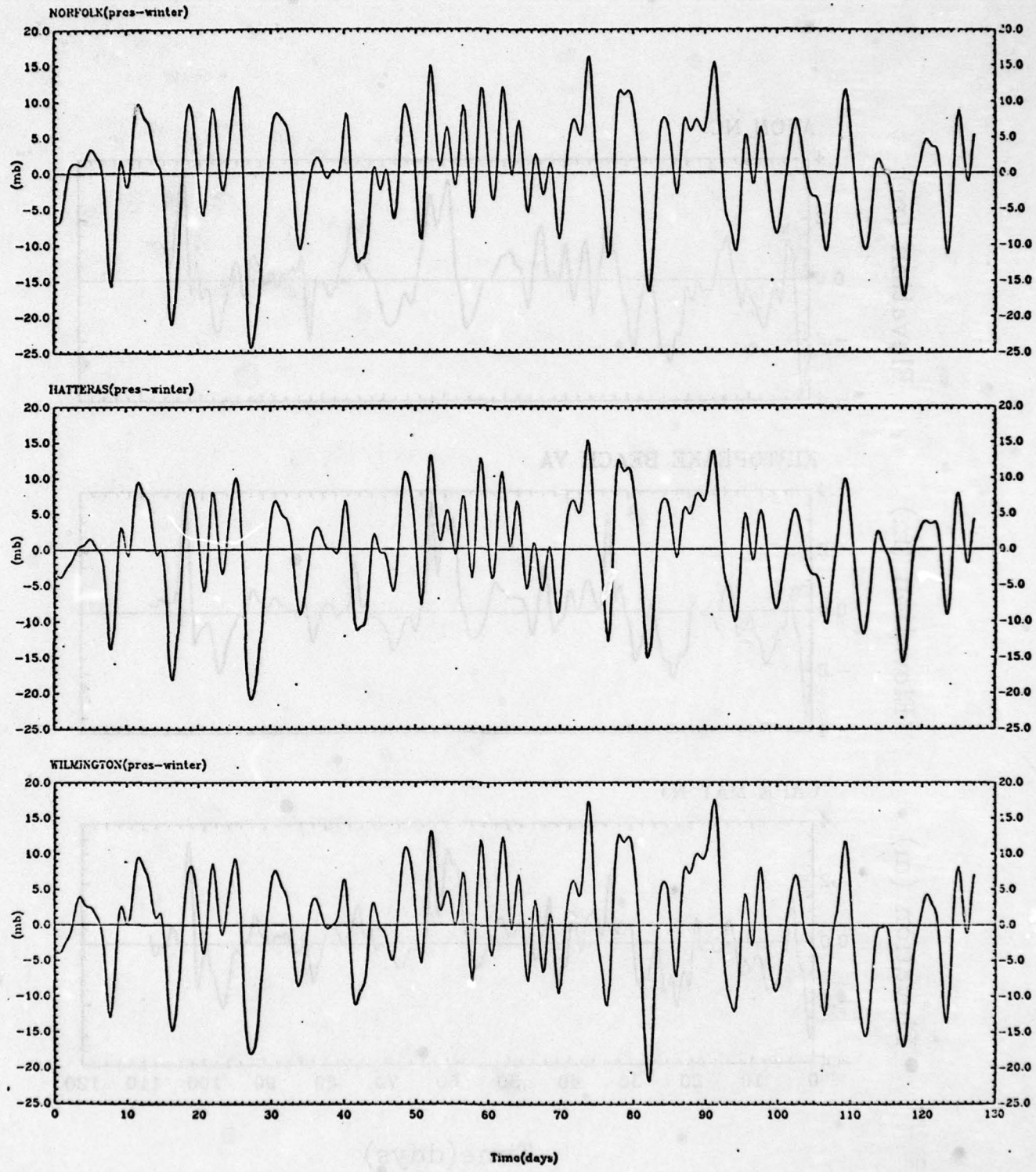

Fig. A.13 Winter atmospheric pressure.

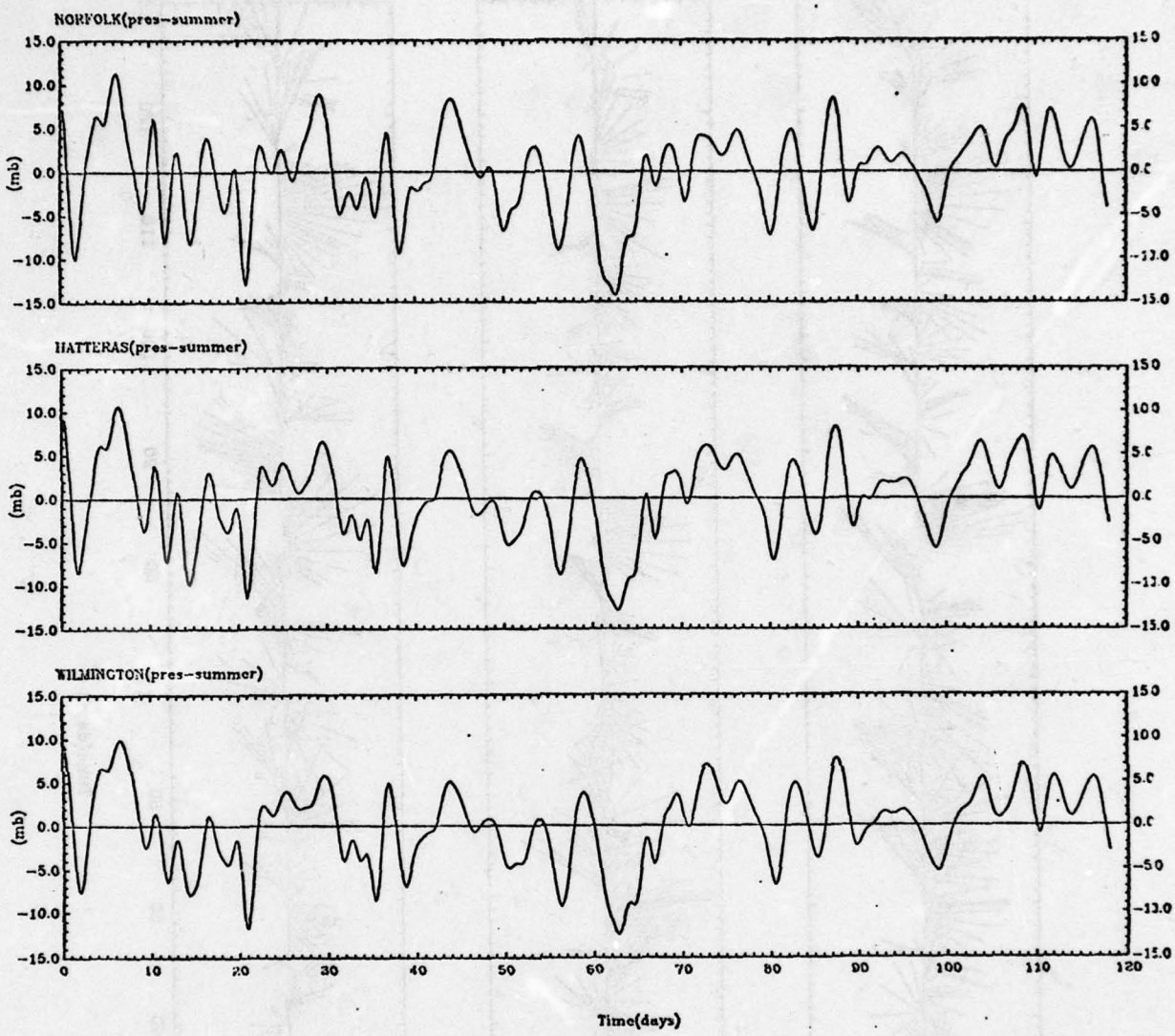

Fig. A.14 Summer atmospheric pressure

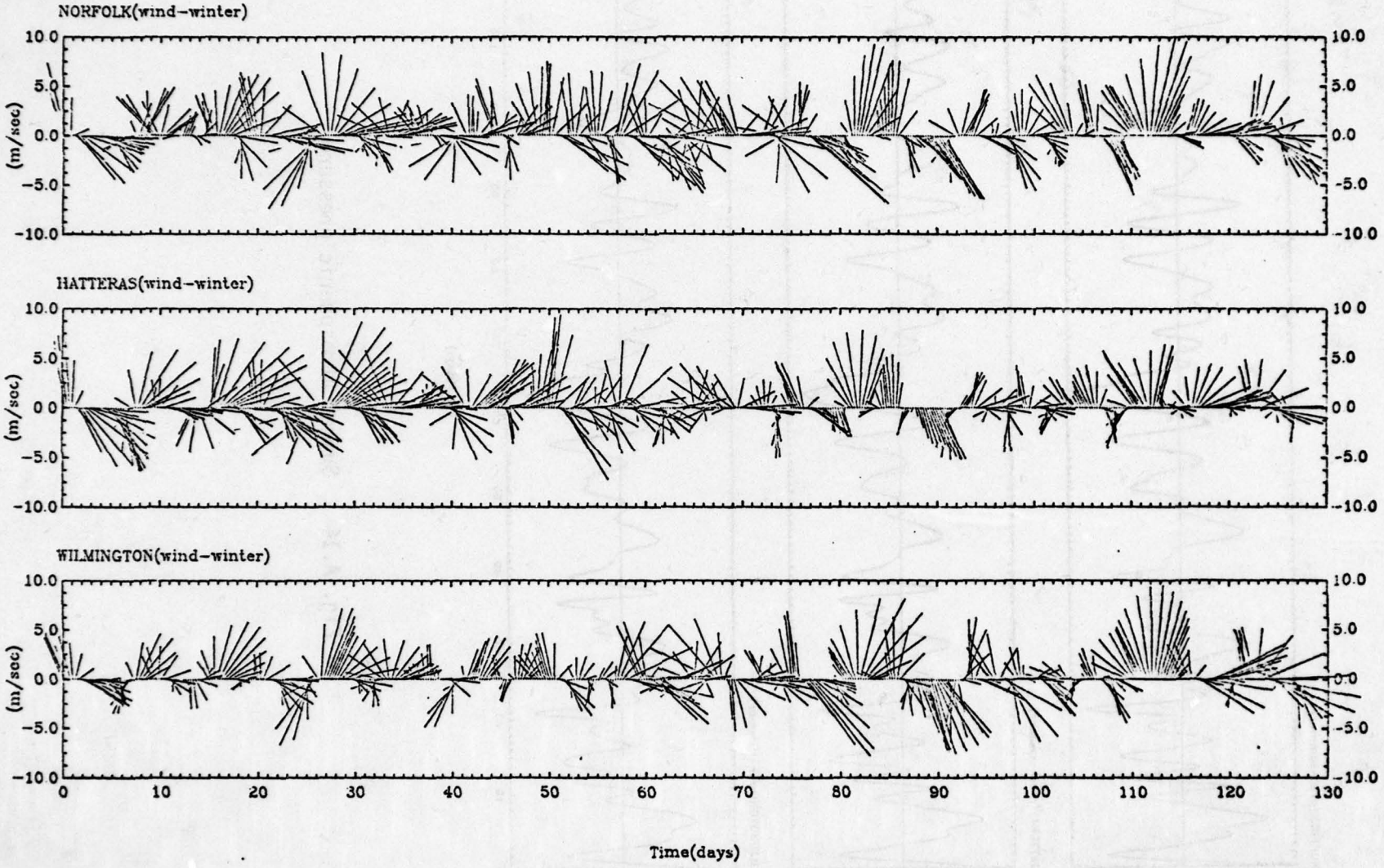

Fig. A.15 Winter wind vector stick plots. The ordinate scale gives the vector magnitude.

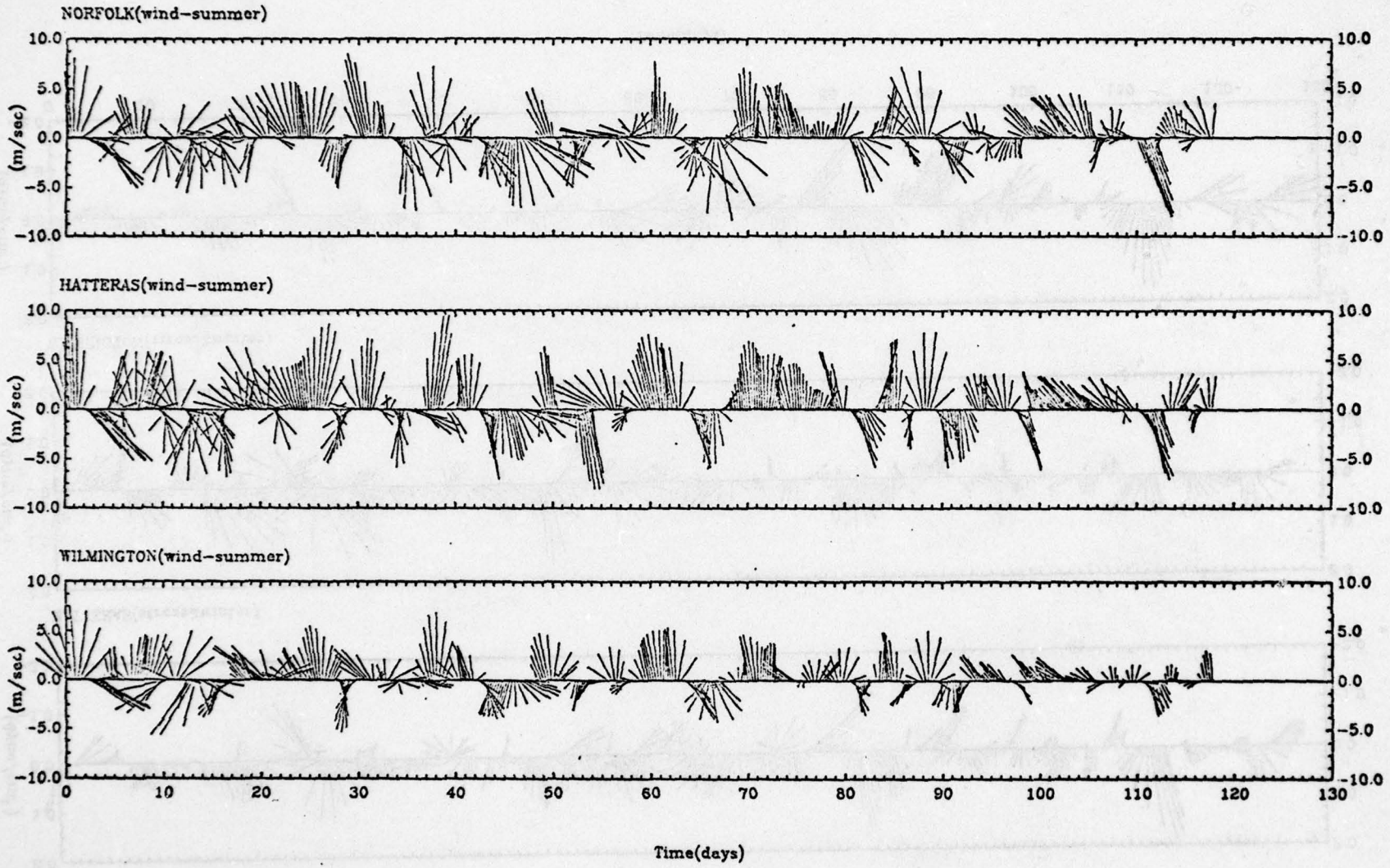

Fig. A.16 Summer wind vector stick plots. The ordinate scale gives the vector magnitude.

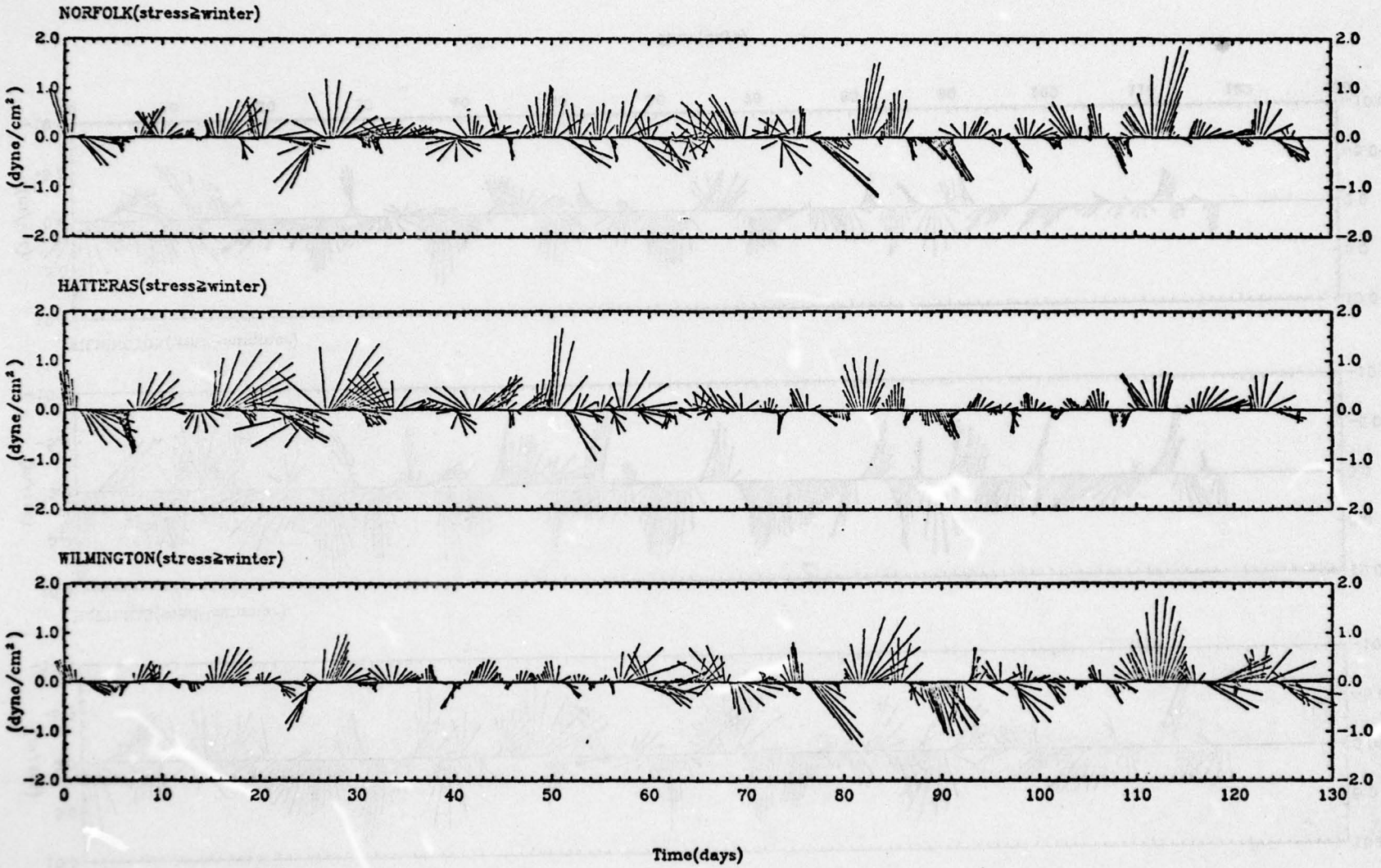

Fig. A.17 Winter wind stress vector stick plots. The ordinate scale gives the vector magnitude.

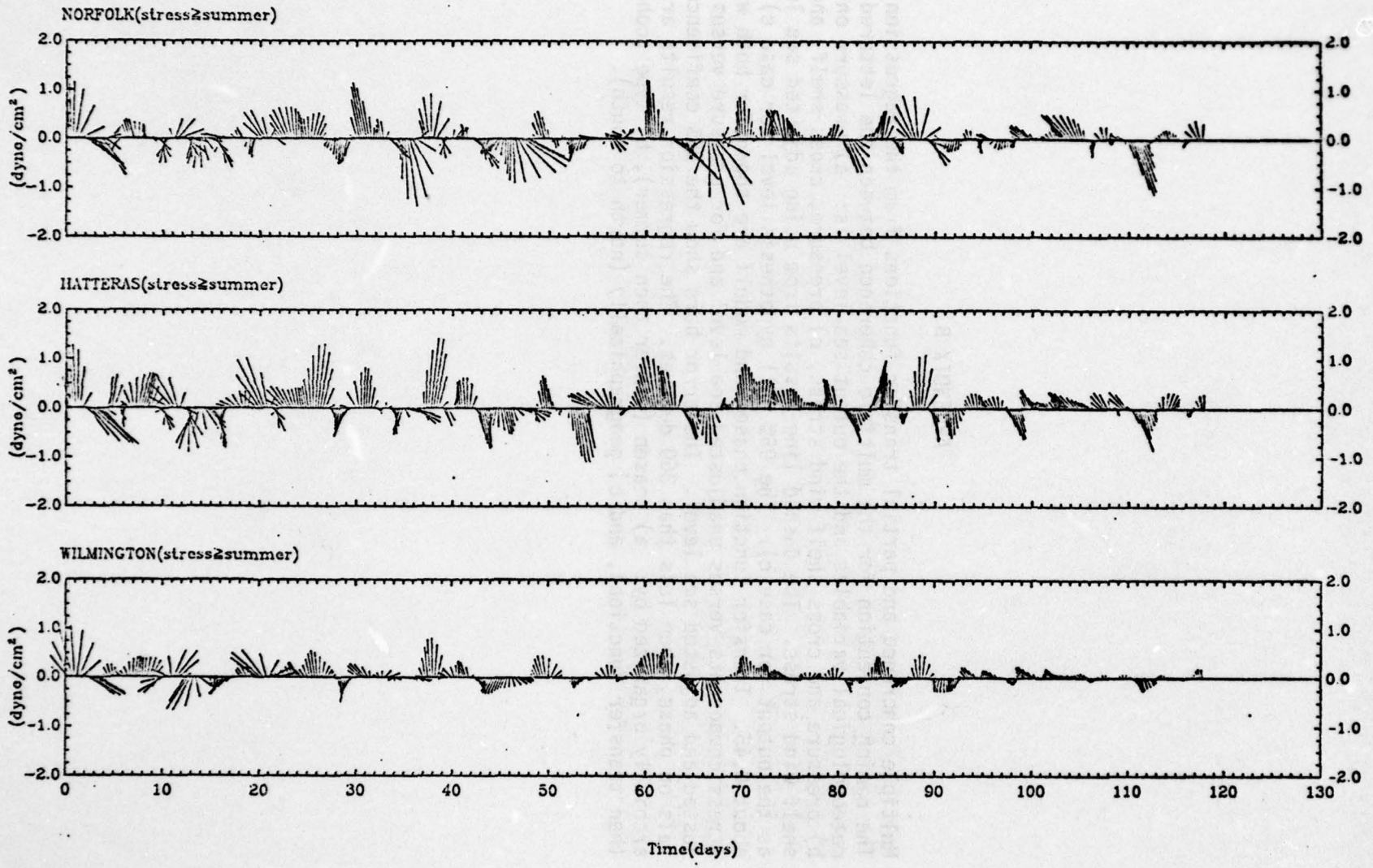

Fig. A.18 Summer wind stress vector stick plots. The ordinate scale gives the vector magnitude.

APPENDIX B

Multiple coherence and partial transfer functions from the regression model. The naming convention for the multiple coherence between the lettered input meteorological variables and the output sea level is: a) pressure only, b) pressure and cross shelf wind stress, c) pressure, cross shelf, and long-shelf wind stress. The dashed line results from using adjusted sea level as the output for case c). The 95% null hypothesis level for case c) is about 0.45. Transfer function phases and moduli are shown for both wind stress components versus unadjusted sea level and for pressure versus unadjusted and adjusted sea level. The error bars show the 95% confidence intervals on phase, when less than 360 degrees. The regression results are hierarchially organized by: a) season (winter then summer), b) type (coherence then transfer function), and c) geographically (north to south).

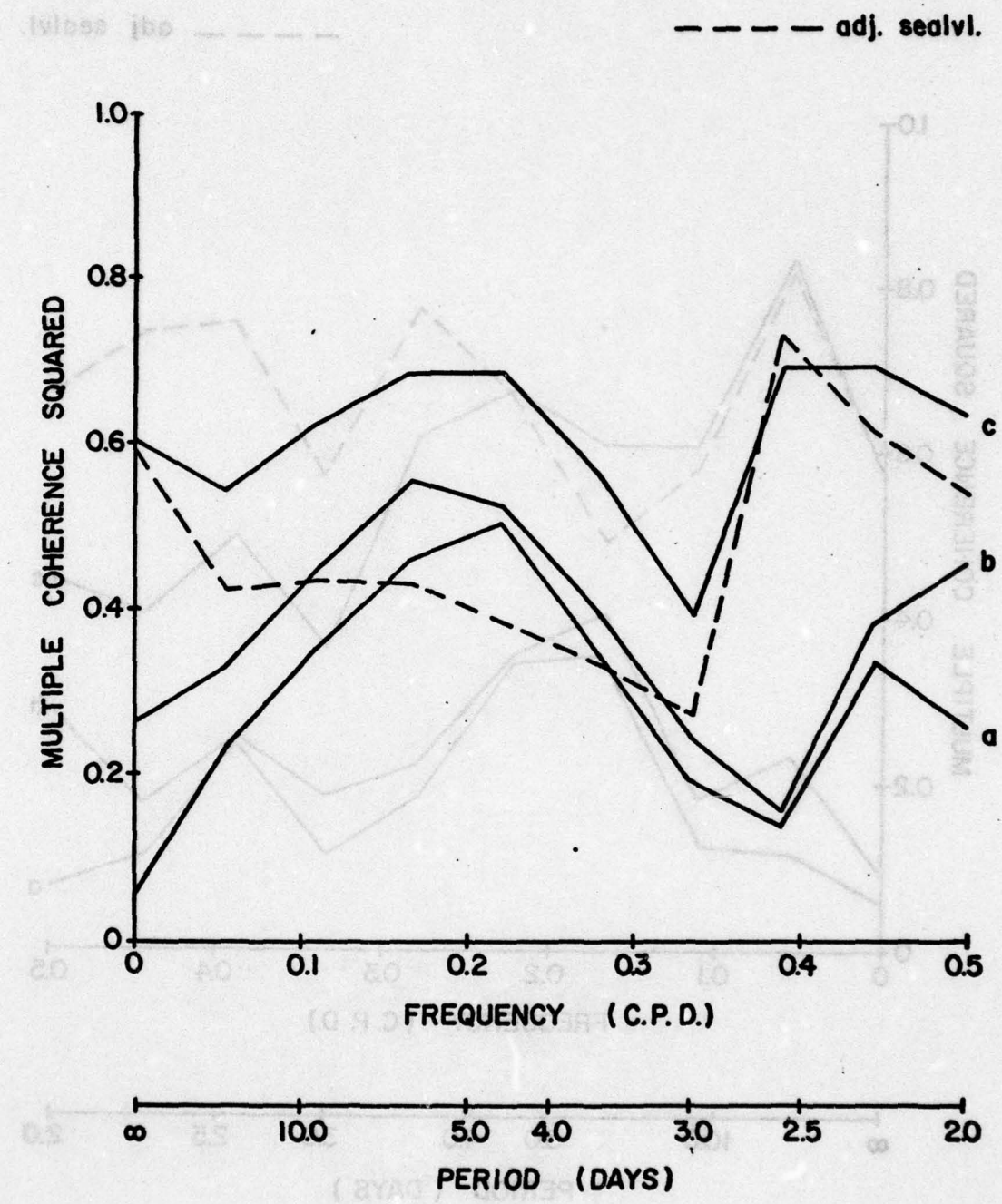

Fig. B1. Winter multiple coherence.

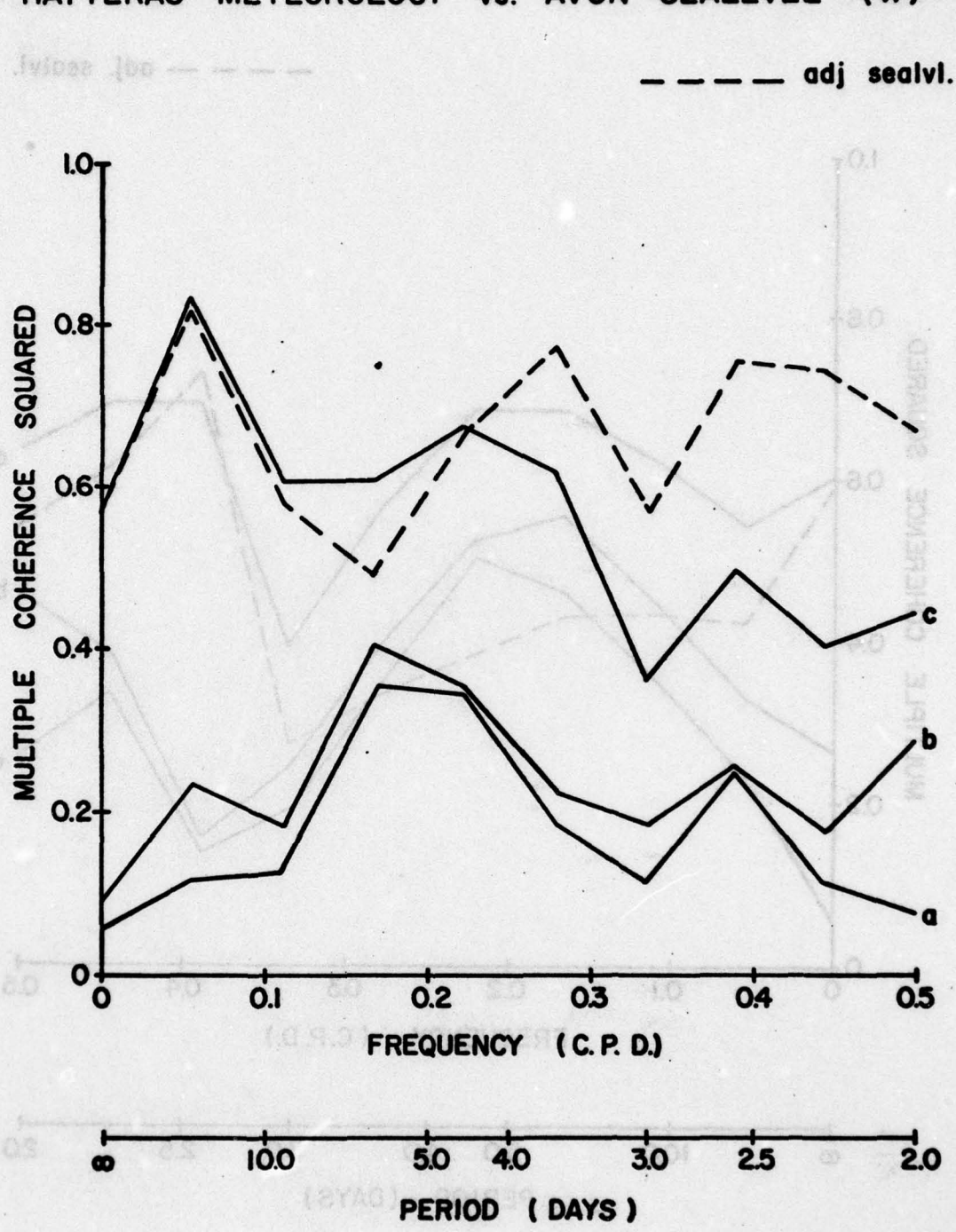

Fig. B2. Winter multiple coherence.

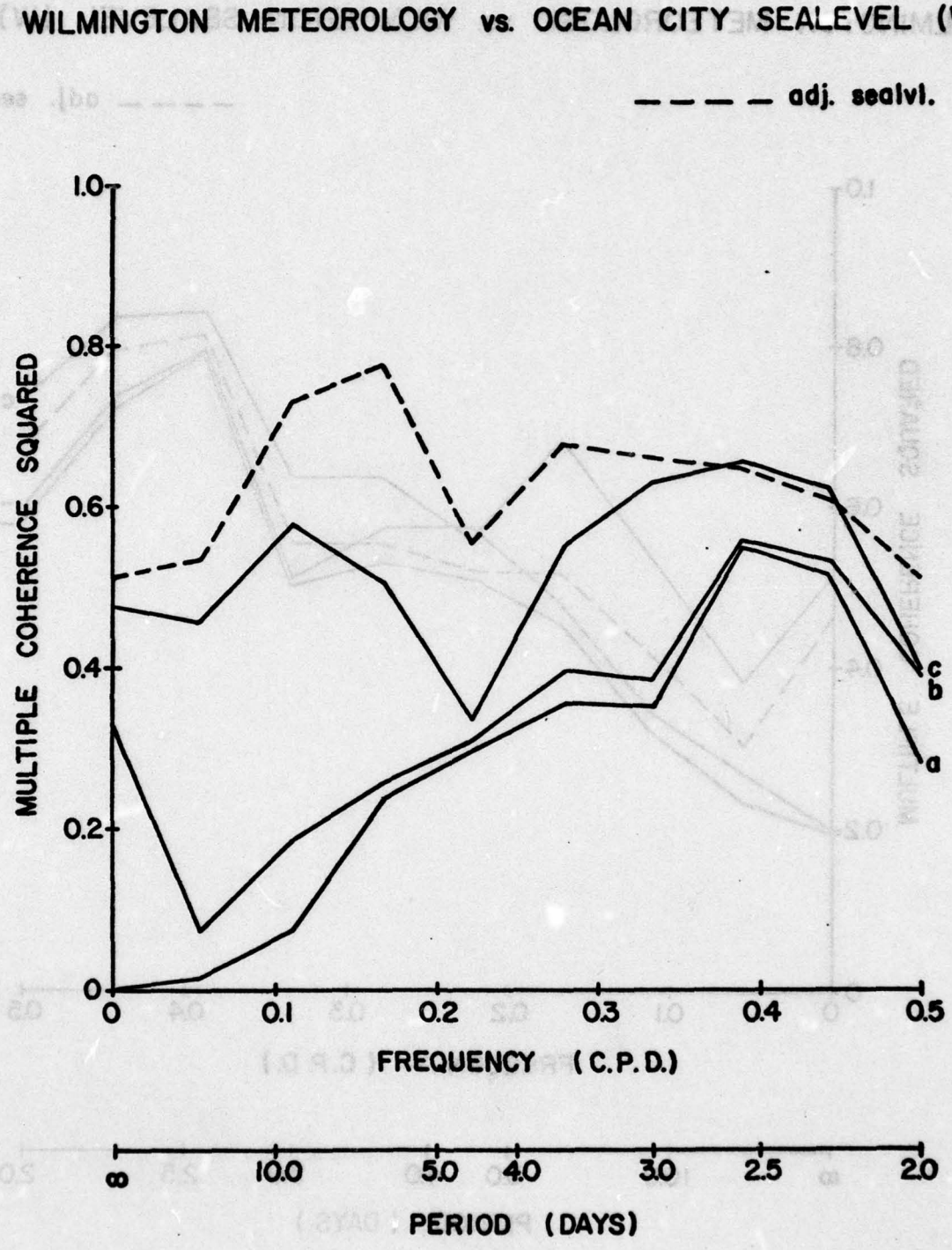

Fig. B3. Winter multiple coherence.

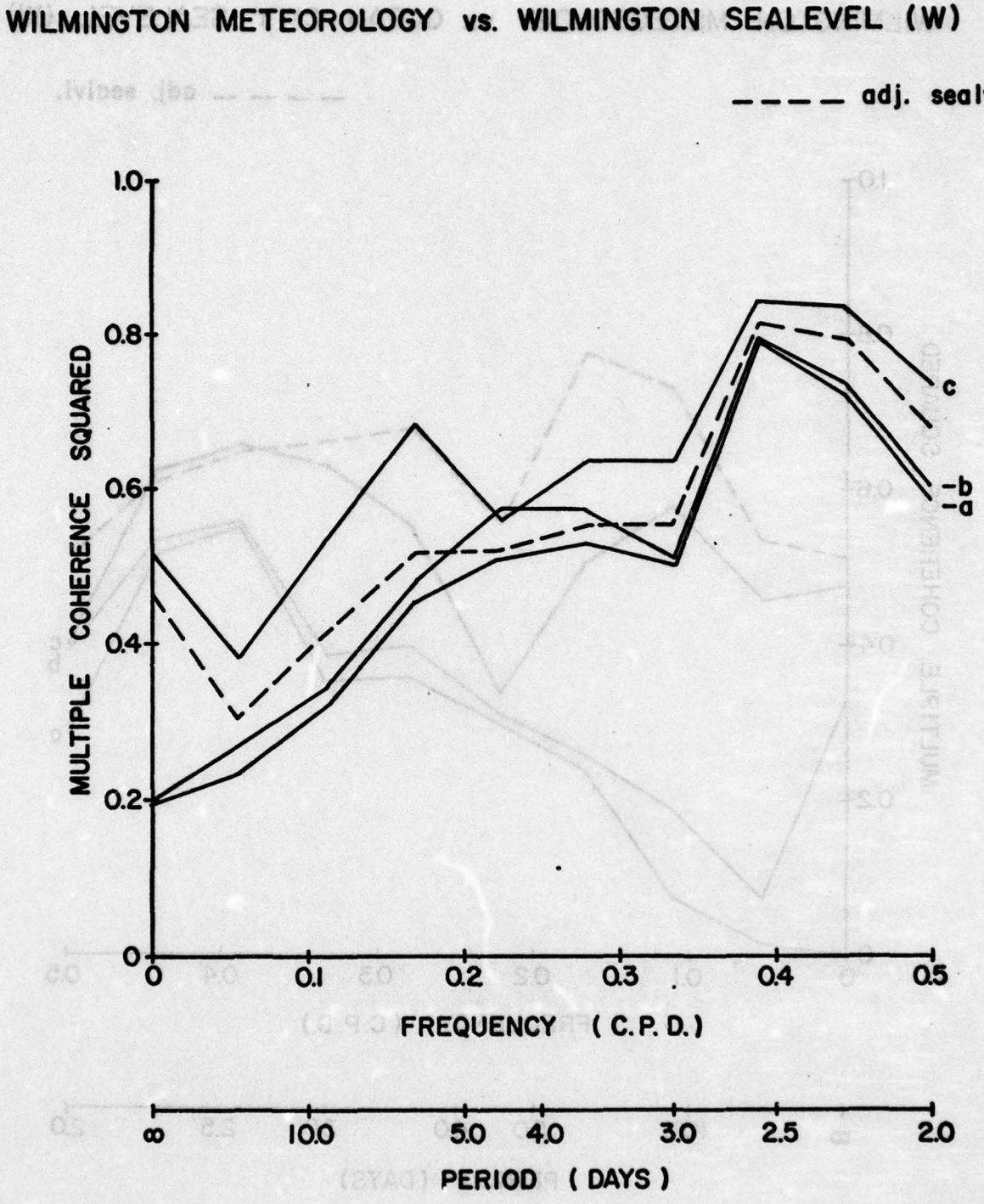

Fig. B4. Winter multiple coherence.

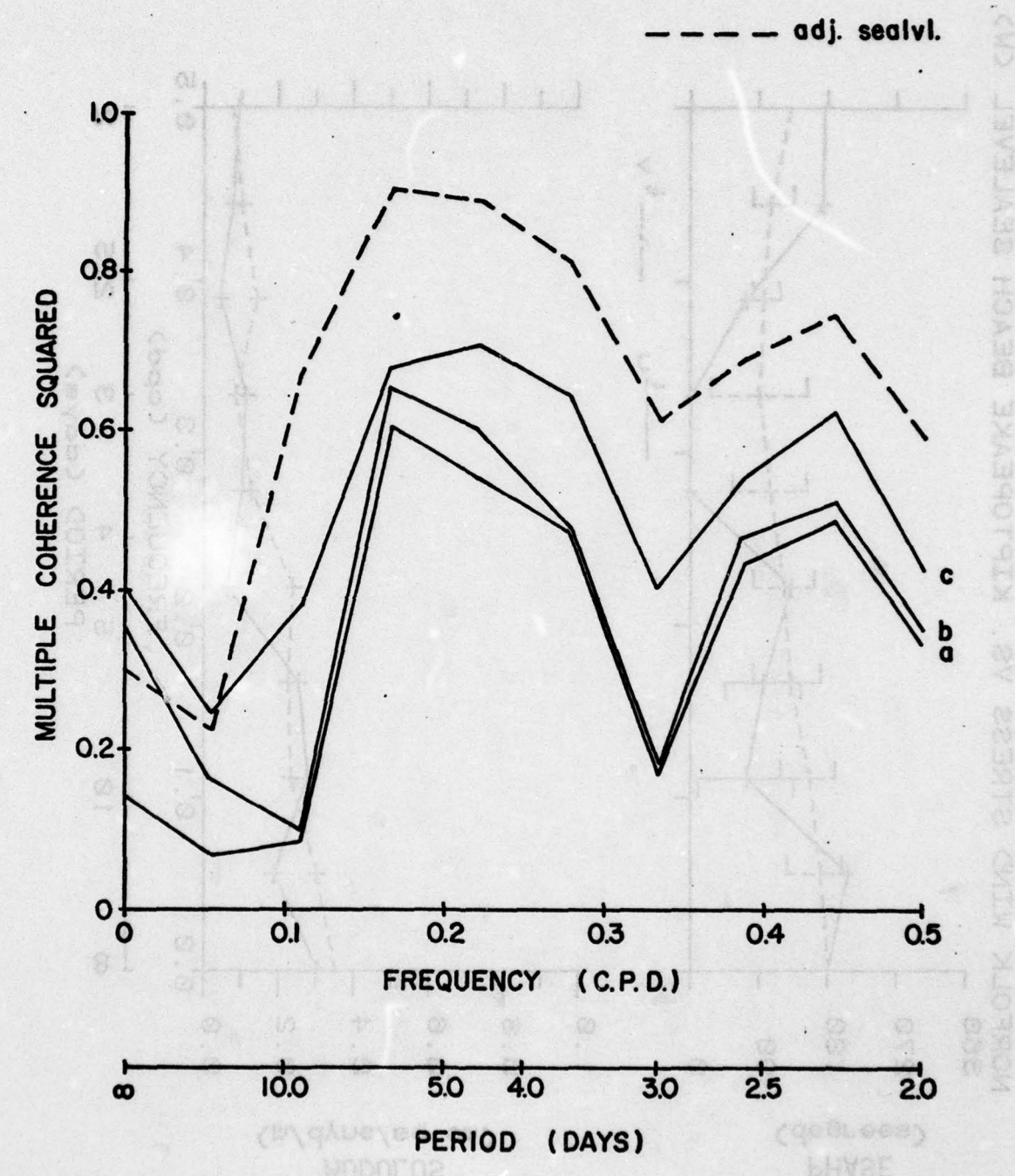

Fig. B5. Winter multiple coherence.

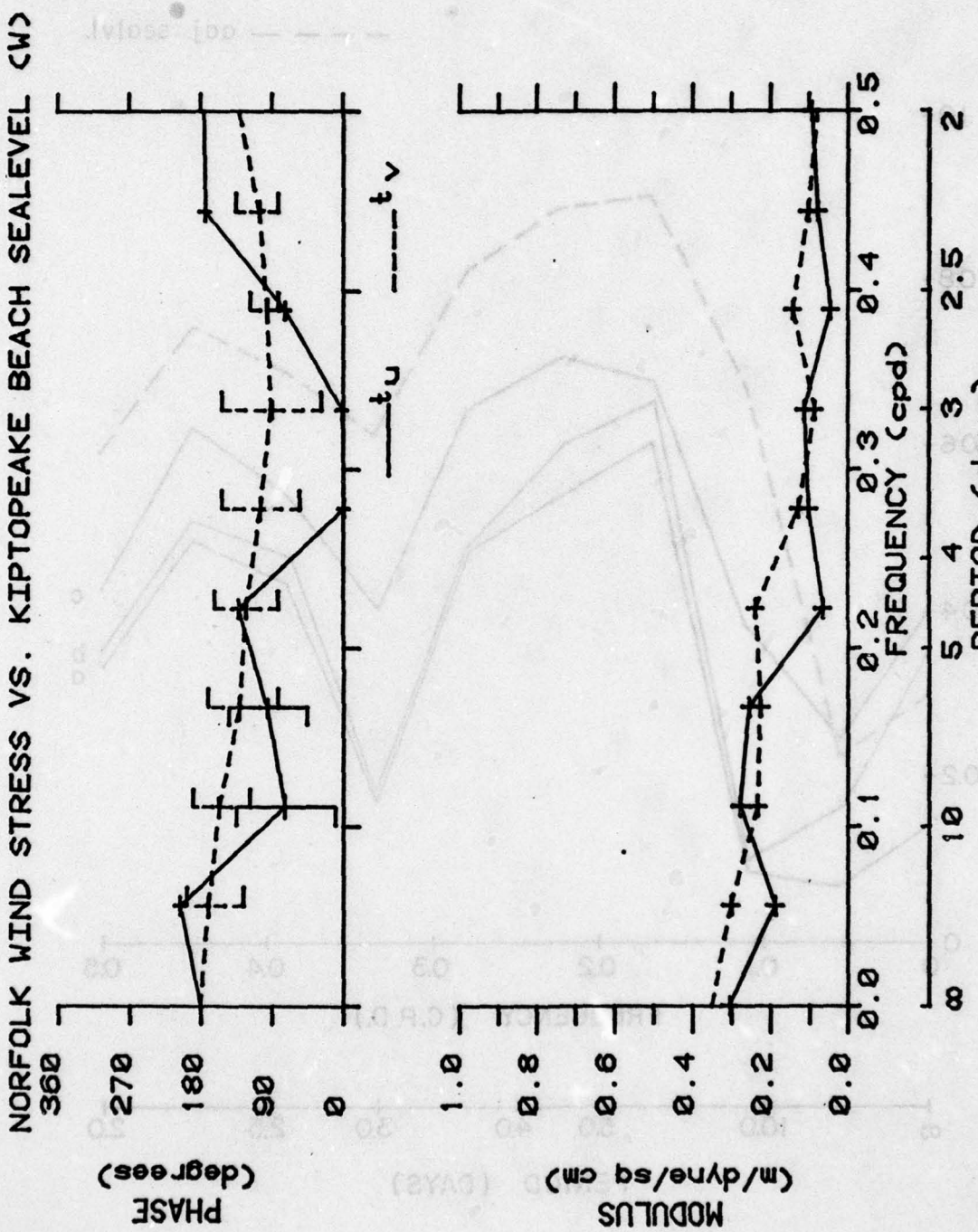

Fig. B6. Winter partial transfer functions.

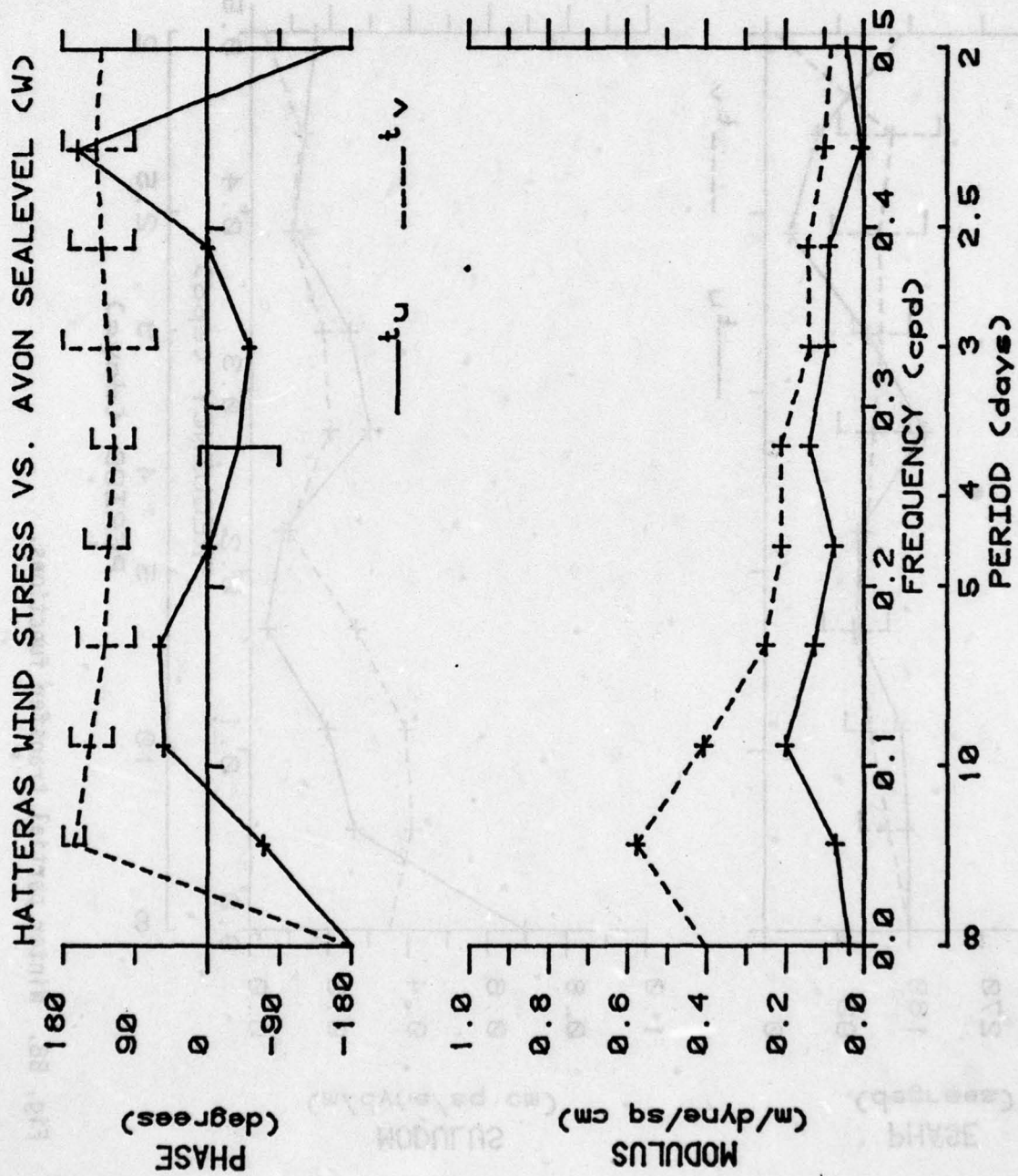

Fig. B7. Winter partial transfer functions.

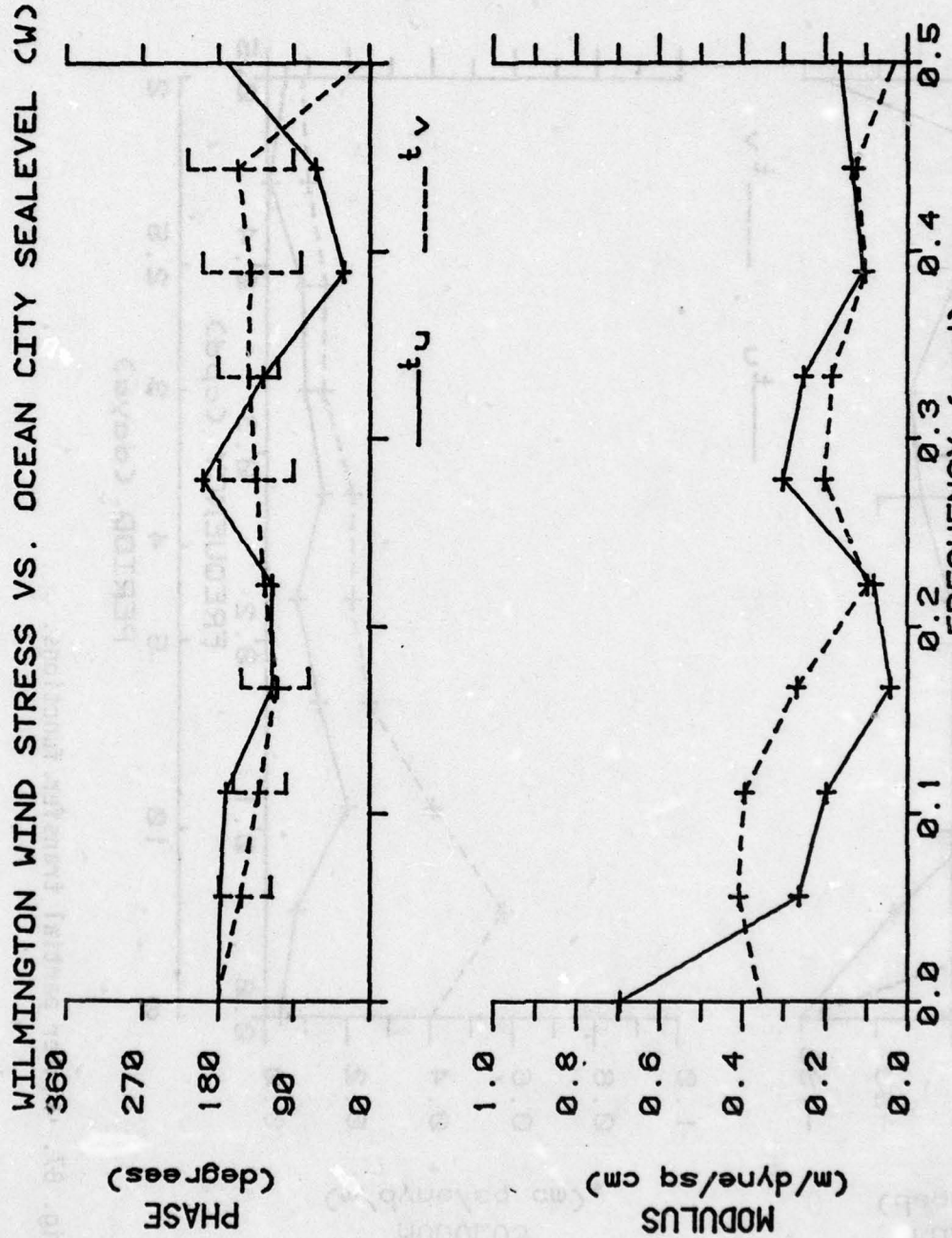

Fig. B8. Winter partial transfer functions.

AD-A072 282 TEXAS A AND M UNIV COLLEGE STATION DEPT OF OCEANOGRAPHY F/G 8/3
LONG WAVE COUPLING OF THE MID AND SOUTH ATLANTIC BIGHTS FORCED --ETC(U)
MAY 79 D A BROOKS N00014-77-C-0354
UNCLASSIFIED TAMU-REF-79-3-T NL

2 OF 2
AD
A072282

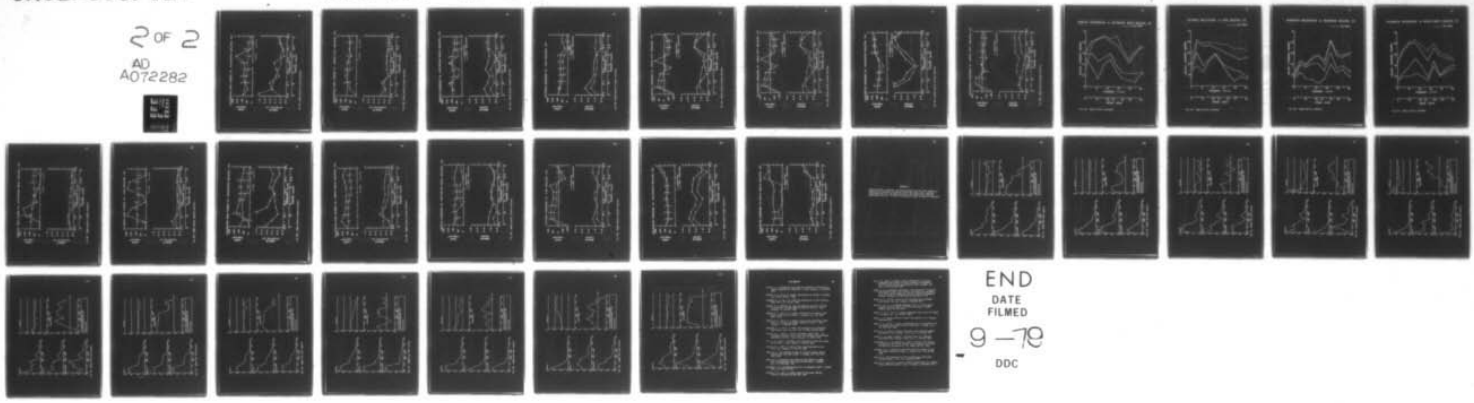

END
DATE
FILMED
9-79
DDC

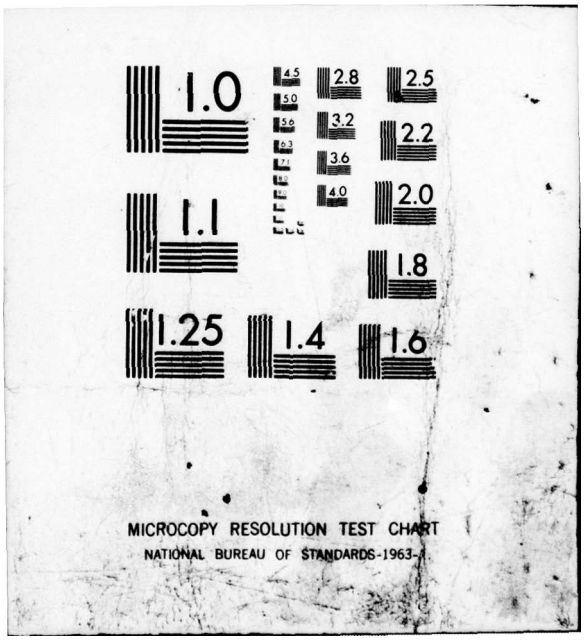
1.0
1.1
1.25
1.4
1.6
1.8
2.0
2.2
2.5
2.8
3.2
3.6
4.0
4.5
5.0
5.6
6.3
MICROCOPY RESOLUTION TEST CHART
NATIONAL BUREAU OF STANDARDS-1963-A

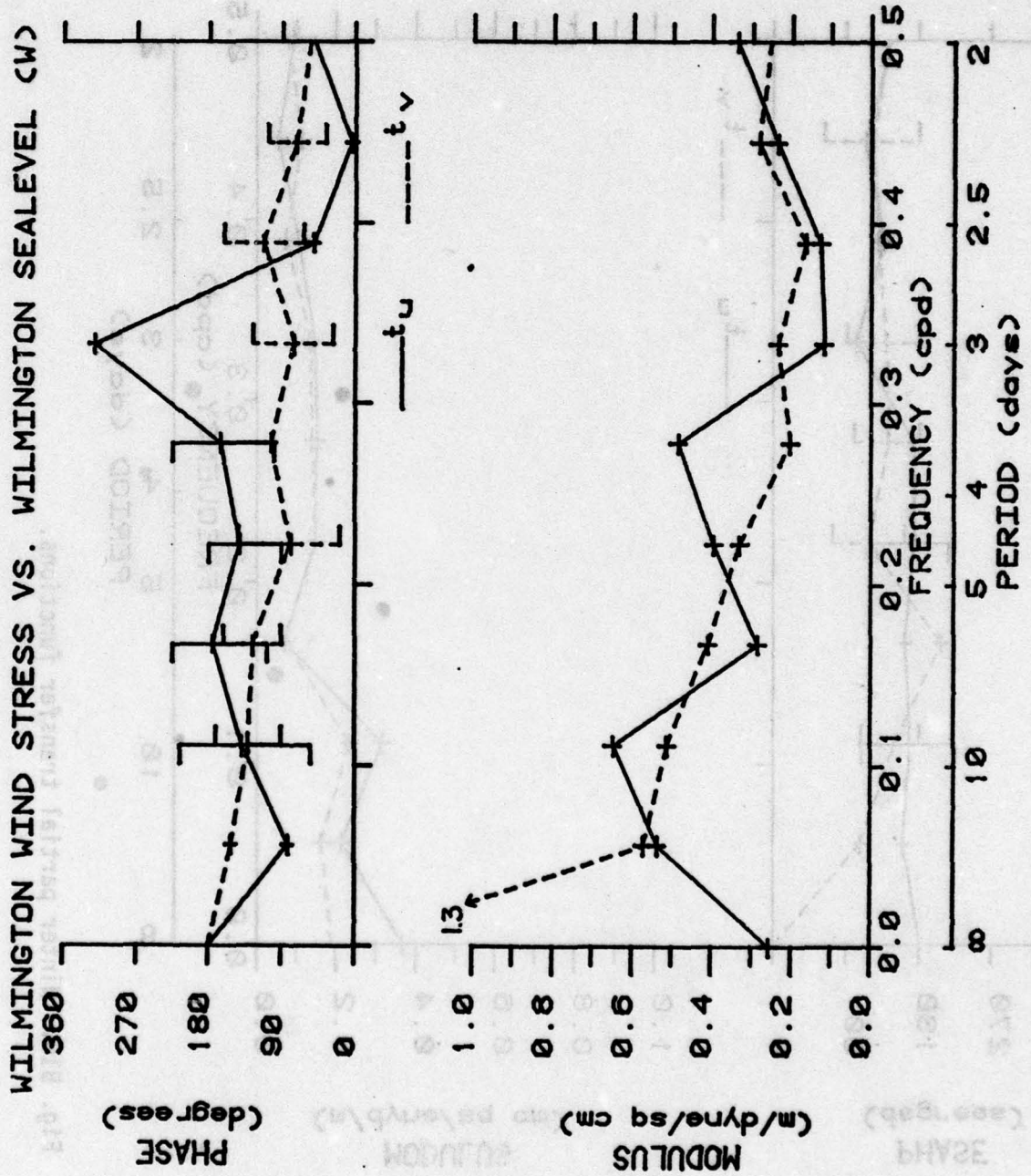

Fig. B9. Winter partial transfer functions.

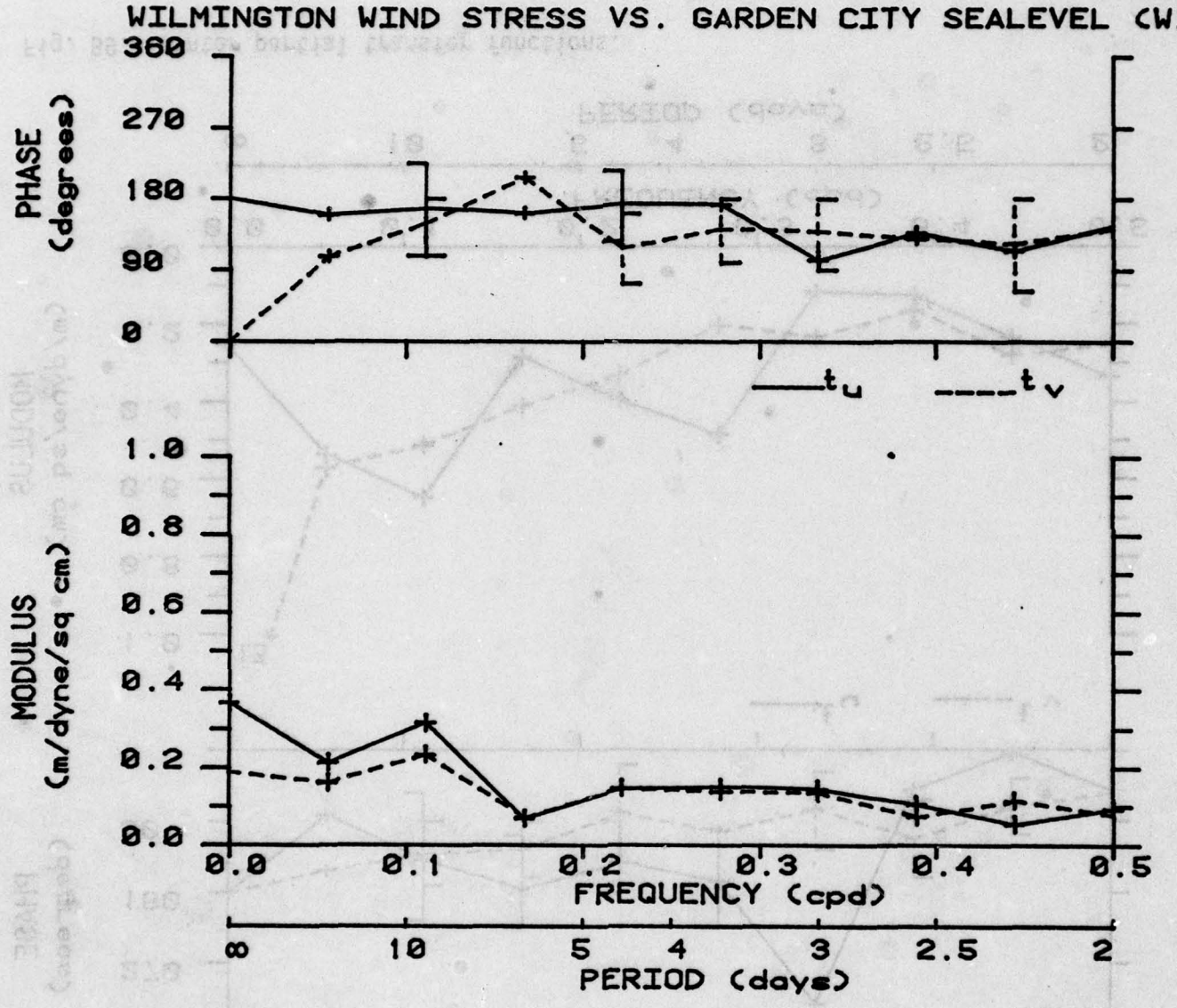

Fig. B10. Winter partial transfer functions.

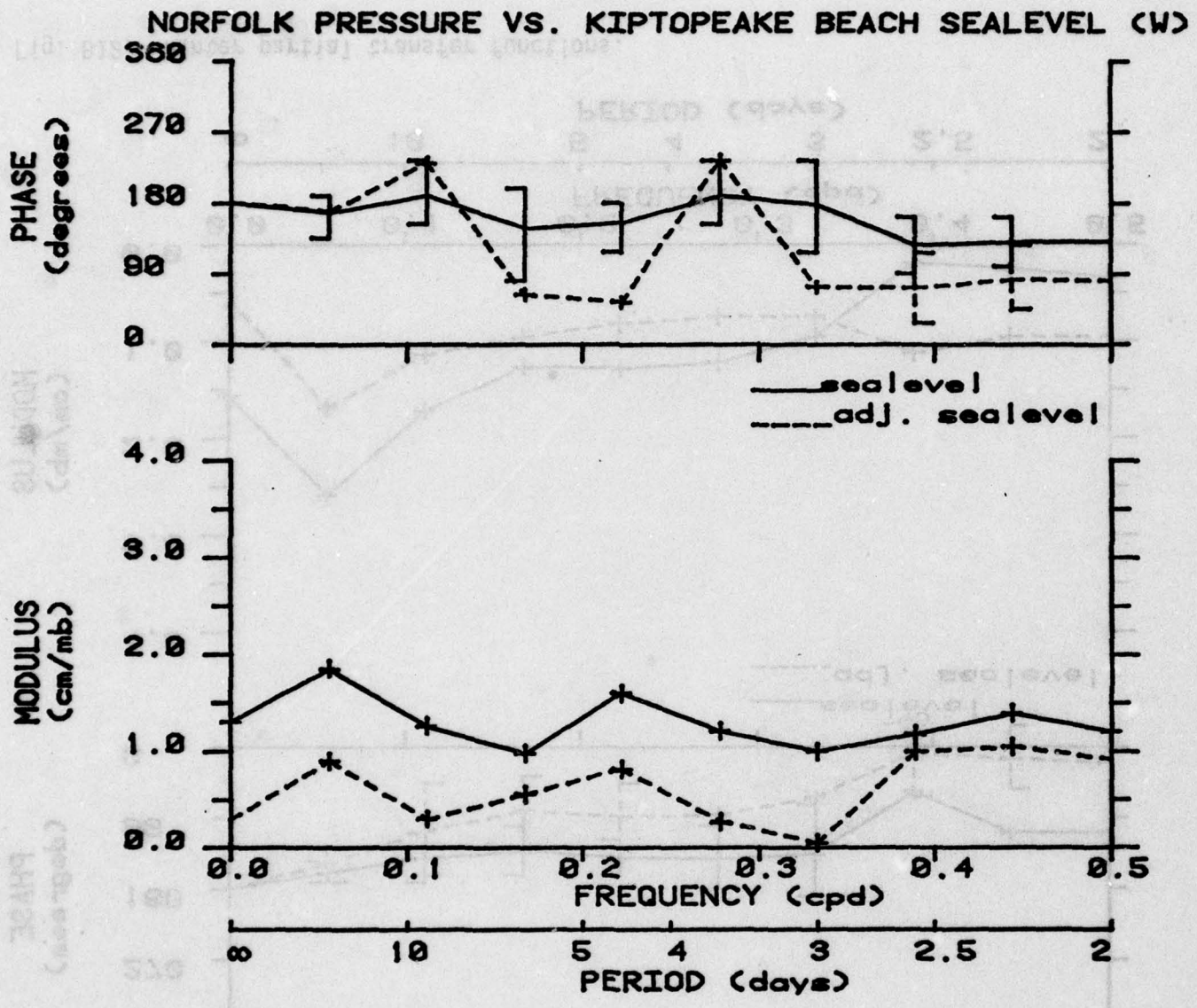

Fig. B11. Winter partial transfer functions.

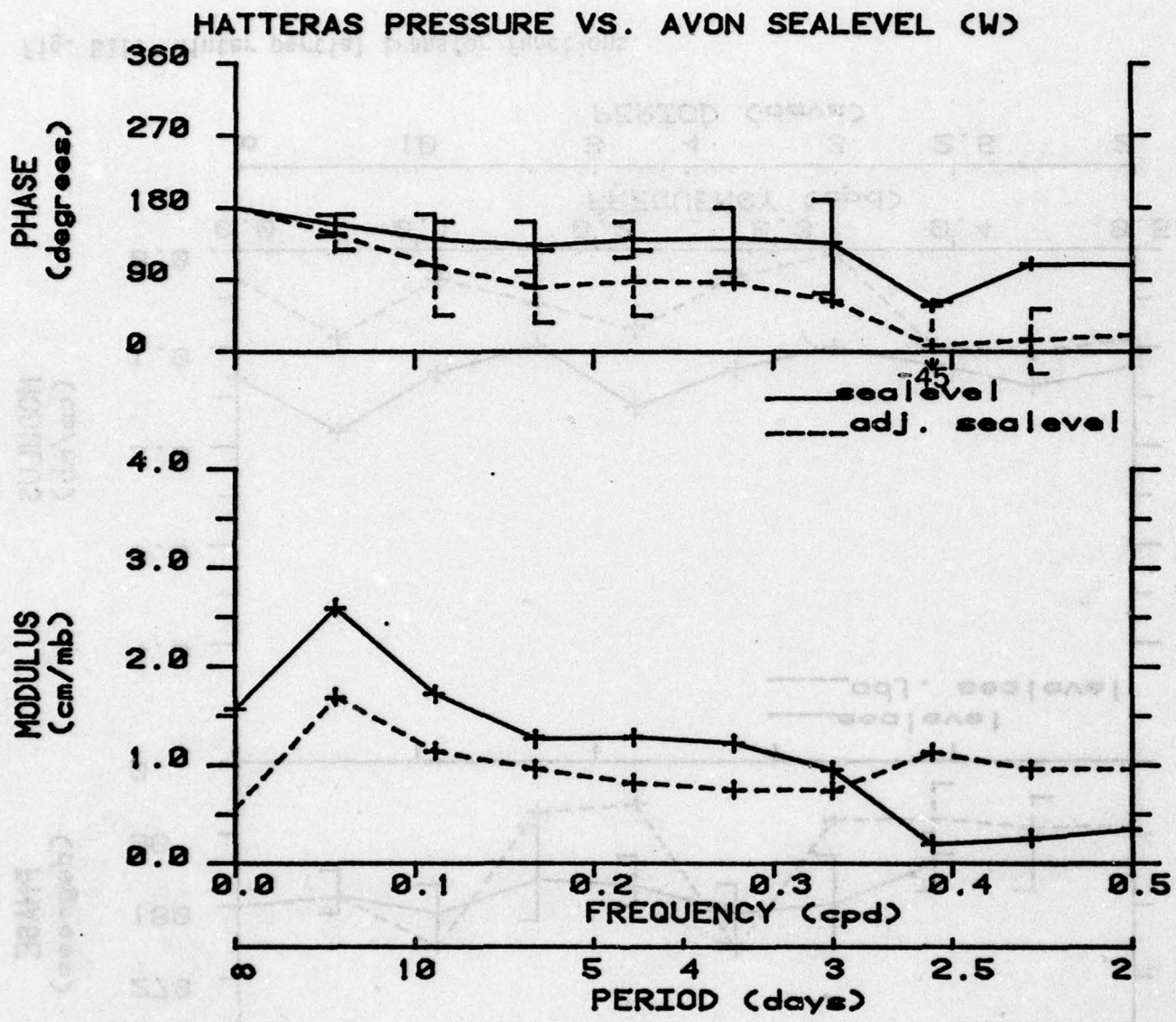

Fig. B12. Winter partial transfer functions.

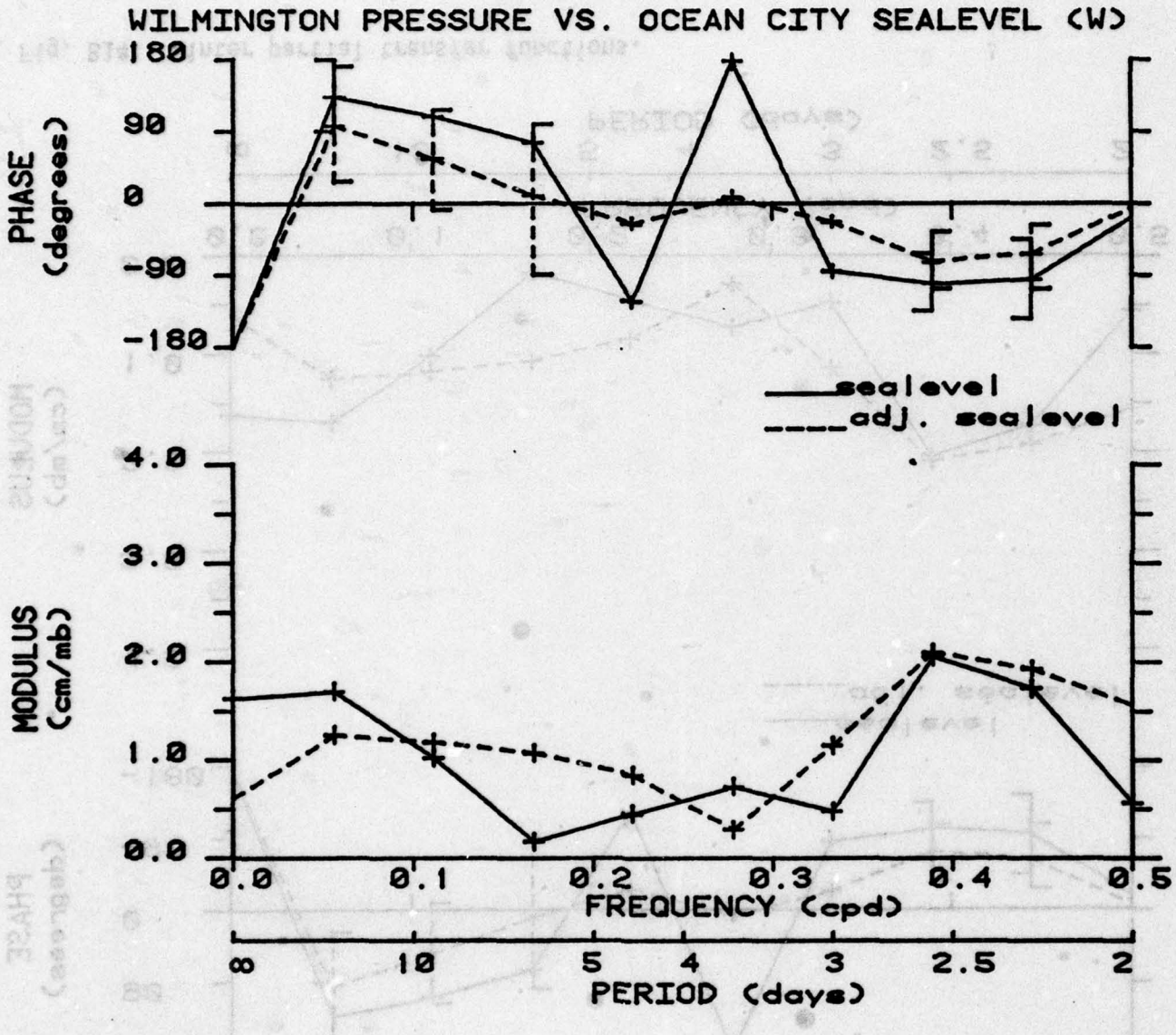

Fig. B13. Winter partial transfer functions.

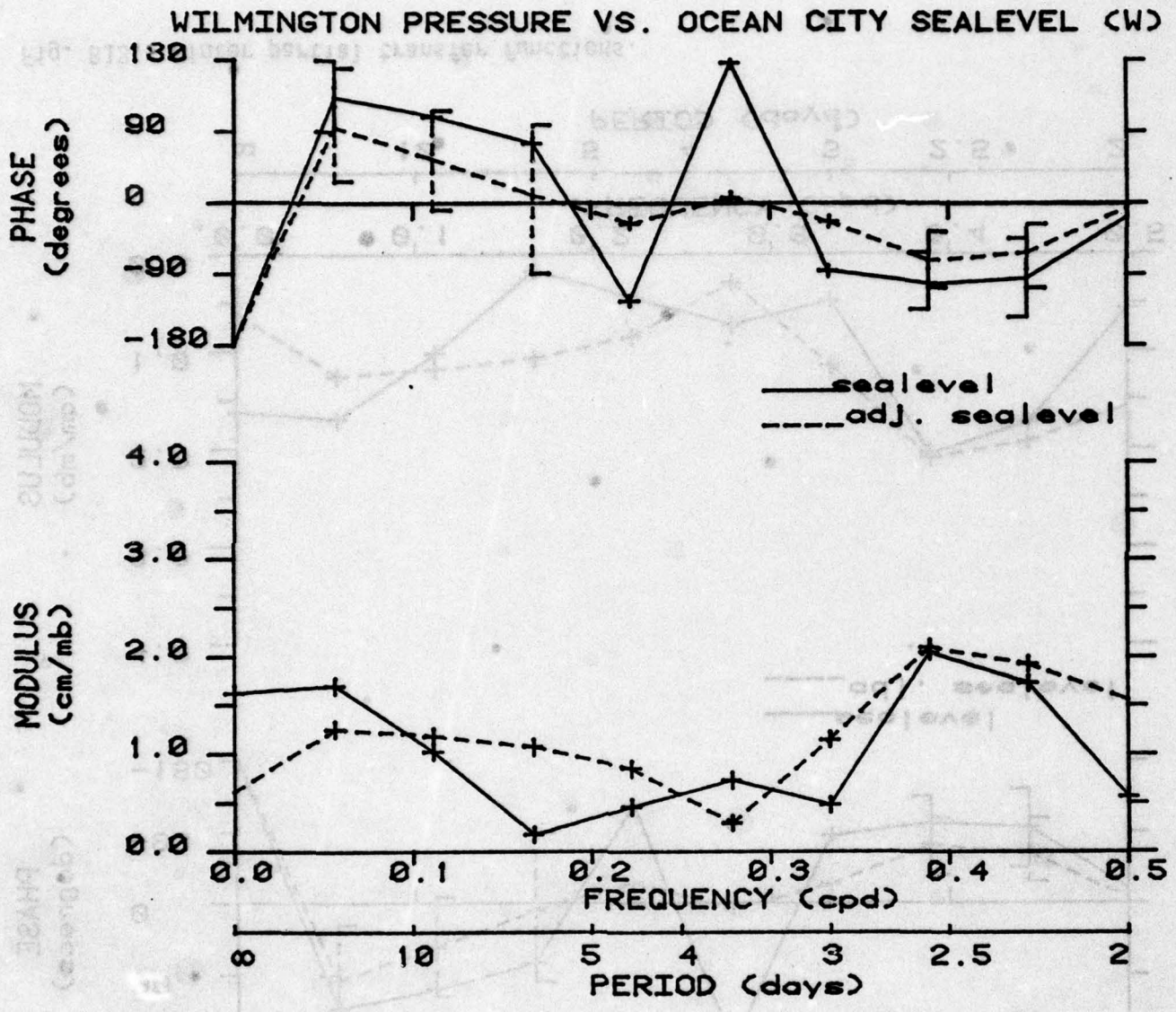

Fig. B14. Winter partial transfer functions.

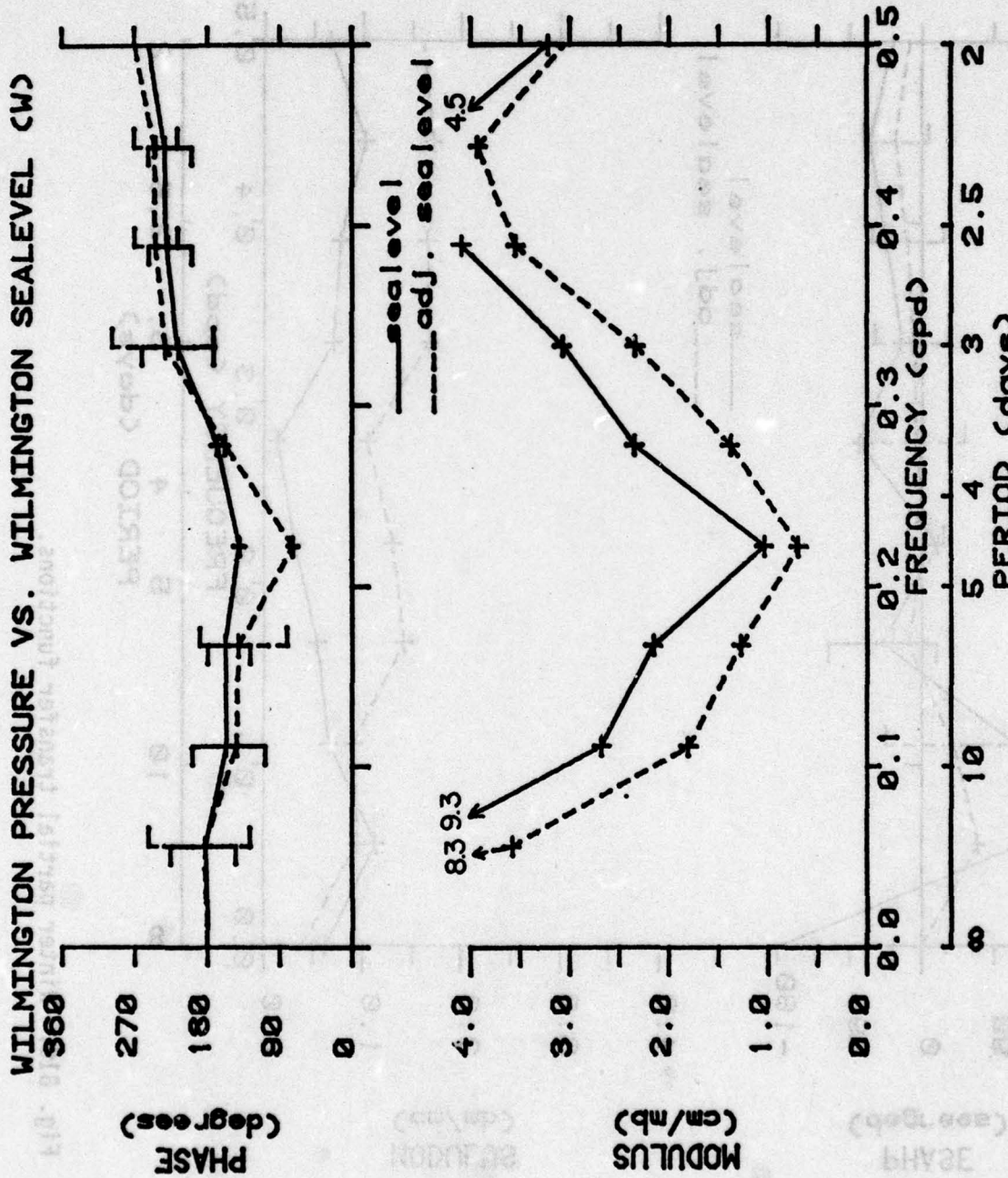

Fig. B15. Winter partial transfer functions.

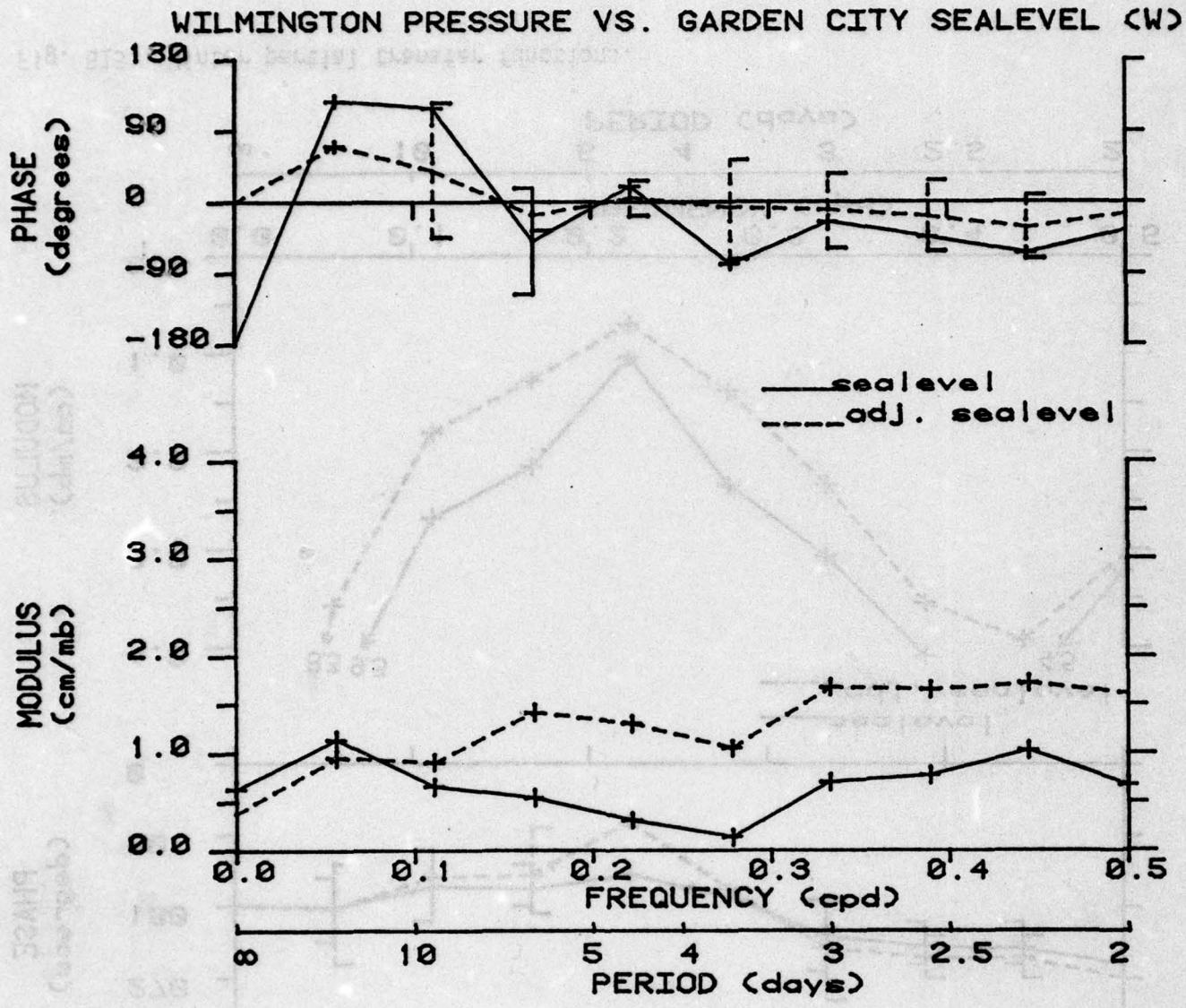

Fig. B16. Winter partial transfer functions.

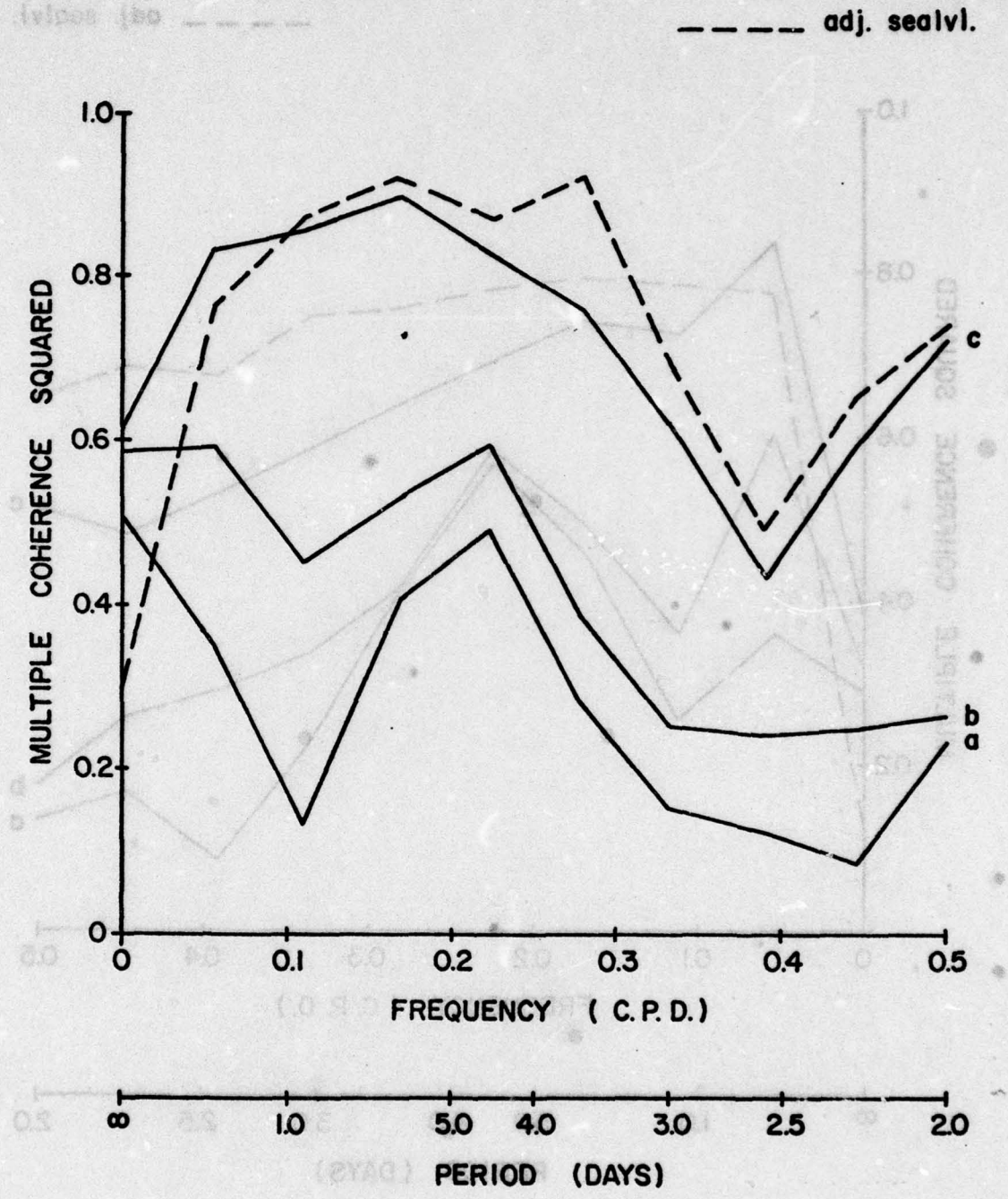

Fig. B17. Summer multiple coherence.

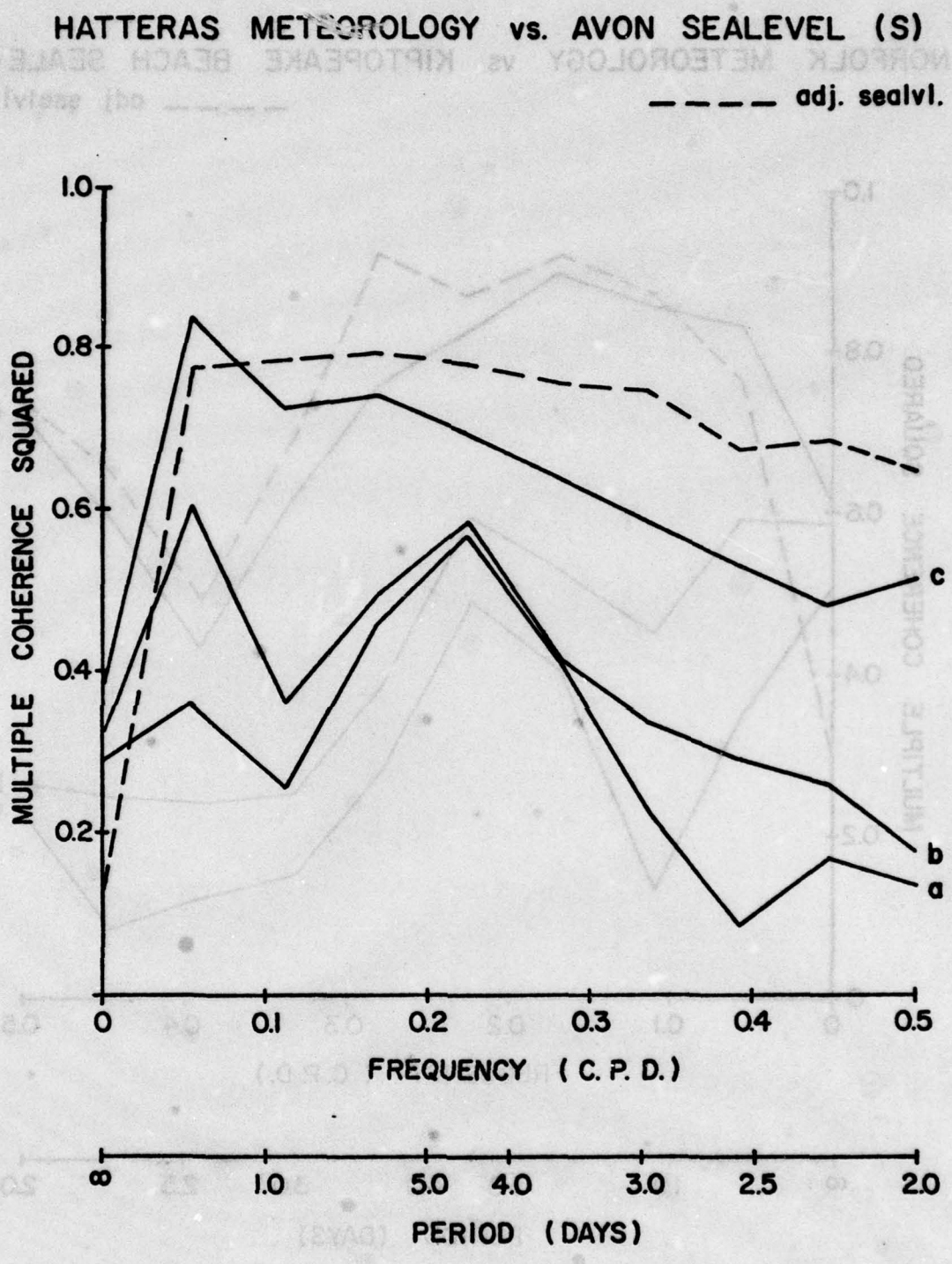

Fig. B18. Summer multiple coherence.

WILMINGTON METEOROLOGY vs. WILMINGTON SEALEVEL (S)

adj. sealvl.

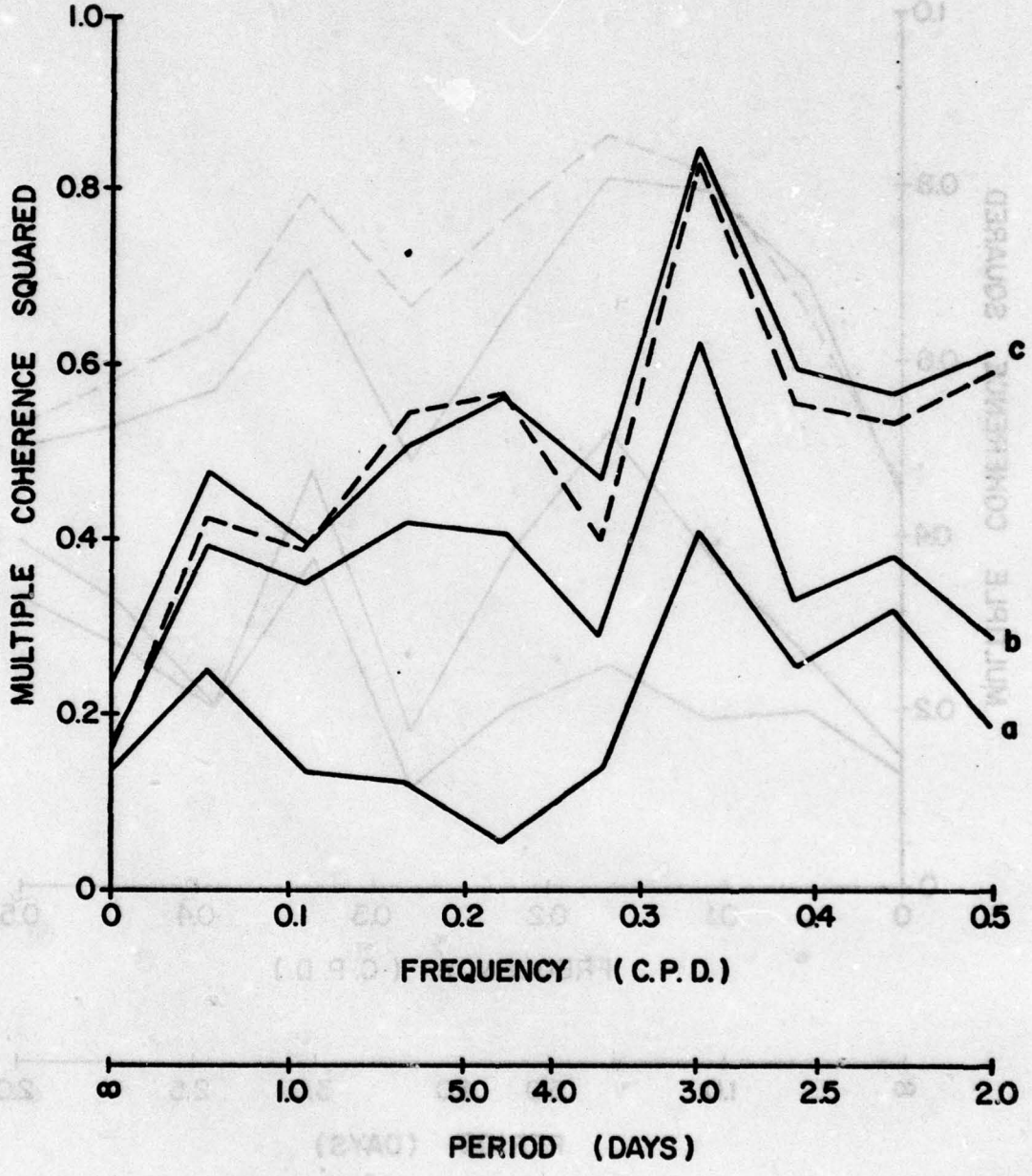

Fig. B19. Summer multiple coherence.

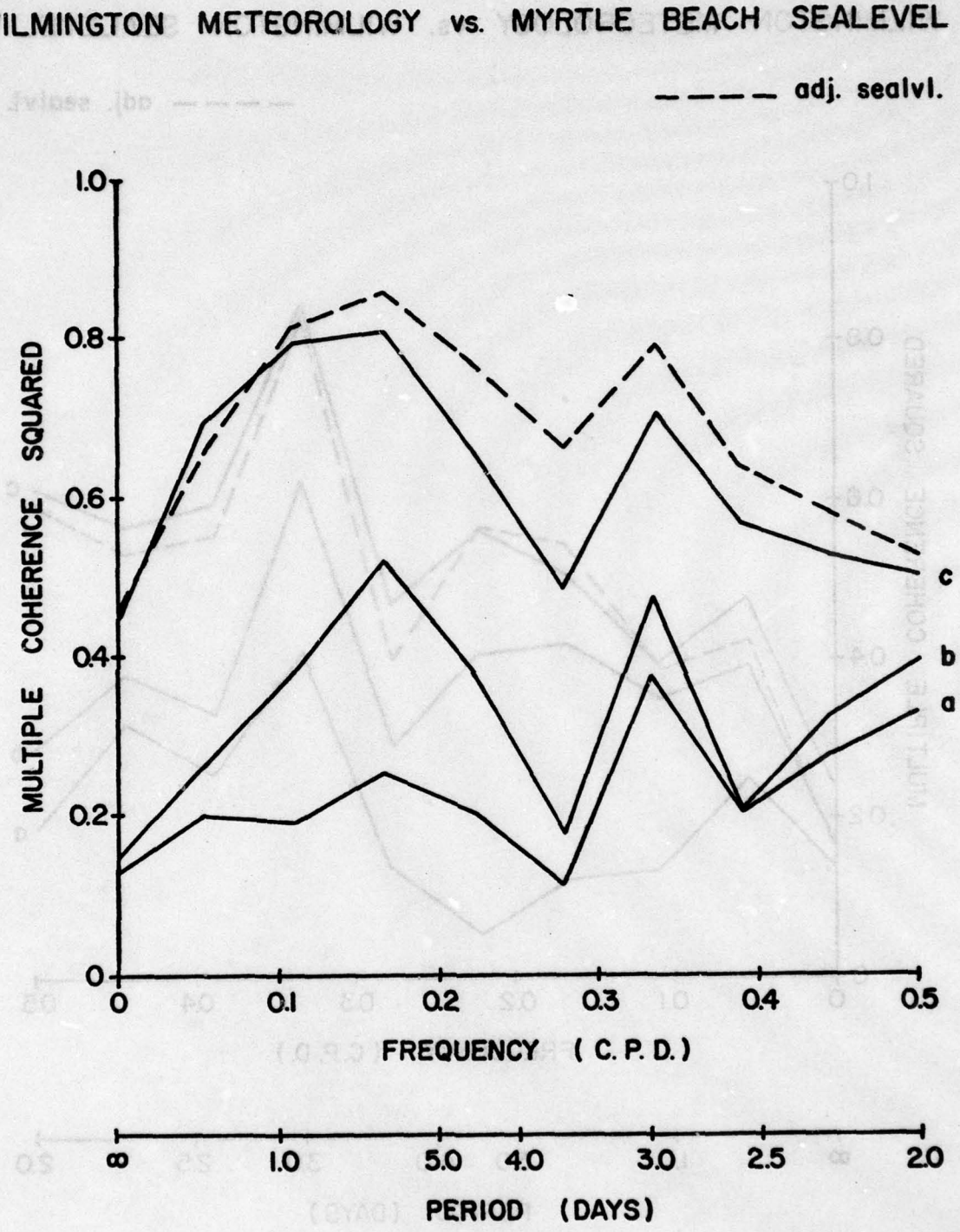

Fig. B20. Summer multiple coherence.

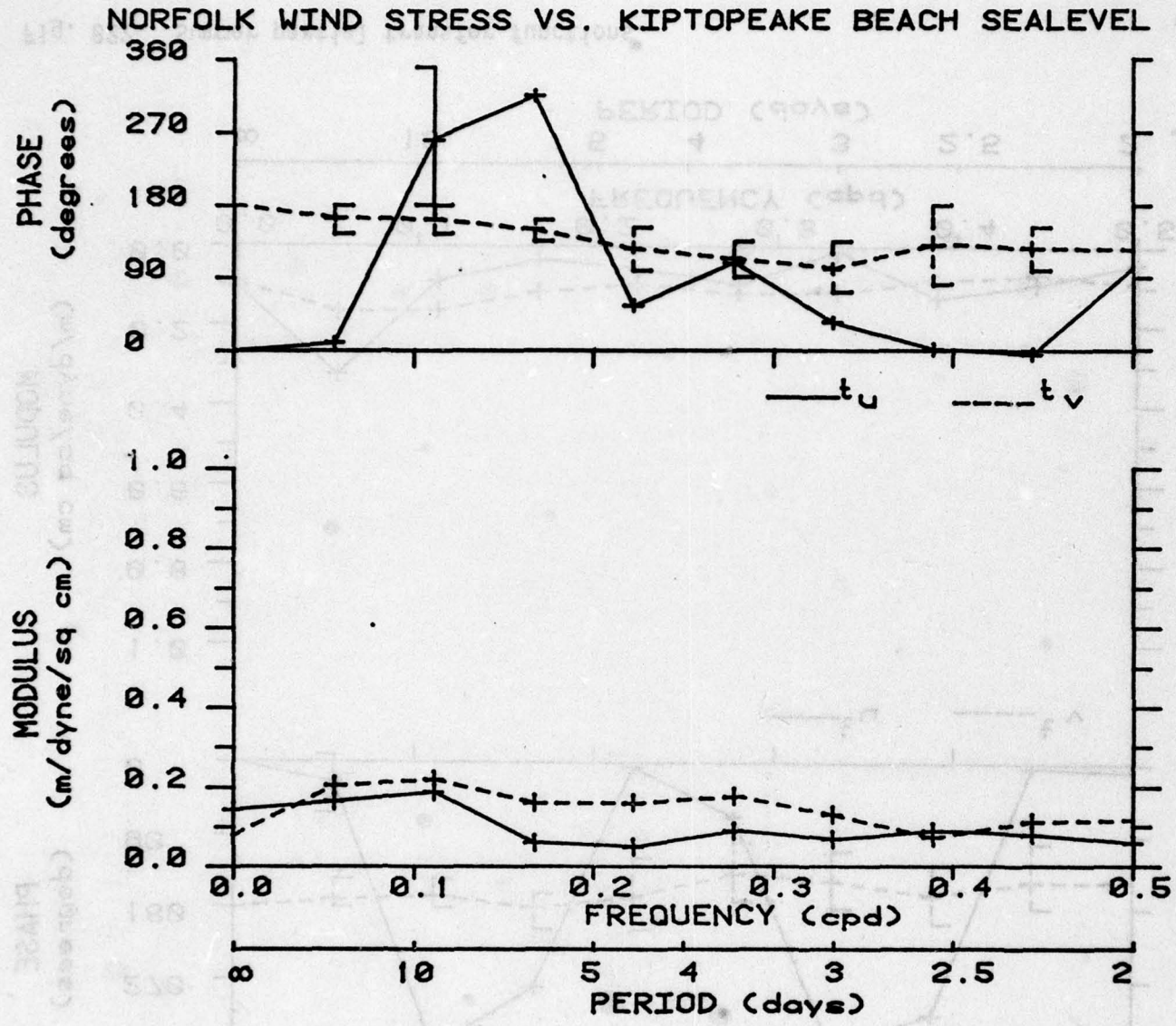

Fig. B21. Summer partial transfer functions.

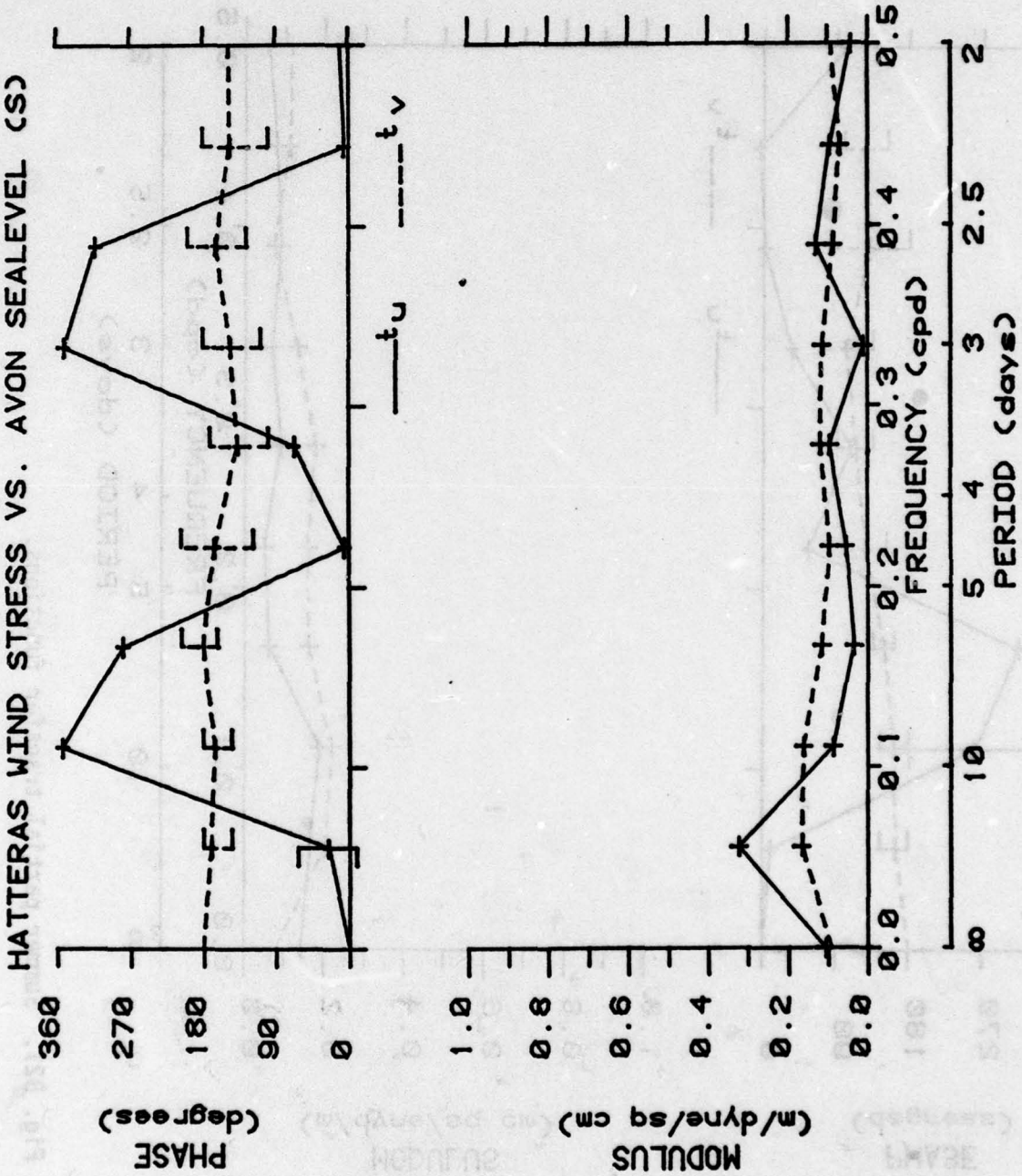

Fig. B22. Summer partial transfer functions.

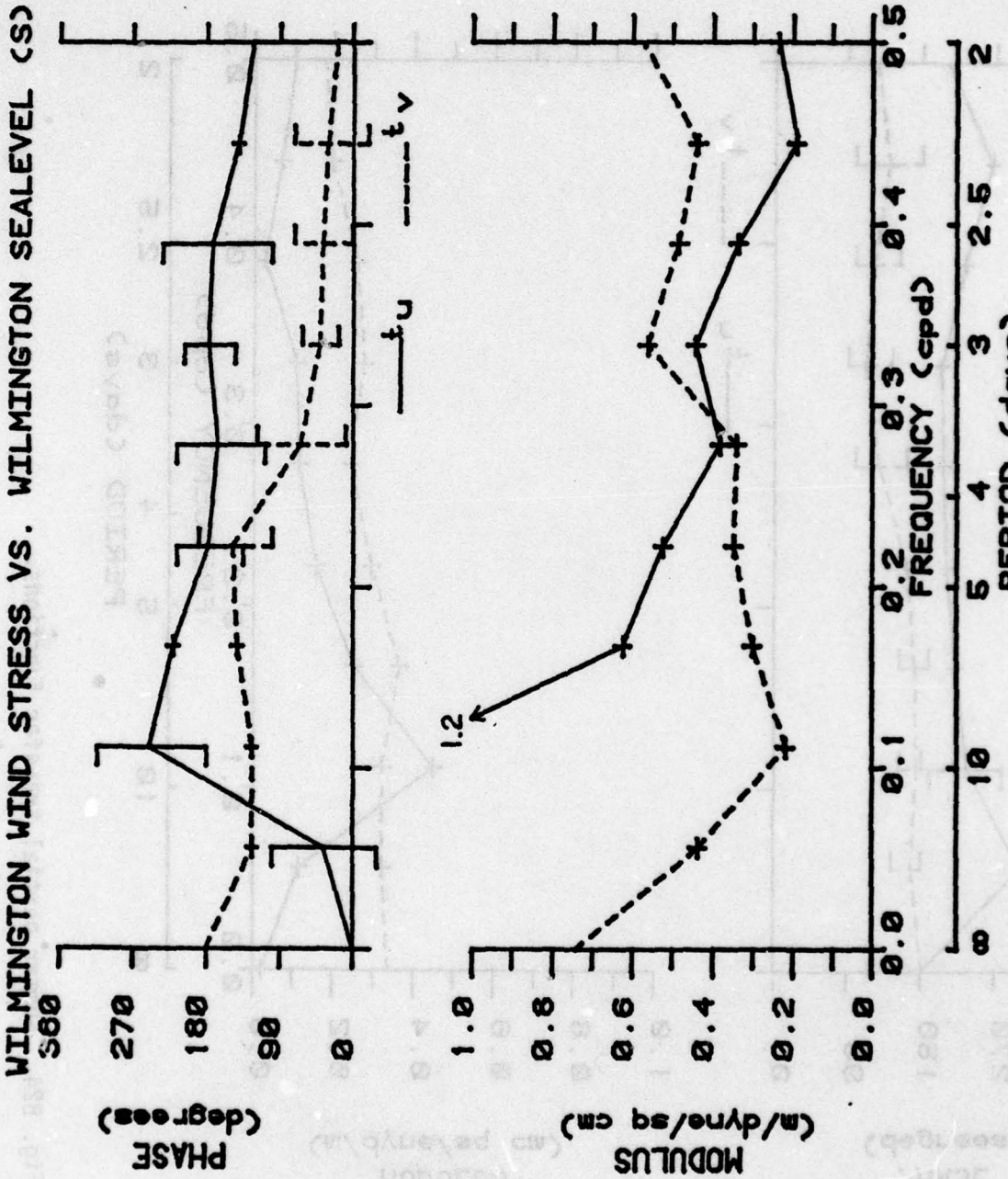

Fig. B23. Summer partial transfer functions.

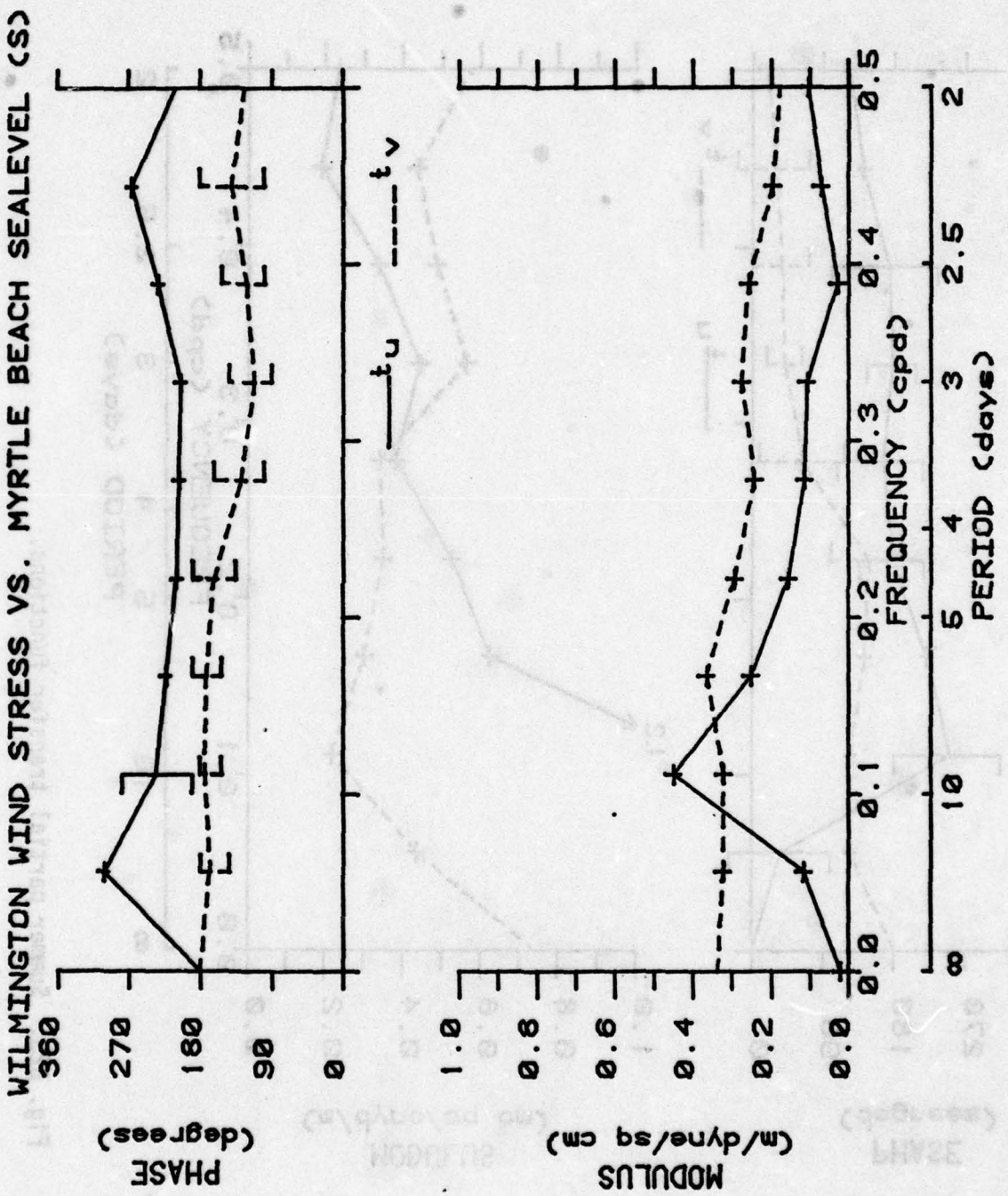

Fig. B24. Summer partial transfer functions.

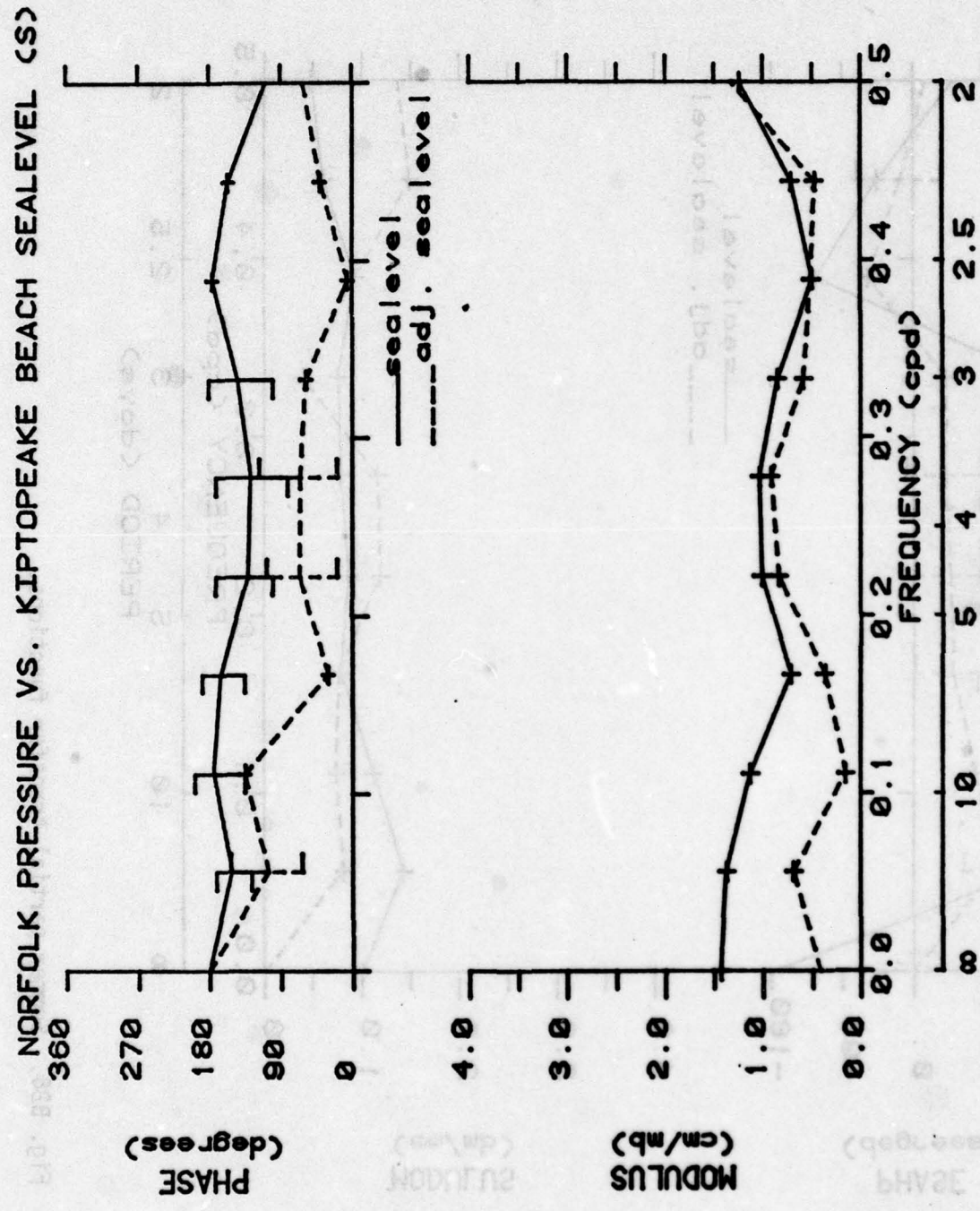

Fig. B25. Summer partial transfer functions.

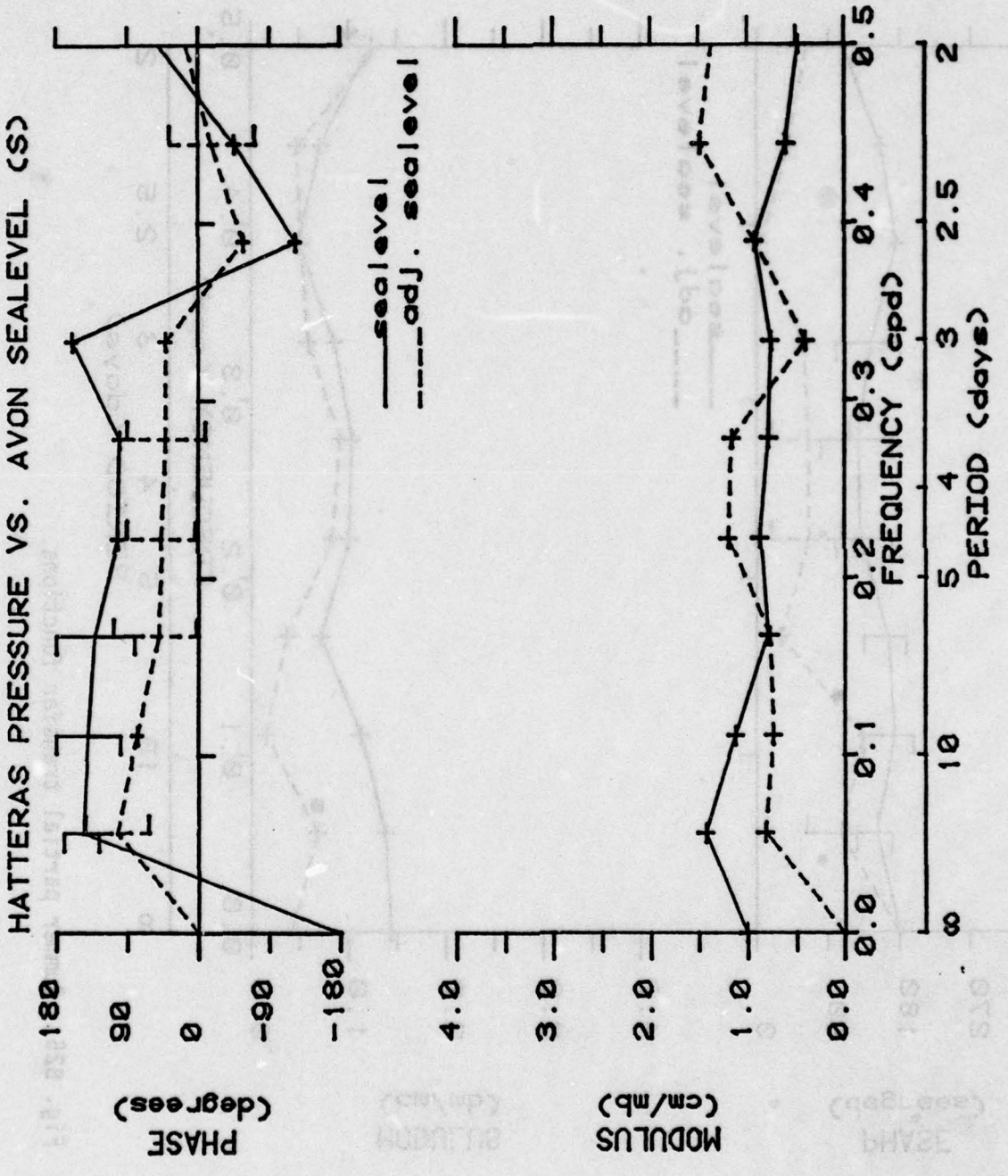

Fig. B26. Summer partial transfer functions.

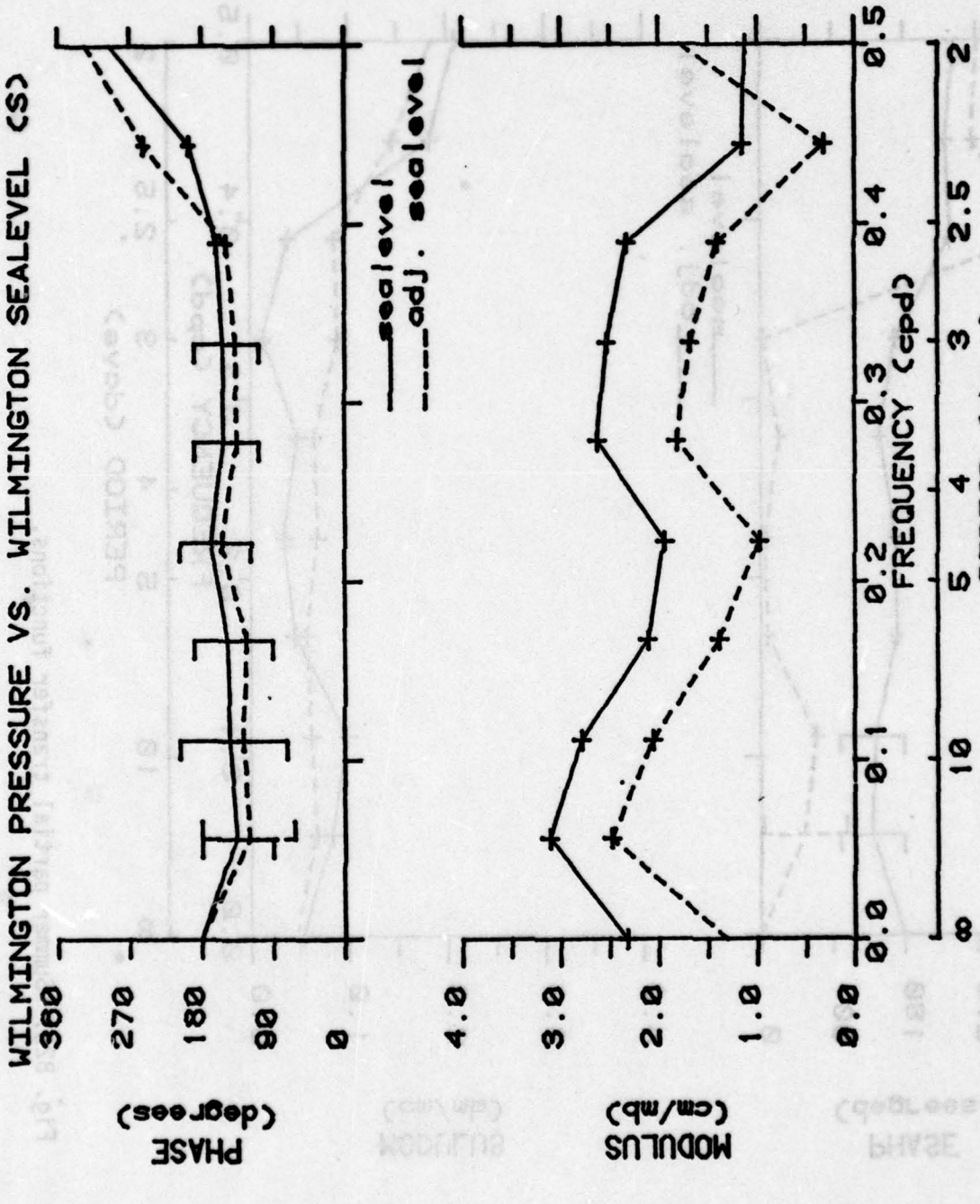

Fig. B27. Summer partial transfer functions.

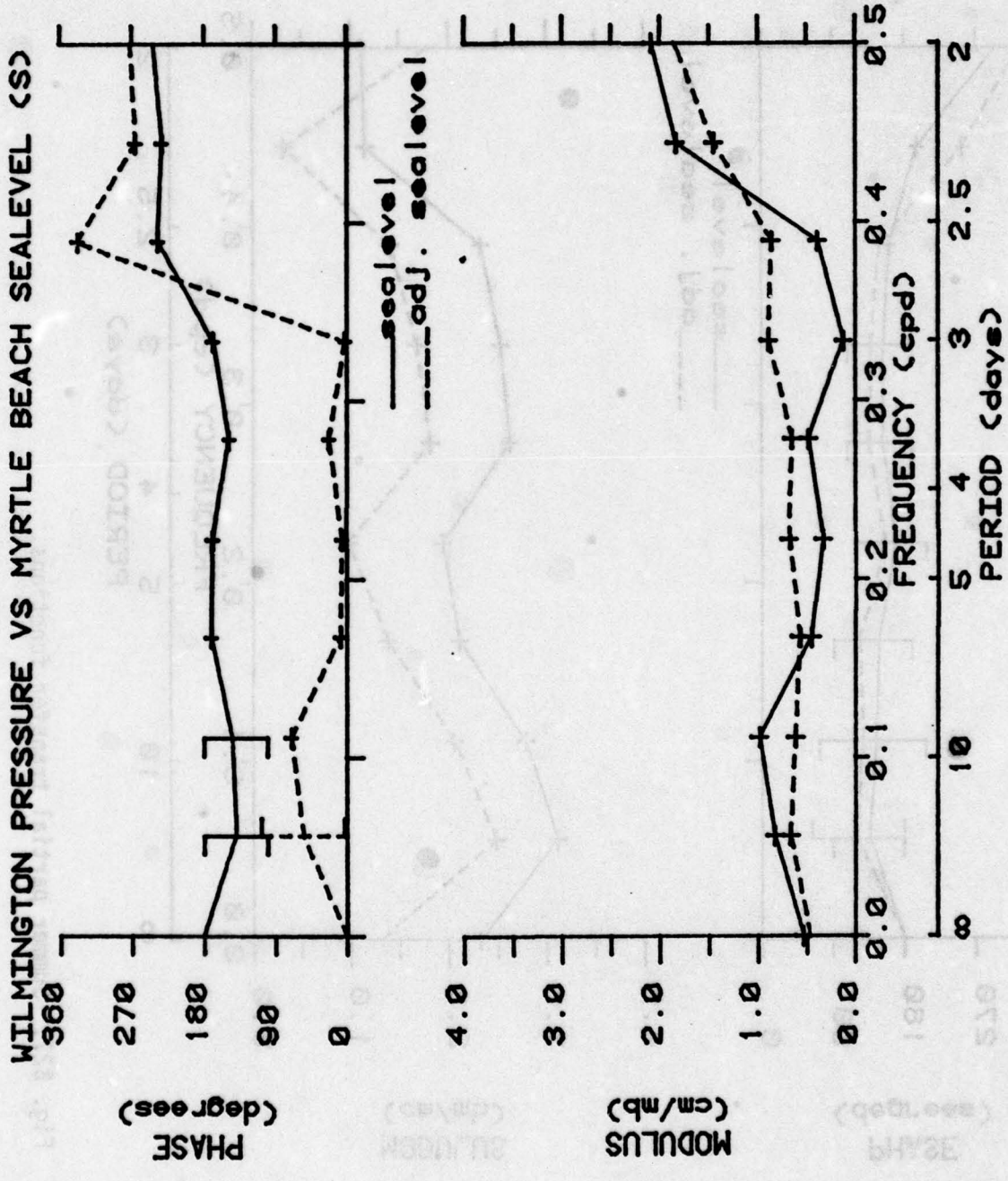

Fig. B28. Summer partial transfer functions.

APPENDIX C

Spectra (m^2/CPD), coherence, and phase (degrees) for sea level station adjacent pairs, proceeding southward, winter and summer cases. Negative phase means that the first-named station in the caption box leads the second-named station. The 95% null hypothesis level is shown for coherence.

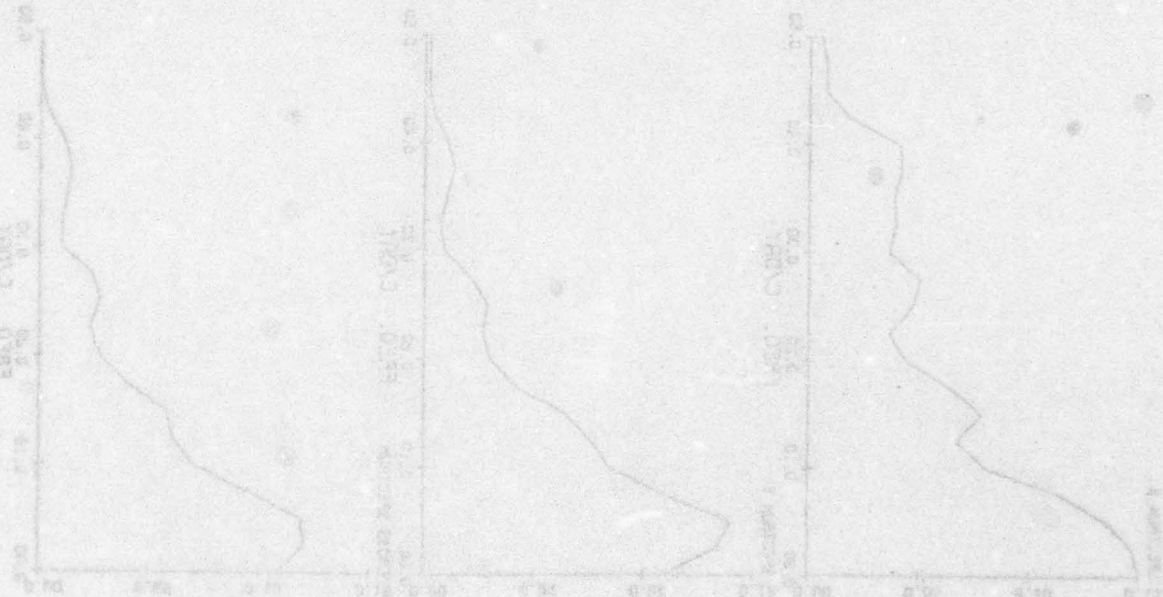

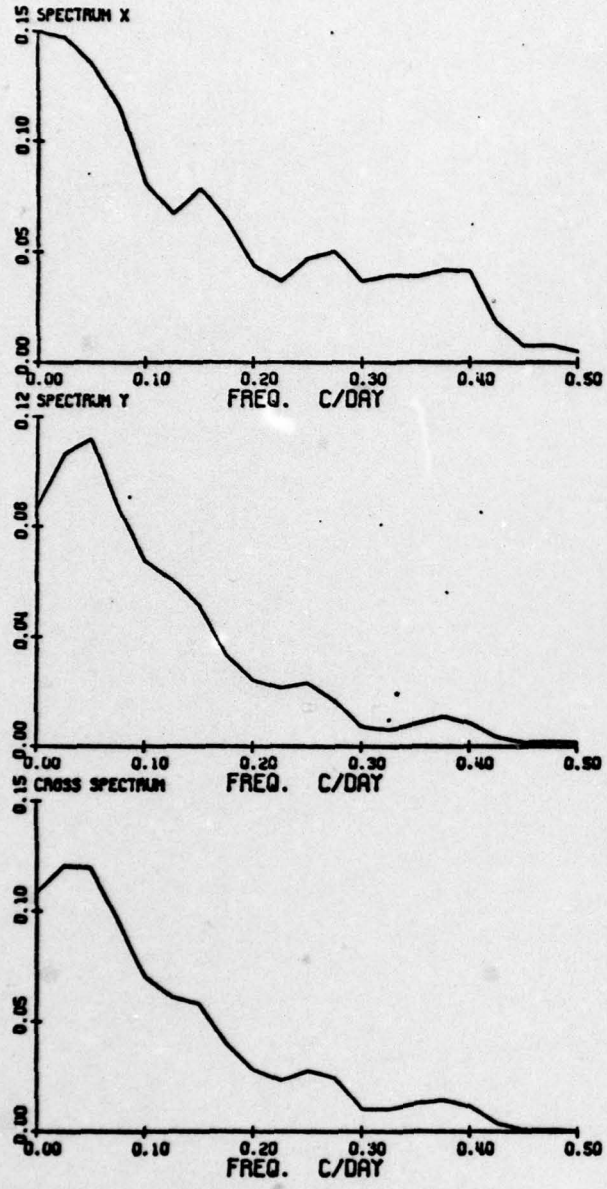

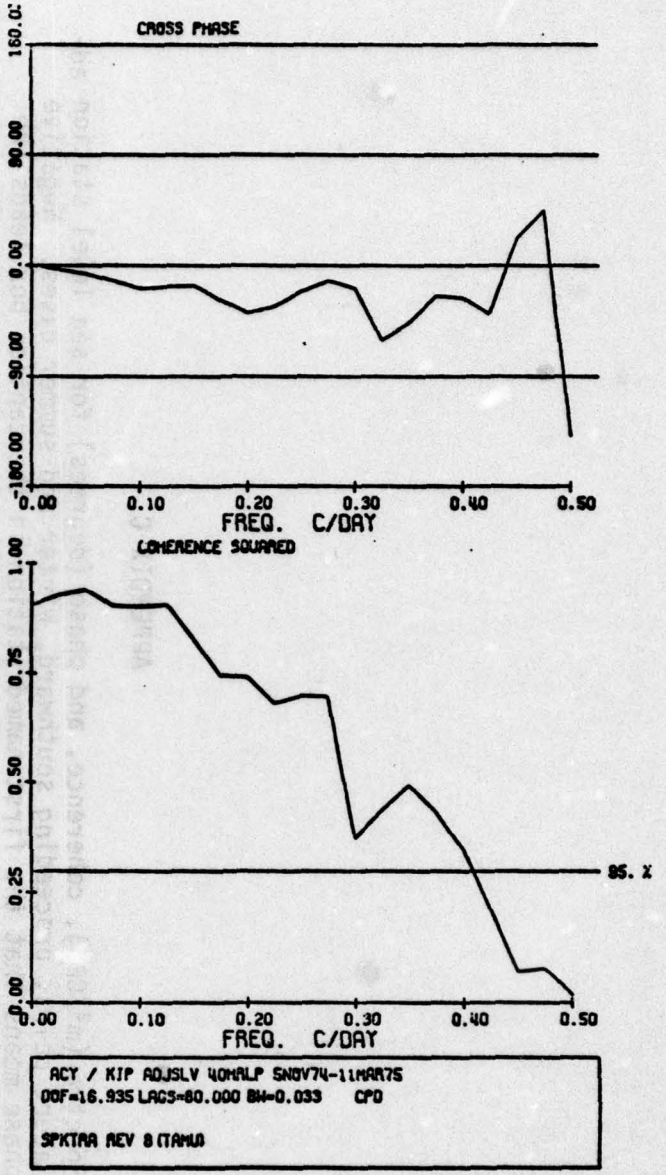

Fig. C1. Winter sea level spectra.

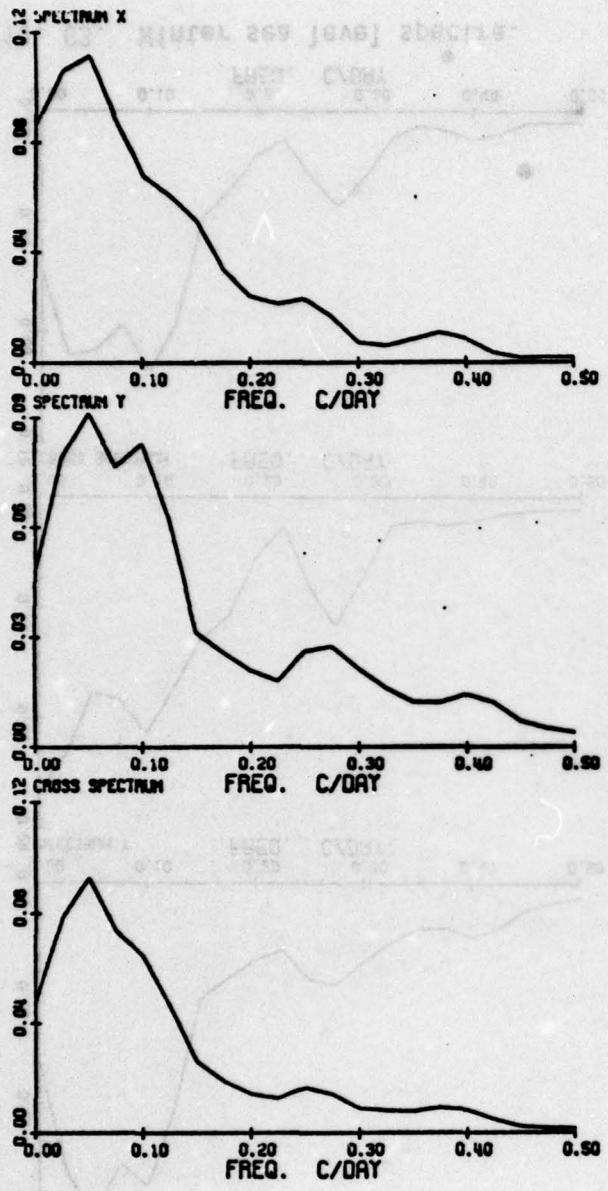

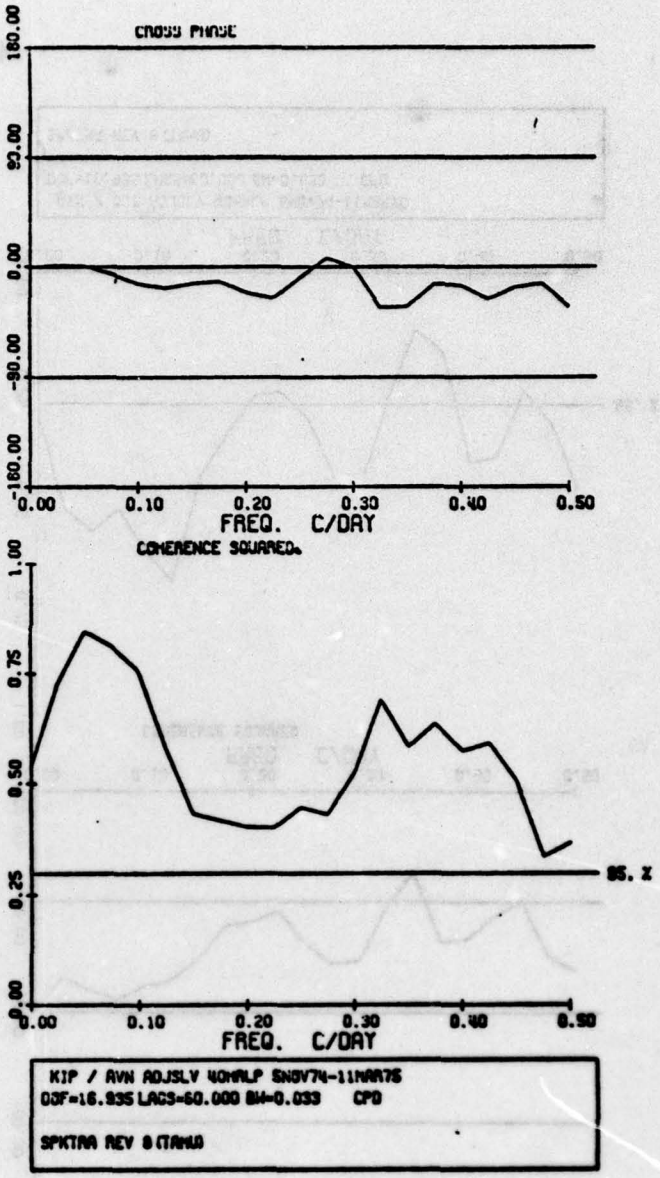

Fig. C2. Winter sea level spectra.

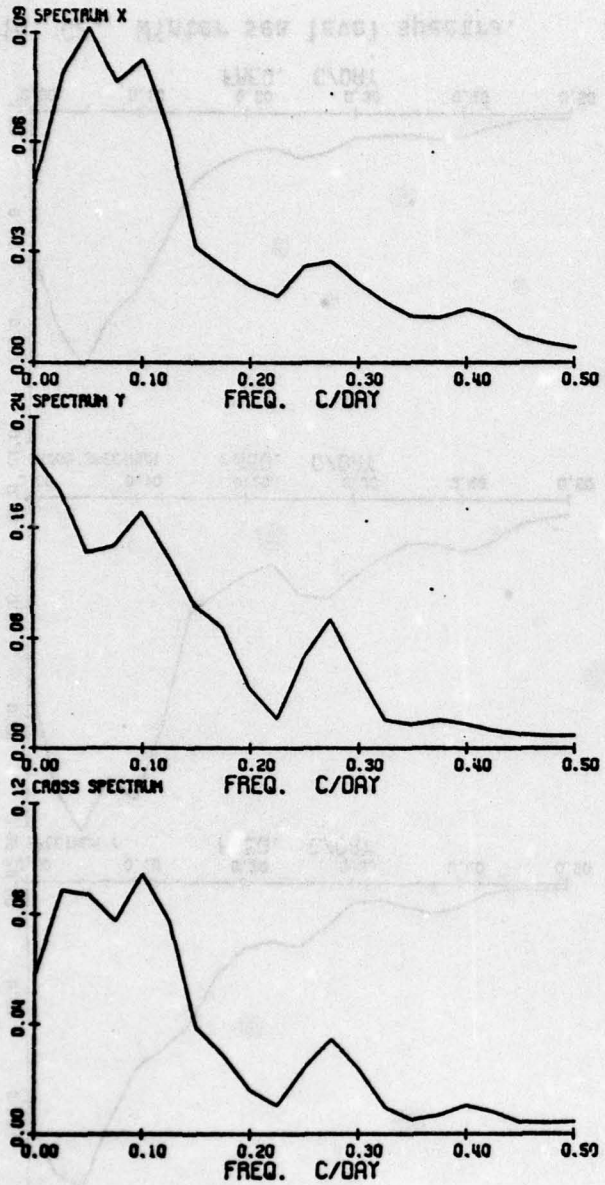

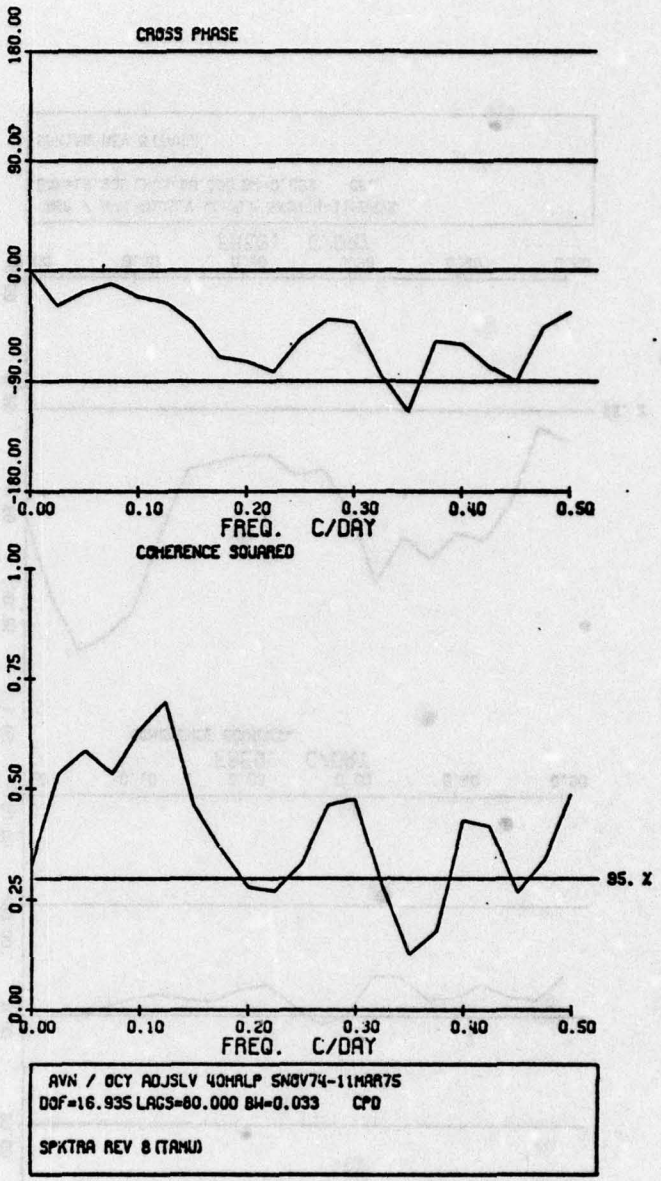

Fig. C3. Winter sea level spectra.

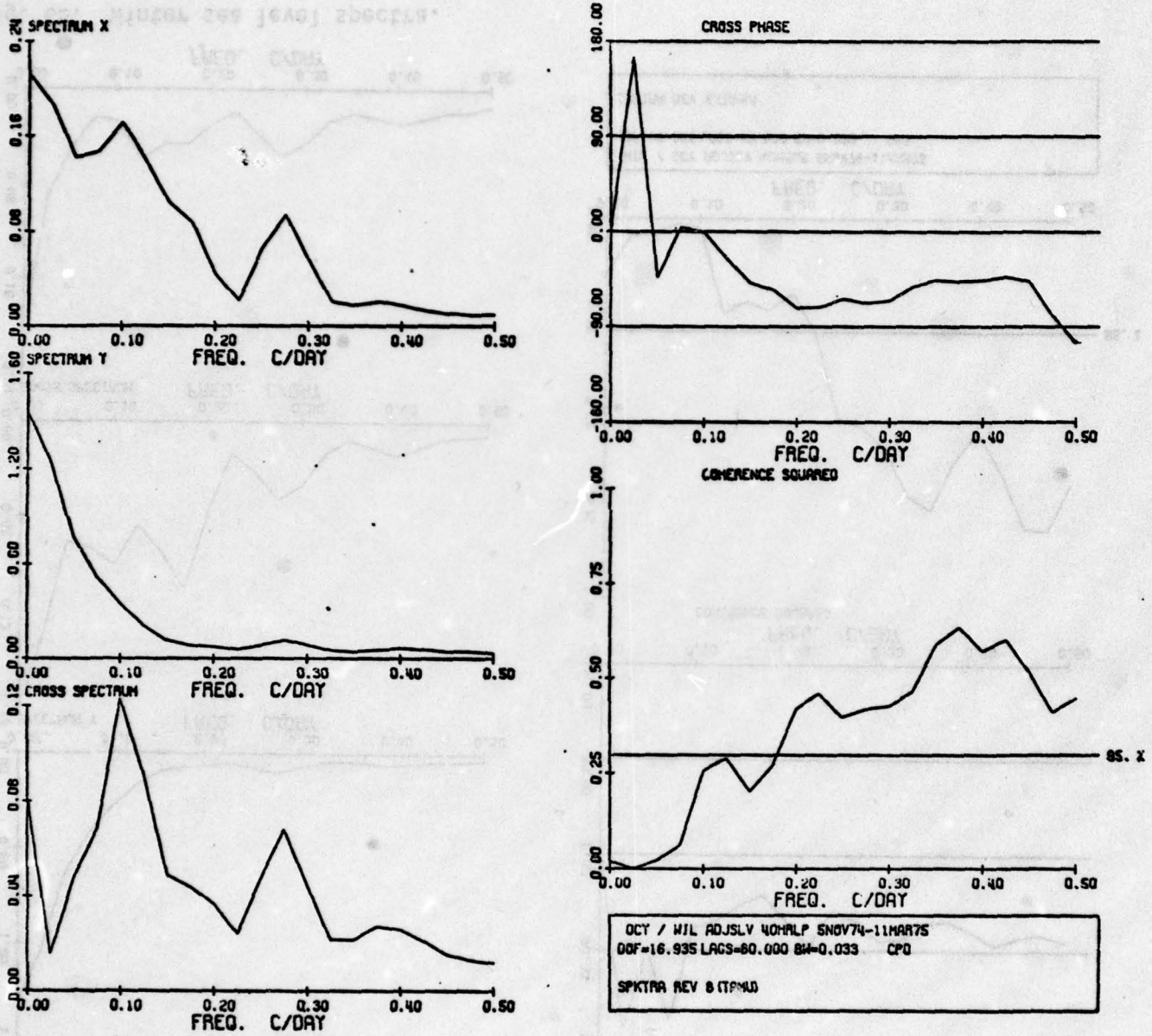

Fig. C4. Winter sea level spectra.

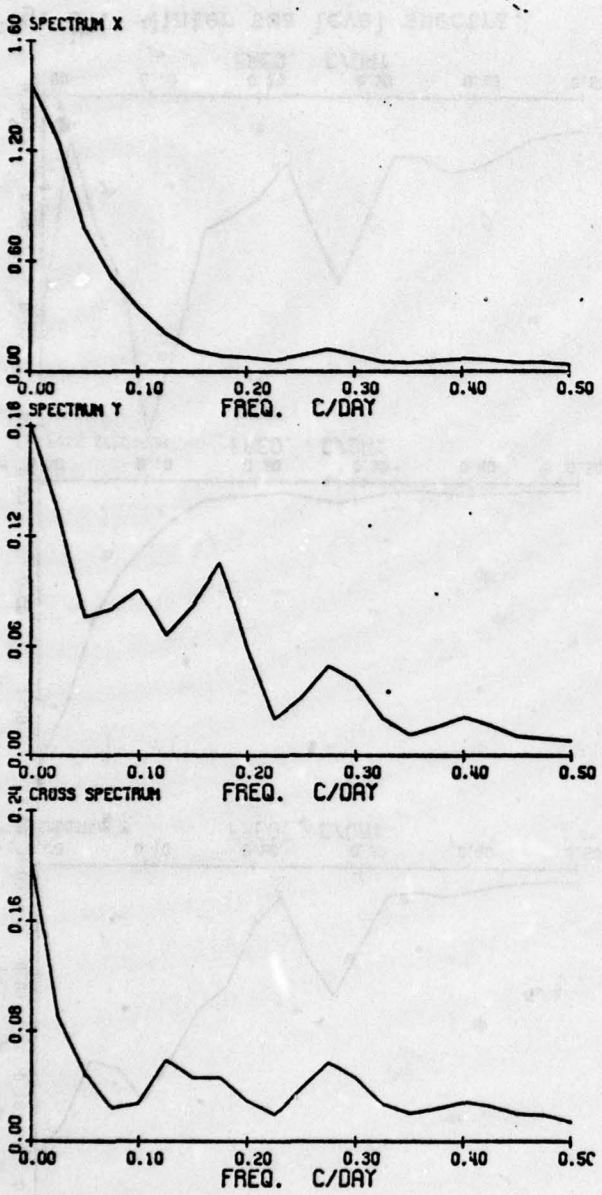

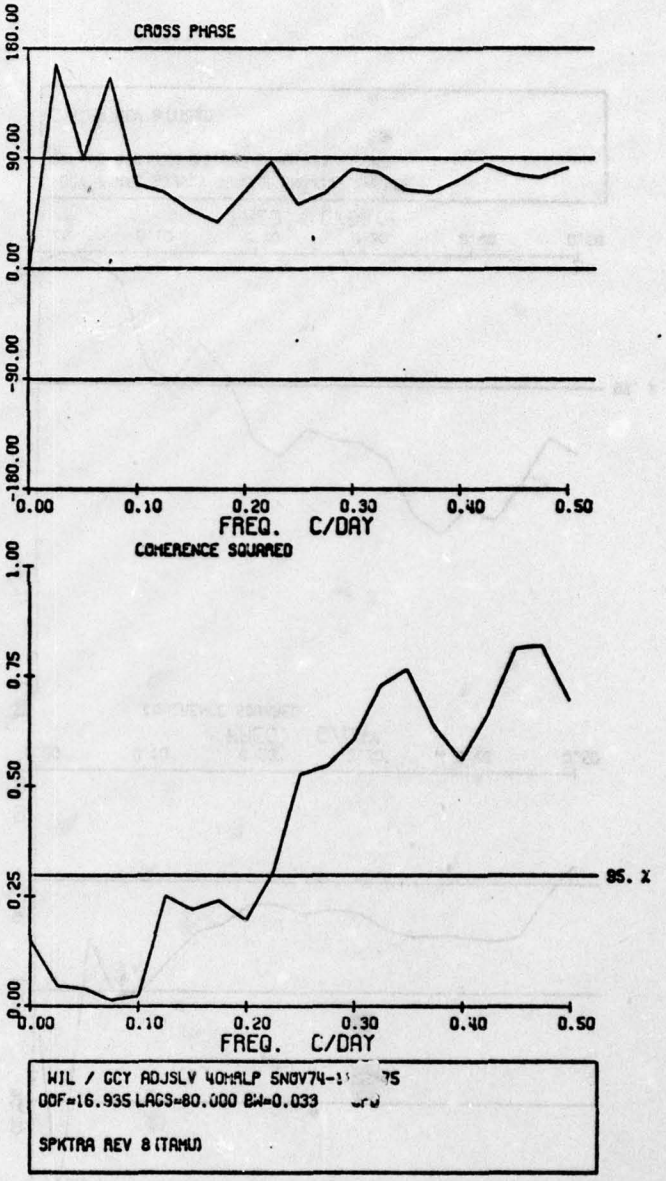

Fig. C5. Winter sea level spectra.

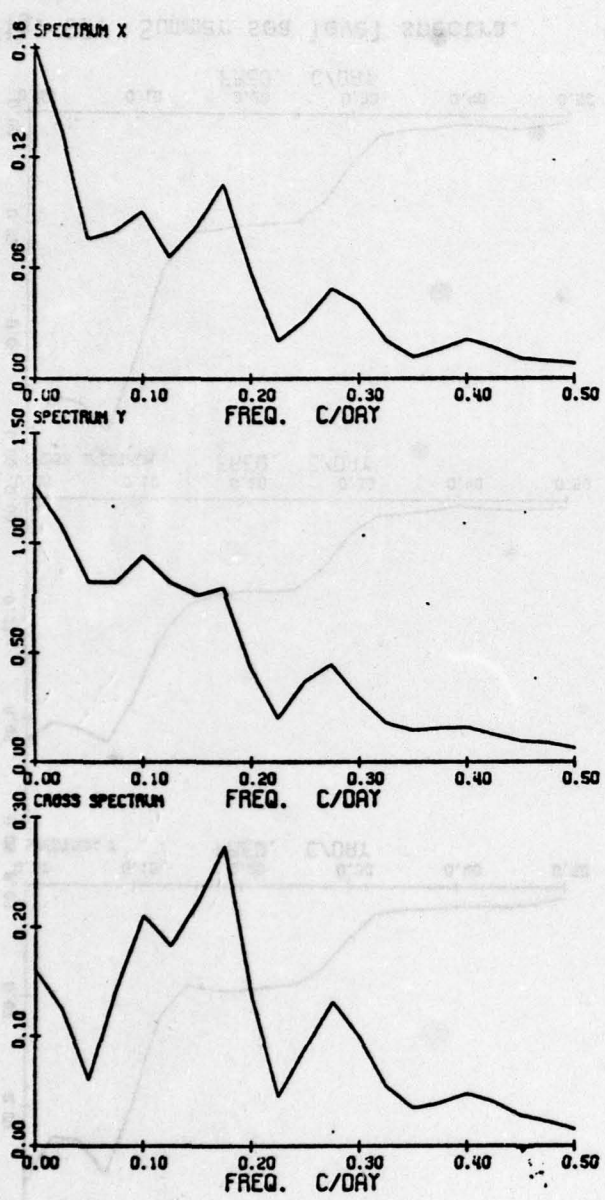

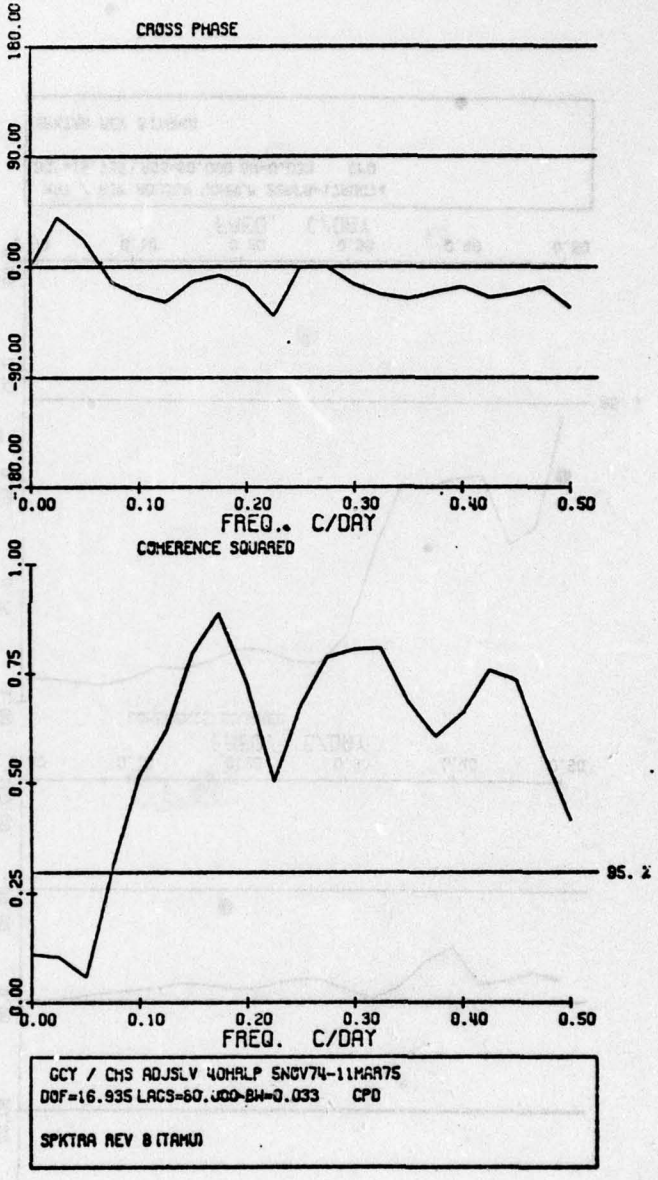

Fig. C6. Winter sea level spectra.

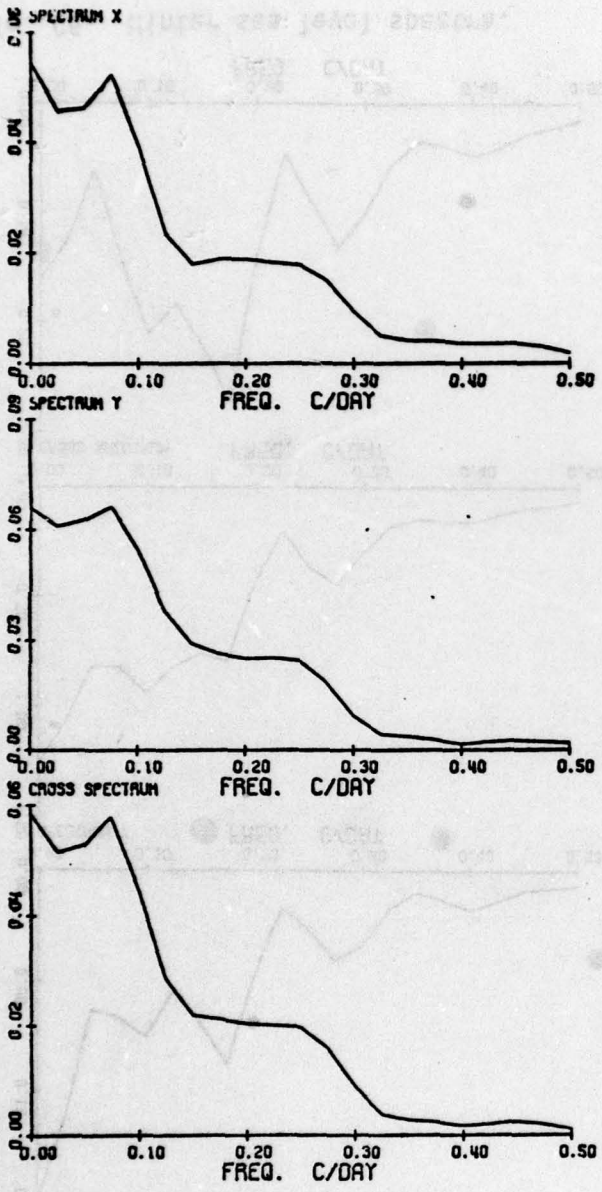

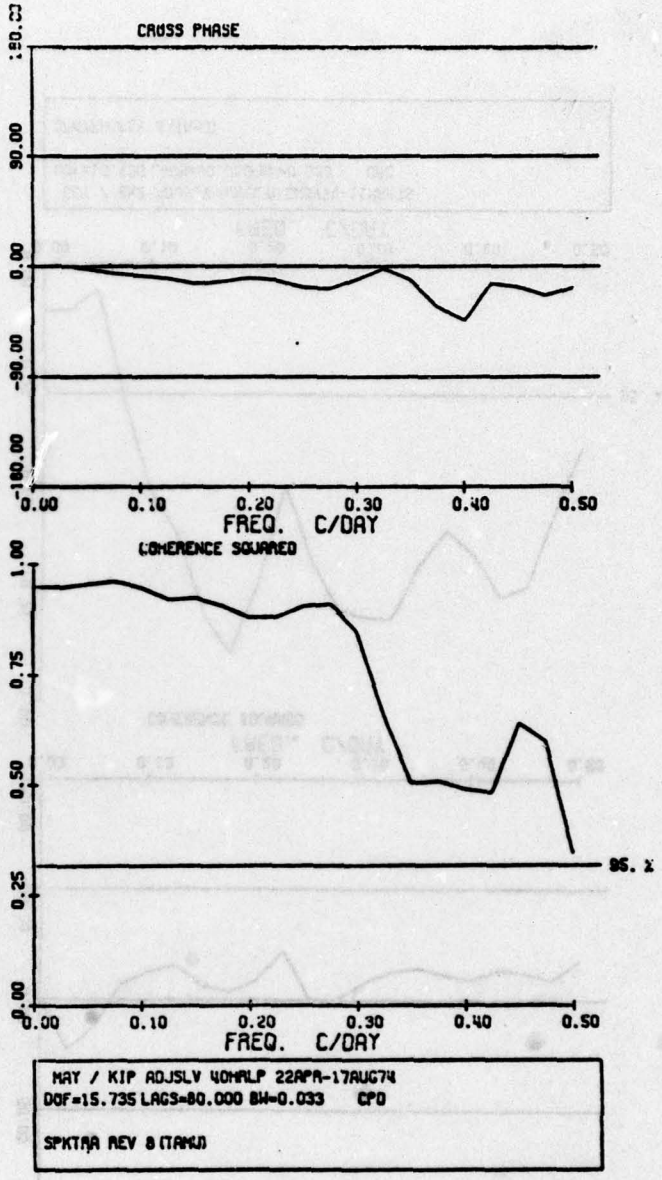

Fig. C7. Summer sea level spectra.

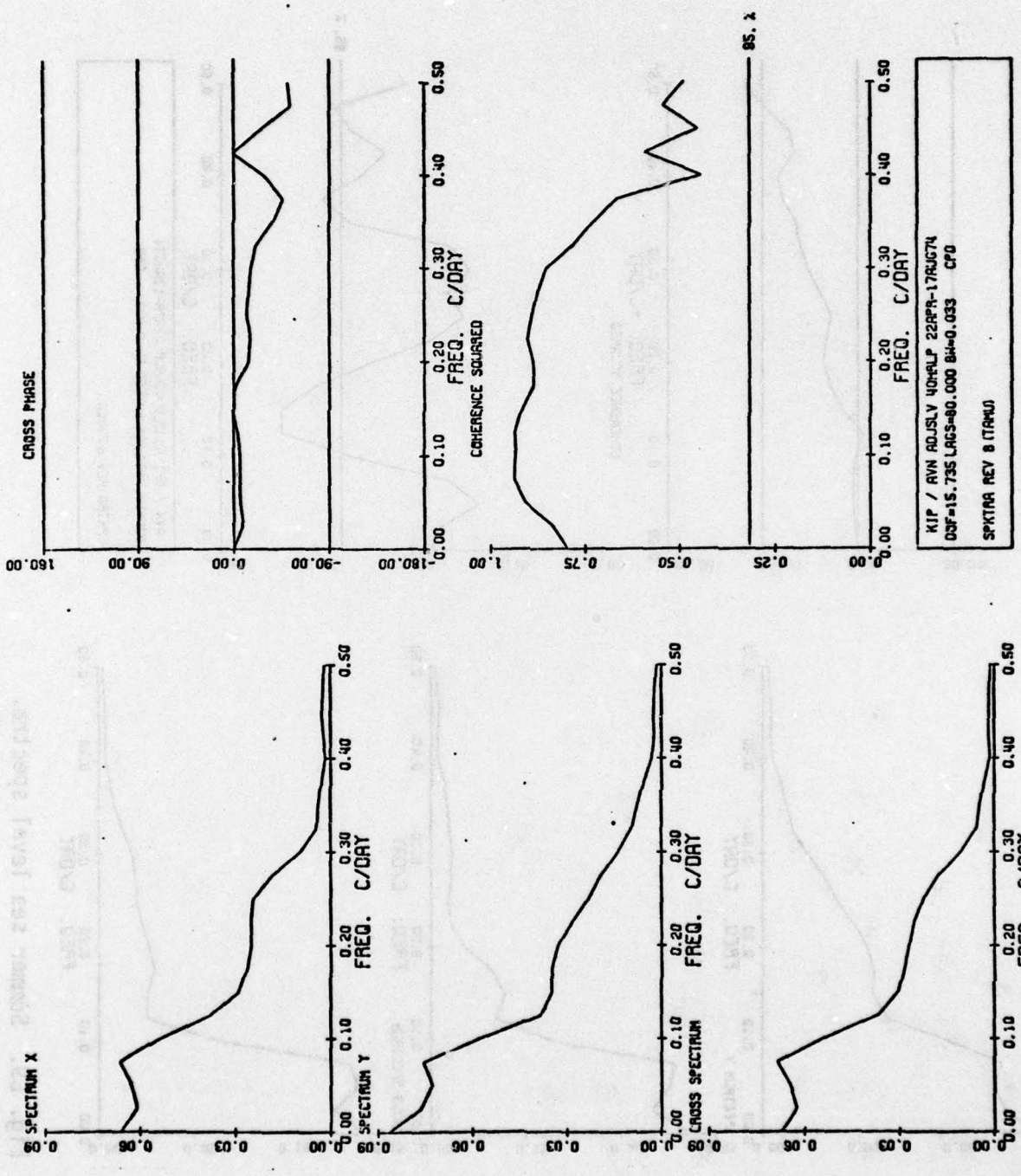

Fig. C8. Summer sea level spectra.

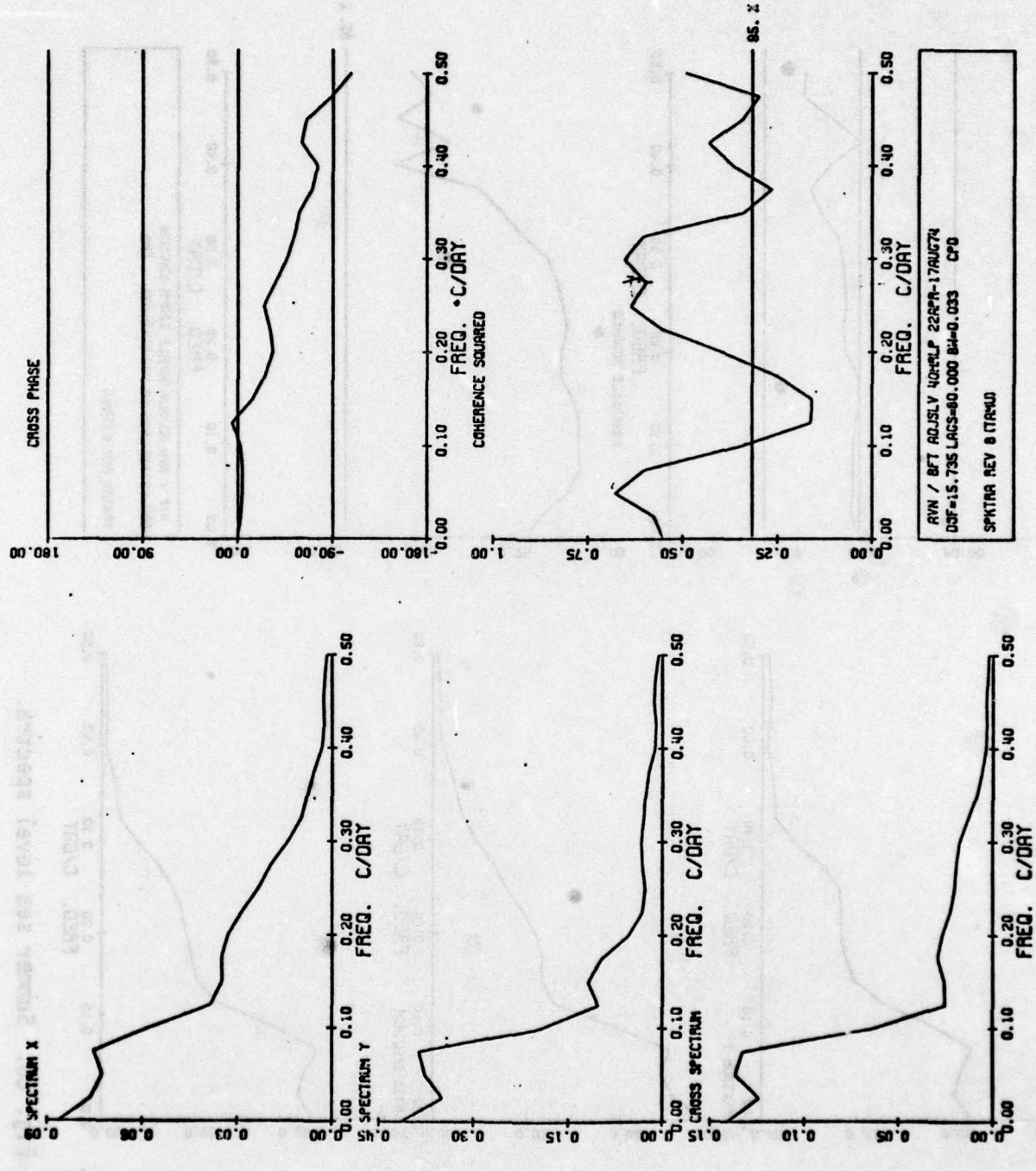

Fig. C9. Summer sea level spectra.

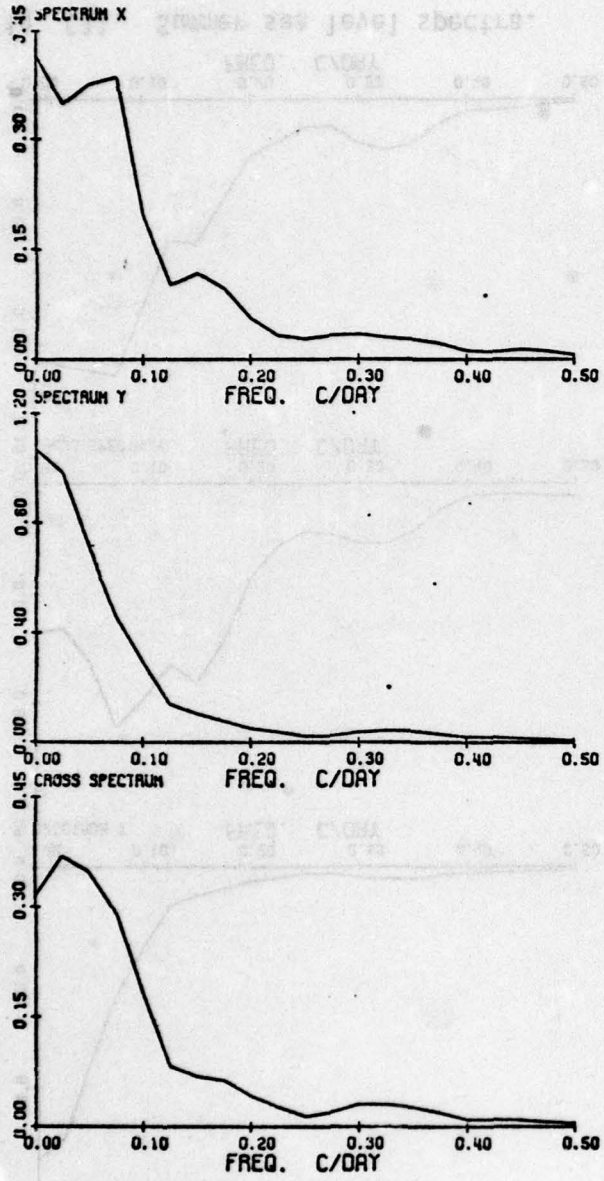

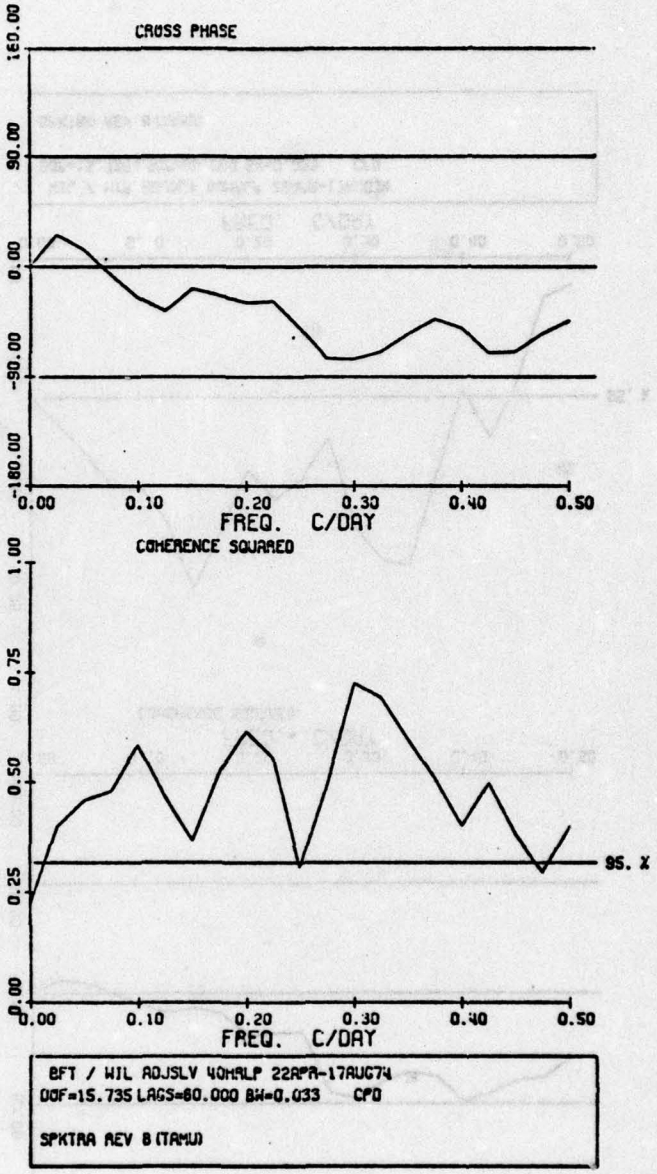

Fig. C10. Summer sea level spectra.

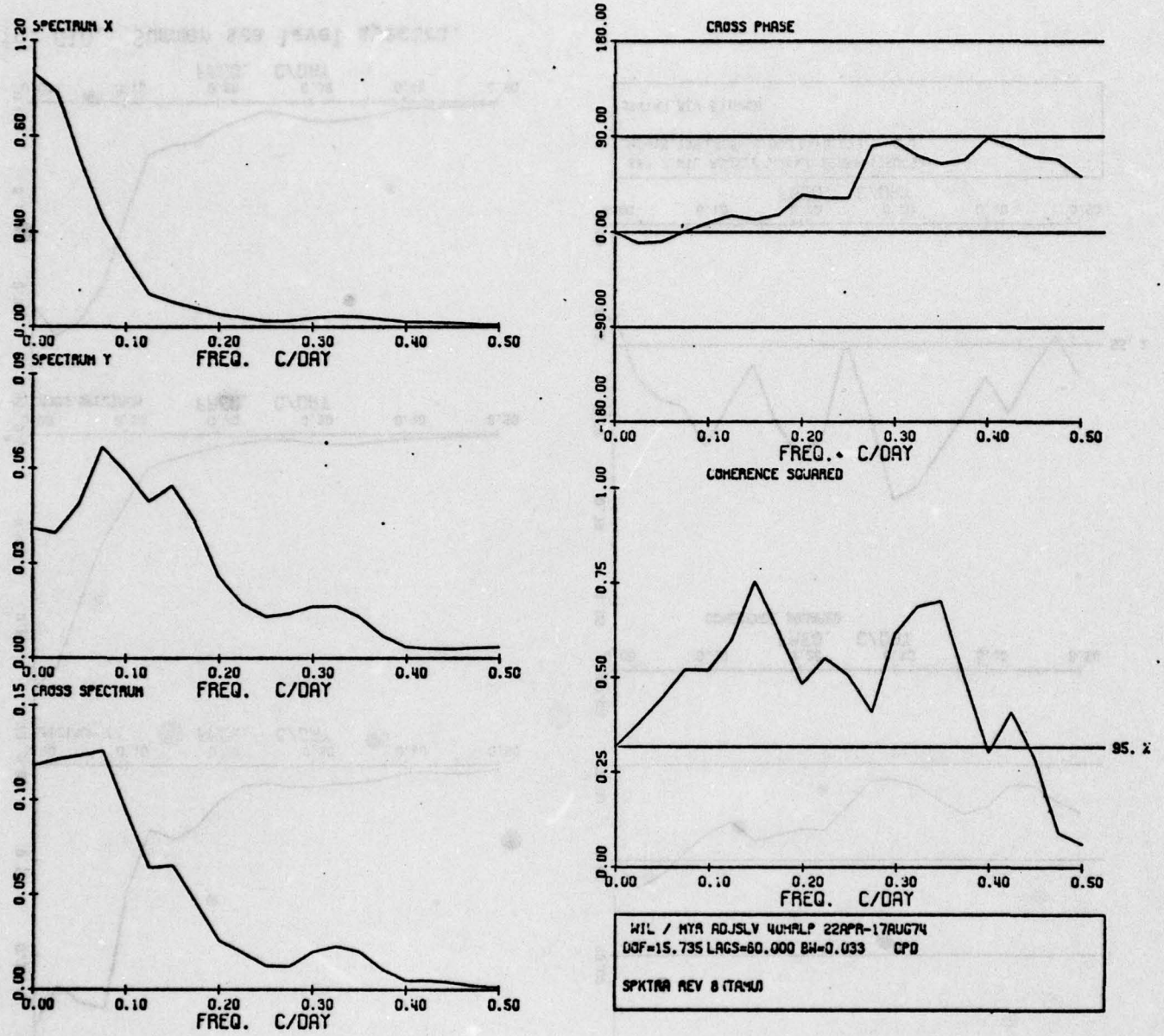

Fig. C11. Summer sea level spectra.

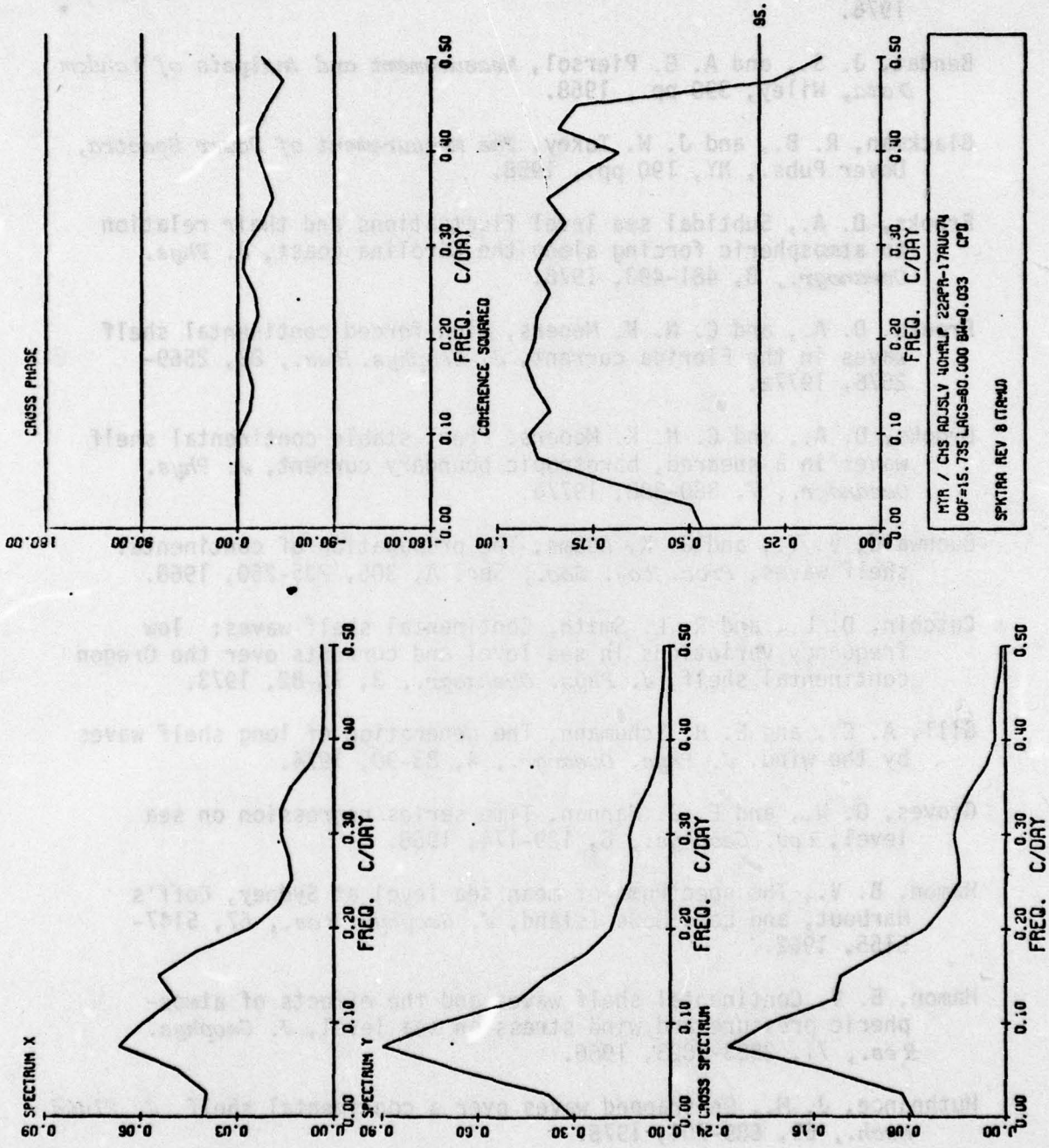

Fig. C12. Summer sea level spectra.

Allen, J. S., Continental shelf waves and alongshore variations in bottom topography and coastline, *J. Phys. Oceanogr.*, 6, 864-878, 1976.

Bendat, J. S., and A. G. Piersol, *Measurememt and Analysis of Random Data*, Wiley, 390 pp., 1968.

Blackman, R. B., and J. W. Tukey, *The Measurement of Power Spectra*, Dover Pubs., NY, 190 pp., 1958.

Brooks, D. A., Subtidal sea level fluctuations and their relation to atmospheric forcing along the Carolina coast, *J. Phys. Oceanogr.*, 8, 481-493, 1978.

Brooks, D. A., and C. N. K. Mooers, Wind-forced continental shelf waves in the Florida current, *J. Geophys. Res.*, 82, 2569-2576, 1977a.

Brooks, D. A., and C. N. K. Mooers, Free, stable continental shelf waves in a sheared, barotropic boundary current, *J. Phys. Oceanogr.*, 7, 380-388, 1977b.

Buchwald, V. T., and J. K. Adams, The propagation of continental shelf waves, *Proc. Roy. Soc.*, Ser. A, 305, 235-250, 1968.

Cutchin, D. L., and R. L. Smith, Continental shelf waves: low frequency variations in sea level and currents over the Oregon continental shelf, *J. Phys. Ocenaogr.*, 3, 73-82, 1973.

Gill, A. E., and E. H. Schumann, The generation of long shelf waves by the wind, *J. Phys. Oceangr.*, 4, 83-90, 1974.

Groves, G. W., and E. J. Hannan, Time series regression on sea level, *Rev. Geophys.*, 6, 129-174, 1968.

Hamon, B. V., The spectrums of mean sea level at Sydney, Coff's Harbout, and Lord Howe Island, *J. Geophys. Res.*, 67, 5147-5155, 1962.

Hamon, B. V. Continental shelf waves and the effects of atmospheric pressure and wind stress on sea level, *J. Geophys. Res.*, 71, 2883-2893, 1966.

Huthnance, J. M., On trapped waves over a continental shelf, *J. Fluid Mech.*, 69, 689-704, 1975.

LeBlond, P. H., and L. A. Mysak, *Waves in the Ocean*, 602 pp., Elsevier, Amsterdam and New York, 1978.

Lee, T. N., and D. A. Brooks, Initial observations of current temperature and coastal sea level response to atmospheric and Gulf Stream forcing on the Georgia shelf, *Geophys. Res. Lett.*, 6 (4), 321-324, 1979.

McKee, W. D., Continental shelf waves in the presence of a sheared geostrophic current, *Lecture Notes in Physics*, 64, edited by D. G. Provis and R. Radok, pp. 212-219, Australian Academy of Sciences, Canberra, and Springer-Verlag, Berlin, 1977.

McKee, W. D., Critical levels for forced Rossby and continental shelf waves, *Pure App. Geophys.*, submitted 1979.

Mooers, C. N. K., J. Fernandes-Partagas, and J. F. Price, Meteorological forcing fields of the New York Bight, U. Miami (RSMAS) report TR 76-8, 1976.

Mooers, C. N. K., and R. L. Smith, Continental shelf waves off Oregon, *J. Geophys. Res.*, 73, 549-557, 1968.

Mysak, L. A., Recent advances in shelf wave dynamics, *Rev. Geophys.*, submitted 1979.

Mysak, L. A., and B. V. Hamon, Low-frequency sea level behavior and continental shelf waves off North Carolina, *J. Geophys. Res.*, 74, 1397-1405, 1969.

Niiler, P. P., and L. A. Mysak, Barotropic waves along an eastern continental shelf, *Geophys. Fluid. Dyn.*, 2, 273-288, 1971.

Rhines, P. B., Edge-, bottom-, and Rossby waves in a rotating stratified fluid, *Geophys. Fluid. Dyn.*, 1, 273-302, 1970.

Richardson, W. S., W. Schmitz Jr., and P. P. Niiler, The velocity structure of the Florida Current from the Straits of Florida to Cape Fear, *Deep-Sea Res.*, 16, (supp), 225-231, 1969.

Robinson, A. R., Continental shelf waves and the response of the sea level to weather systems, *J. Geophys. Res.*, 69, 367-368, 1964.

Wang, D. P., Low frequency sea level variability on the Middle Atlantic Bight, *J. Mar. Res.*, submitted 1979.

Wang, D. P., and C. N. K. Mooers, Coastal-trapped waves in a continuously stratified ocean, *J. Phys. Oceanogr.*, 6, 853-863, 1976.